Dissertation

zur Erlangung des Doktorgrades der Fakultät für Biologie
der Ludwig-Maximilians-Universität München

A screen to identify factors in translation-dependent retrograde signaling

Vorgelegt von
Lukas Mittermayr

München, im Juli 2013

Erstgutachter : Prof. Dr. Dario Leister

Zweitgutachter: Dr. Tatjana Kleine

Tag der mündlichen Prüfung: 30.09.2013

Summary

Chloroplasts are crucial for life on earth as they are able to convert the sunlight into chemical energy. Hence, the understanding of chloroplast biogenesis and its regulation is necessary to support attempts to manipulate these processes and to promote the search for new sources of renewable energy. Effective communication between the cell organelles is required as most of the proteins are encoded in the nucleus and transported post-translationally into chloroplasts and mitochondria, where they form large complexes – such as the photosystems – together with proteins encoded in the chloroplast genome. Signal information originating from the nucleus is called anterograde signaling, in contrast to the signals deriving from the organelles, which are known as retrograde signals.

The *prolyl-tRNA synthase 1* (*prors1*) mutant was identified as a very good candidate for research of plastid as well as mitochondria retrograde signaling pathways due to its impairment of organellar translation, which has been shown to be involved in retrograde signaling processes. In this thesis, to further investigate this pathway, a genetic forward screen with mutagenized *prors1* mutants was performed. As marker for the suppression screen, luciferase was chosen and *LHCB* promotors were placed in front of it. Upon screening of 13377 plants, 360 mutants of the M3 generation were found to show a rescue of the luciferase expression and/or the growth performance, and 19 of these *relaxed LHCB suppression* (*rls*) mutants were further characterized. To verify the internal *LHCB* transcript levels, the expression of nuclear-encoded photosynthesis associated genes and translation of the corresponding proteins were measured. As it has been observed before that the *prors1* mutant exhibits a retarded growth and strongly reduced photosystem II (PSII) performance, hence the growth and PSII performance of the *rls* mutants was investigated. Moreover, the content of chlorophyll *a* and *b* was detected as well as the starch amount at the end of the dark period and at the end of the light period. From these analyses, three *rls* mutants (*rls2(1.2)*, *rls2(3)* and *rls478*) were chosen to identify the respective mutation responsible for the suppression of the *prors1* phenotype. All three mutations were localized via positional cloning on chromosome **V**. With a next generation mapping approach (combining next generation sequencing with fine mapping), possible causative mutations for the *rls2(3)* and *rls478* mutants (in *AT5G36320* for *rls2(3)* and in *AT5G09360* for *rls478*) were finally identified.

Zusammenfassung

Ohne Chloroplasten wäre das Leben auf der Erde wie man es kennt nicht vorstellbar, denn sie wandeln die Energie des Sonnenlichts in chemische Energie um. Dabei spielt die Kommunikation zwischen den einzelnen Zellkompartimenten eine entscheidende Rolle, denn ein Großteil der Proteine wird im Zellkern kodiert und anschließend post-translational in die Zellkompartimente transportiert, wo sie zusammen mit den vor Ort kodierten Proteinen größere Einheiten wie die Photosysteme im Chloroplasten bilden. Der Informationsfluss vom Zellkern zu den Organellen wie Chloroplasten und Mitochondrien wird anterograder Signalweg genannt, der Signalweg von den Zellkompartimenten zurück zum Kern retrograd.

Die *prors1* Mutante ist für die Untersuchung des Translations-abhängigen retrograden Signalwegs hervorragend geeignet, da sie eine Beeinträchtigung der Translation in den Organellen vorweisen kann. Mit Hilfe eines „genetic forward screens“ von mutagenisierten *prors1* Pflanzen sollten in der vorliegenden Arbeit neue Mutanten gefunden werden, die bei der Untersuchung der Translations-abhängigen retrograden Signalwege helfen könnten. Von den 13377 getesteten Pflanzen zeigten 360 in der M3-Generation eine Unterdrückung des *prors1* Phänotyps und somit bessere Werte als die Elterngeneration vor der Mutagenese. Im weiteren Verlauf dieser Arbeit wurden 19 dieser *rls* (*„relaxed LHCB suppression“*) Mutanten physiologisch charakterisiert. Es wurde das Wachstum der *rls* Mutanten analysiert, und mittels der Chlorophyllfluoreszenz die Leistung des Photosystems II ermittelt. Neben der Bestimmung von Chlorophyll *a* und *b* wurde außerdem der Stärkegehalt untersucht. Darüber hinaus wurde das Expressionslevel von kernkodierten Genen, welche an der Photosynthese beteiligt sind, ebenso bestimmt wie der dazugehörige Proteingehalt. Aufgrund der Ergebnisse dieser Messungen wurden drei Mutanten (*rls2(1.2)*, *rls2(3)* und *rls478*) gewählt, für welche bestimmt werden sollte, welche Mutation für den *rls* Phänotyp verantwortlich ist. Für die drei Mutanten wurde dazu eine Grobkartierung durchgeführt und für jede Mutante jeweils eine Region auf dem Chromosom **V** gefunden. Mittels einer Kombination aus „next generation sequencing“ Technologie mit bekannten Kartierungsmethoden konnte außerdem für *rls2(3)* (in einem Exon von *AT5G36320*) und *rls478* (in einem Exon von *AT5G09360*) die mögliche Mutation identifiziert werden, welche für den *rls* Phänotyp verantwortlich zu sein scheint.

Table of contents

List of abbreviations:

µE	microeinstein
µg	microgramm
µl	microliter
µm	micrometer
µmol	micromolar
1-qP	proportion of closed PSII
bp	base pair
CAPS	cleaved amplified polymorphic sequences
chl *a*	chlorophyll *a*
chl *b*	chlorophyll *b*
Col-0	Columbia-0
ddH_2O	double distilled water
EMS	ethyl methanesulfonate
flu	fluorescent in blue light
F_v/F_m	maximum quantum yield of PSII
g	g-force (the force of gravity)
GFP	green fluorescent protein
gun	genome uncoupled mutant
GUS	β-glucuronidase
h	hour
iML	improved Maximum Likelihood
kb	kilobase
L*er*	Landsberg *erecta*
LUC	luciferase
m	meter
M2	second mutagenized generation
M3	third mutagenized generation
M4	fourth mutagenized generation
mb	mega base
mg	milligramm
min	minute
ml	milliliter

mM	millimolar
MRPL	mitochondrial ribosome protein L
ms	millisecond
NGE	nuclear gene expression
NGS	next generation sequencing
NPQ	nonphotochemical fluorescence quenching
pam	photosynthesis altered mutant
PCR	polymerase chain reaction
PGE	plastid gene expression
PhANGs	Photosynthetic Associated Nuclear Genes
PRORS1	prolyl-tRNA-synthethase 1
PRPL	plastidial ribosome protein L
PSII	photosystem two
PTM	plastid transmembrane transcription factor
rls	relaxed LHCB suppression
RLU	relative luminescence unit
ROS	reactive oxygen species
SNP	single nucleotide polymorphism
SRM	SNP ratio mapping
SSLP	simple sequence length polymorphisms
stdv	standard deviation
v/v	volume per volume
w/v	weight per volume
Φ_{II}	effective quantum yield of PSII

1. Introduction

Chloroplasts and mitochondria originate from free-living prokaryotic organisms and became stable integrated organelles by a process called endosymbiosis (Dyall et al. 2004). During evolution, the conversion from endosymbionts to organelles was accompanied by a massive transfer of genomic DNA from the organelles to the nucleus (Kleine et al. 2009). In nowadays plastids, merely ~5% of the chloroplast-located proteins are encoded by the chloroplast genome, whereas the majority of proteins is encoded in the nucleus and is imported post-translationally into the chloroplast (Abdallah et al. 2000). Hence, most of the chloroplast multi-protein complexes including the photosystems are a mosaic of subunits encoded by both the nucleus and the chloroplast genome. This arrangement requires a coordinated expression of nuclear genes encoding plastid-localized proteins with expression of plastidic genes. This coordinated expression is accomplished by bidirectional signaling cascades that send the information from the nucleus to the organelles (anterograde signaling) and pathways required for signaling from plastids to the nucleus (retrograde signaling) (Chan et al. 2010; Enami et al. 2012; Jung and Chory 2010; Kakizaki et al. 2009; Kleine et al. 2009; Leister 2005; Nott et al. 2006; Pesaresi et al. 2007; Pogson et al. 2008; Terry and Smith 2013; Woodson and Chory 2008) (Figure 1). Additional to their role as biochemical factories, plastids act as sensors for changing environmental conditions and different developmental stages to coordinate regulatory mechanisms.

Hence, the communication between the plastids and the nucleus is essential during initial developmental stages of the plastids (biogenic control) and in the adult stage to react to changes in the environment (operational control) (Pogson et al. 2008).

1.1 Retrograde signaling

The first evidence for retrograde signaling (“plastid signals“) was found in two barley mutants with morphologically aberrant plastids that possess a defect in plastid protein synthesis (Bradbeer et al. 1979). This results in a down-regulation of nuclear-encoded plastid proteins, suggesting that a plastid signal was emitted that repressed the nuclear expression of photosynthetic genes (Bradbeer et al. 1979). Today it is known that several distinct processes exist in plastids that trigger signaling pathways to regulate specific genes and regulons in the nucleus. To achieve this, the cytosolic

and plastid signaling pathways have to operate together to ensure the correct responses in the different cellular compartments (Fernandez and Strand 2008). Plastid signals are moreover responsible for the coordination of the cell cycle and coupling of DNA replication (Kobayashi et al. 2009). Additionally, interorganellar communication plays a role in other cellular processes, including intercellular communication via plasmodesmata (Burch-Smith et al. 2011) or the transition from cell proliferation to cell expansion (Andriankaja et al. 2012).

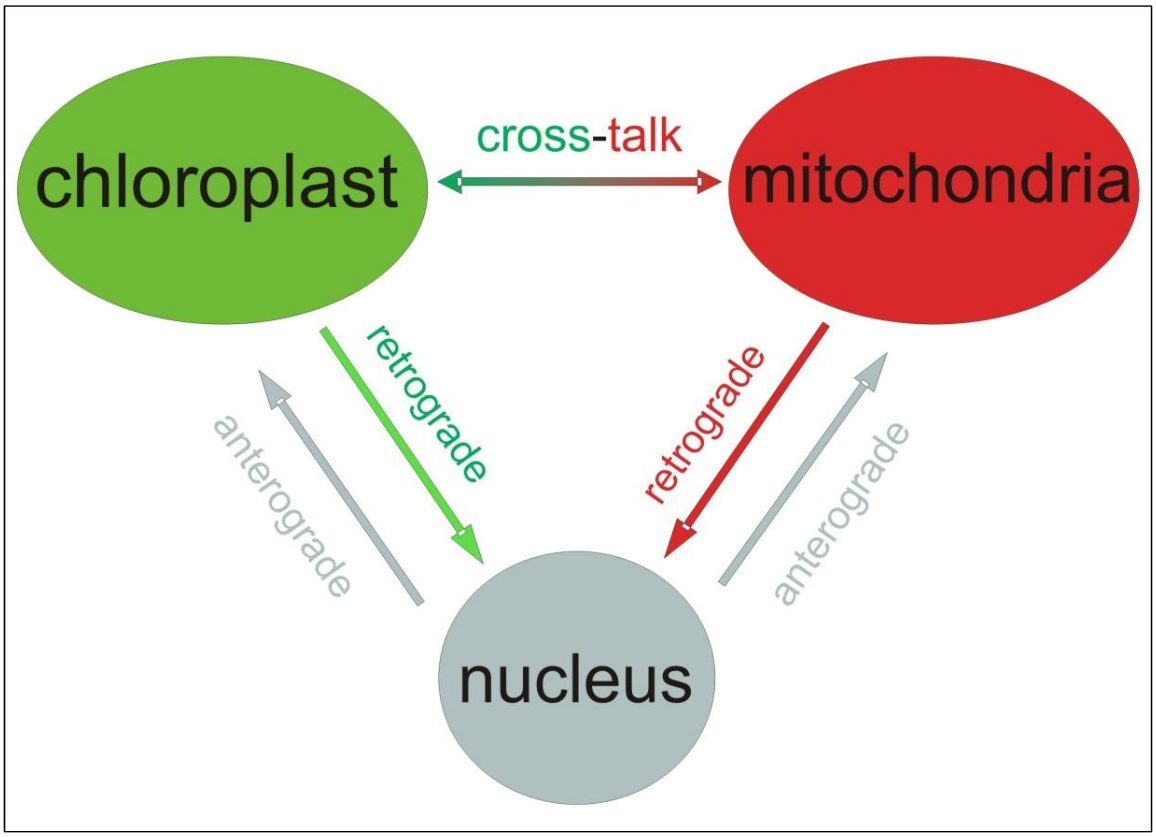

Figure 1: Signaling networks in the plant cell. The flow of information from the nucleus (grey) to the organelles (green and red) is called “anterograde” signaling, whereas the plastid and mitochondrial signals to the nucleus are called “retrograde”. The interorganellar communication between chloroplasts and mitochondria is depicted as “cross-talk”. Adapted from Woodsen and Chory, 2008.

The major “classical“ signals/pathways that are thought to mediate retrograde signaling include (i) the organellar gene expression, (ii) reactive oxygen species (ROS) and (iii) proteins. More recently, several metabolites were discussed as an additional class of retrograde signaling molecules (see chapter 1.1.1 – 1.1.4).

1.1.1 Organellar gene expression as source for retrograde signaling

The knowledge about “developmental” plastid signals regulating early chloroplast biogenesis derives primarily from studies using herbicides like norflurazon or lincomycin that inhibit function and development of the organelle (Nott et al. 2006). Norflurazon is an inhibitor of phytoene desaturase and therefore of carotenoid biosynthesis which causes photobleaching of plants (Oelmüller et al. 1986). Lincomycin, on the other hand, is an inhibitor of the 70S ribosome and thus of plastidic (and mitochondrial) translation (Sullivan and Gray 1999). Studies using these herbicides demonstrated that inhibition of plastid gene expression and/or tetrapyrrole biosynthesis lead to down-regulation of Photosynthetic Associated Nuclear Genes (PhANGs), as they are sensitive to the functional state of the plastids (Susek et al. 1993; Larkin et al. 2003).

By applying genetic screens in *Arabidopsis thaliana,* six *genome uncoupled mutants* (*gun*) were identified which express PhANGs, even upon photobleaching with norflurazon (Susek et al. 1993; Woodson et al. 2011). The genes *GUN2*-*GUN6* encode for proteins that play a role in tetrapyrrole biosynthesis, functioning in the branch point of heme and chlorophyll biosynthesis (Mochizuki et al. 2001, Larkin et al. 2003; Woodson et al. 2011). Moreover, the plastid gene expression (PGE) pathway was discovered with the help of the chloroplast translation inhibitor lincomycin (Sullivan and Gray 1999). From the six *gun* mutants, only *gun1* affects the PGE pathway, as the mutant shows a rescue of plastid signaling after norflurazon and lincomycin treatment, suggesting that plastid translation is necessary for full *LHCB* transcription (Koussevitzky et al. 2007).

1.1.1.1 The mutant *prors1* as an alternative for research of the PGE pathway

In earlier studies, Columbia-0 (Col-0) *Arabidopsis thaliana* plants were mutagenized with T-DNA transposons and the resulting lines were screened for plants exhibiting a decreased effective quantum yield (*Fv*/*Fm*) of photosystem II (PSII) (Varotto et al. 2000). With this approach, mutations were identified that are localized in the 5´untranslated region of the nuclear gene encoding PROLYL-tRNA-SYNTHETASE1 (PRORS1), leading to the leaky mutants *prors1-1* and *prors1-2* (Pesaresi et al. 2006). The function of PRORS1 is crucial for plants, as all proteins encoded by the organelle genomes contain at least one proline residue, hence only leaky mutants survive the embryo stage. The *PRORS1* transcript of the leaky mutants *prors1-1* and *prors1-2* is

reduced to 50% and 25%, respectively, which was found to cause a down-regulation of transcripts for proteins of the photosynthetic light reaction and an up-regulation of other chloroplast proteins (Pesaresi et al. 2006). These effects are stronger in *prors1-2* than in *prors1-1*, and they were moreover shown to be independent from light and photooxidative stress, as they are not associated with the ROS levels in leaves and are thus unaffected during darkness (Pesaresi et al. 2006). Interestingly, PhANGs are down-regulated in the double mutant *prpl11mrpl11* similar to *prors1-2*. By contrast, expression of PhANGs is only slightly down-regulated in the single mutants *prpl11* (impaired in the plastid ribosomal L11 protein) and *mrpl11* (impaired in the mitochondrial ribosomal L11 protein). These mutants were used as controls because of their impairment of organellar translation either exclusively in chloroplasts (*prpl11*) or in mitochondria (*mrpl11*). The observed translational defect in the double mutant is not due to an additive effect of the single mutants, as *prpl11* and *prpl11mrpl11* were found to feature the same photosynthetic performance and thylakoid protein composition (Pesaresi et al. 2006). Thus, analysis of retrograde signaling induced by inhibition of organellar translation in the *prors1* mutant is a very good alternative to applying inhibitors of protein synthesis.

1.1.1.2 The tetrapyrrole pathway and its metabolites as signaling source and molecules

The so far best characterized retrograde signaling pathway involves intermediates of tetrapyrrole biosynthesis. The four major tetrapyrrole molecules synthesized in the chloroplast are chlorophyll, heme, siroheme and phytochromobilin. Disruption of the tetrapyrrole pathway by *e.g.* the transient accumulation of the intermediated Mg-protoporphyrin IX was described to cause a clear effect on the expression of PhANGs and thus on organellar gene expression (Strand et al. 2003; Pontier et al. 2007; Zhang et al. 2011; Figure 2).

Current studies revealed that heme is a very important signaling molecule during chloroplast biosynthesis (Woodson et al. 2011) and for circadian clock adjustment (Salome et al. 2013). Moreover, the combination of the effects from different metabolites (“metabolite signature”) is hypothesized to be responsible for the regulation of PhANGs (Pfannschmidt 2010).

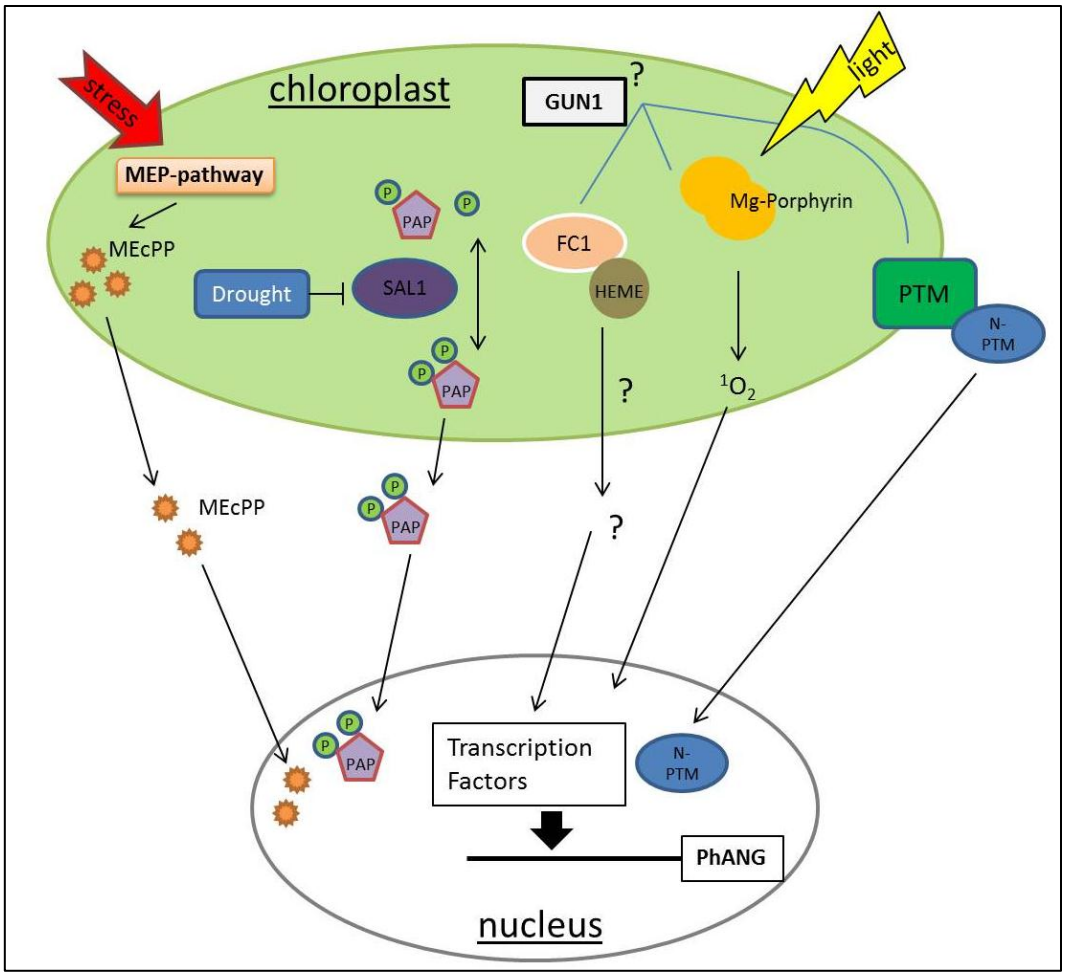

Figure 2: Retrograde signaling from chloroplast to nucleus. Stress mediated induction of methylerythritol cyclodiphosphate (MEcPP) levels functions as a sensor and a communication signal to the nucleus to induce stress responsive genes through alteration of nuclear architecture and functional dynamics. Drought stress and high light inhibits the activity of the bifunctional phosphatase SAL1 leading to accumulation of the phosphonucleotide PAP in the chloroplast. PAP travels to the nucleus and induces stress associated gene expression. The mode of action of heme functioning as a regulator of expression of photosynthesis-associated nuclear genes (PhANGs) remains elusive. Under oxidative stress conditions, which lead to accumulation of chlorophyll precursors such as Mg-porphyrins, a signal mediated by singlet oxygen ($^1O_2$), regulates the expression of PhANGs. PTM acts as a general stress sensor in the outer envelope membrane. GUN1-mediated response activates a protolytic mechanism where the N-terminal part of N-PTM is released. This N-PTM peptide travels to the nucleus and induces transcription factors. For further details, see text.
P, phosphate; FC1, ferrochelatase1; PTM, plastid transmembrane transcription factor; MEP, methylerythritol phosphate

1.1.2 Reactive oxygen species (ROS) as signaling molecules

Stress conditions that affect the photosynthetic electron transport rate often result in higher ROS levels (Elstner 1991). Singlet oxygen ($^1O_2$) produced by PSII and superoxide anion generated by photosystem I (PSI) - which is further metabolized to H_2O_2 - are the most common ROS found in the chloroplast (Mullineaux and

Karpinsky 2002; Appel and Hirt 2004). ROS can cause irreversible oxidative damage to cells, hence plant cells had to develop pathways to convert ROS into harmless metabolites. However, ROS were described to act as retrograde signals themselves by increasing antioxidant enzyme production or by adjusting the photosynthetic machinery to optimize photosynthetic electron transport (Lee et al. 2007). A breakthrough in understanding ROS signaling was achieved by analysis of the *fluorescent in blue light* (*flu*) mutant, which features a strong accumulation of protochlorophyllide, a chlorophyll precursor excitable by light, in the dark. A posterior shift from dark to light leads to a rapid accumulation of $^1O_2$ in the chloroplast, followed by a stop of growth and cell death (Meskauskiene et al. 2001). It is suggested that $^1O_2$ is able to travel short distances and even crosses membranes (Skovsen et al. 2005), thus capable of acting outside the chloroplast as well (Figure 2). Accumulation of ROS has been shown to result in major changes of nuclear gene expression, *e.g.* $^1O_2$ accumulation in the *flu* mutant affects expression of ~1400 nuclear genes (Lee et al. 2007; Galvez-Valdivieso and Mullineaux 2010).

1.1.3 Proteins as signaling molecules

Proteins functioning as signaling molecules have to translocate from the plastids through the cytosol to the nucleus. An example for this is the chloroplast envelope-bound homeodomain transcription factor (PTM, Figure 2). Activation of proteolytic cleavage of PTM is triggered by retrograde signals, leading to detachment of the N-terminus of the protein, which subsequently enters the nucleus where it activates the expression of *ABI4* (Sun et al. 2011). *ABI4* was found to function in regulation of nuclear gene expression via retrograde signaling (Koussevitzky et al. 2007).

1.1.4 Metabolites acting as signaling molecules

Metabolites involved in retrograde signaling are synthesized in the plastids and subsequently translocate to the cytosol and into other cellular compartments (Terry and Smith 2013). Recent studies focused on characterization of metabolites that affect nuclear gene expression including 3´phosphoadenosine 5´phospaht (PAP) and the isoprenoid precursor methylerythritol cyclodiphosphate (MEcPP) (Figure 2). The amount of the phosphonucleotide 3´phosphoadenosine 5´phospaht (PAP), which accumulates as response to drought and high light conditions, is regulated by the

SAL1 enzyme by dephosphorylation of PAP to AMP. SAL1 is located exclusively in chloroplasts and mitochondria, whereas PAP activates nuclear-encoded high light response genes (Estavillo et al. 2011). MEcPP is produced by the plastidial methylerythritol phosphate (MEP) pathway and activates the expression of selected stress response nuclear genes coding for plastid-localized proteins by alteration of nuclear architecture and functional dynamics (Xiao et al. 2012).

1.2 Next generation mapping

1.2.1 Forward genetic screening

Generally, a genetic screen is used to identify and select for individuals possessing a phenotype of interest in a mutagenized population and genes responsible for a particular phenotype are identified. Once a mutation is localized, secondary screens allow further dissection of the function of the identified mutation. Variations of these secondary screens include (i) enhancer screens, which aim at finding mutations that enhance the mutant phenotype and (ii) suppressor screens, which identify mutants that suppress (alleviate) the mutant phenotype (Page and Grossniklaus 2002). Such secondary screens are unbiased and therefore lead to new insights into interactions between the genes of interest. With the help of reporter genes, even hidden phenotypes are accessible for forward genetics. In these approaches, the promotor of a specially regulated gene is fused to a reporter gene like the firefly luciferase (LUC), β-glucuronidase (GUS) or green fluorescence protein (GFP). After mutagenesis and screening for altered expression of the reporter gene, genetically interesting loci can be selected and identified with further experiments (characterization and mapping of mutant).

1.2.2 Mapping mutants

By methods of classical genetics, a gene is located (mapped) to a chromosome position by crossbreeding with individuals that possess other traits, followed by performing statistics on the frequency of the inherited traits (Figure 3). Instead of phenotypic traits, today single nucleotide polymorphisms (SNPs) are markers most commonly used for mapping approaches, since they are very frequent between different varieties of organisms including the *Arabidopsis thaliana* accessions Col-0 and Landsberg *erecta* (L*er*) (Nordborg et al. 2005; Lu et al. 2012).

1.2.3 Positional cloning

In a first step of mapping the locus causing a specific phenotype, the positional cloning approach (rough mapping) is applied. With this method, a genetic interval is detected, which contains the mutation of interest, by excluding all other parts of the genome. Therefore, PCR-based molecular markers including simple sequence length polymorphisms (SSLPs) and cleaved amplified polymorphic sequences (CAPS) are most commonly applied. These markers are widely used due to (i) their ease of handling, (ii) their low costs, as they are PCR-based and (iii) the fact that they are co-dominant, i.e. they deliver information for both alleles providing the maximum information that can be obtained from a mapping population (Lukowitz et al. 2000).

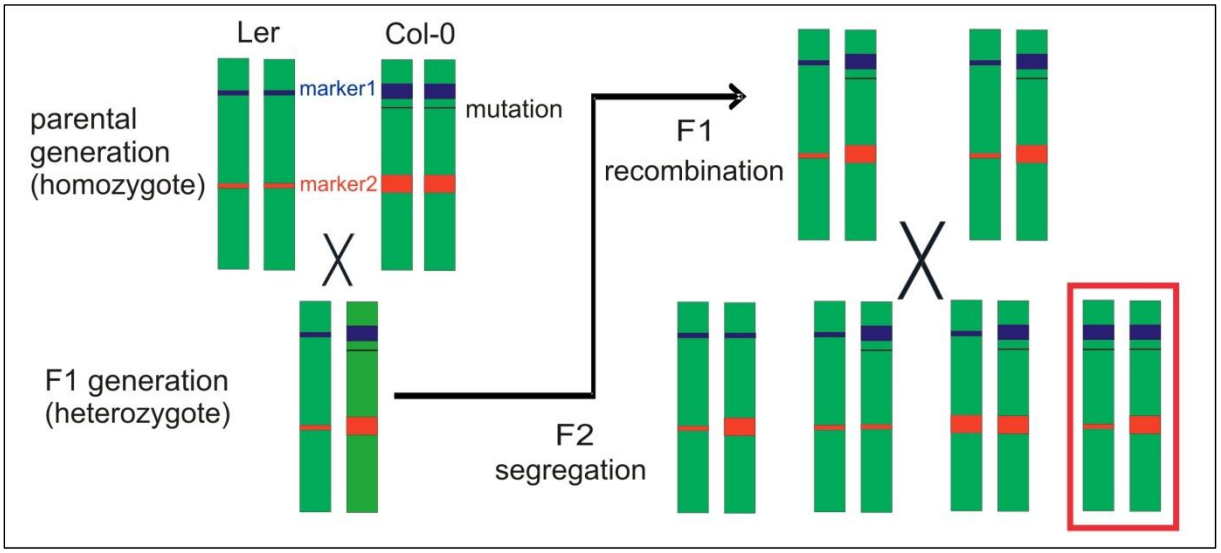

Figure 3: Generation of a mapping population in *Arabidopsis thaliana*. By crossing of the Col-0 accession with the L*er* accession, heterozygous plants are obtained in the F1 generation (depicted by the markers, blue and red). During meiosis in the F1 generation, recombination takes place. The analysis of the F2 generation (mapping population) with the help of markers leads to identification of the region of the mutated loci. A marker is linked to a mutation if no recombination event occurs between the position of the marker and the position of the mutation. In this case, the marker shows a homozygous pattern (red box) for the parental accession with the mutation in this chromosomal region.

The SSLP markers take advantage of the variability of short repetitive sequences, as the length of the repetition differs between the accessions, which are easily visualized on agarose gels (Bell and Ecker 1994). CAPS markers on the other hand use the polymorphic restriction sites for the mapping purpose: exclusively the PCR fragments of one accession contain a restriction site, which is not present in the PCR fragments of the other accession. After digestion of the PCR products, the different band pattern is analyzed on agarose gels as well (Konieczny and Ausubel 1993).

1.2.4 Mapping by next generation sequencing

One of the broad spectrums of applications of next generation sequencing (NGS) is its use to identify mutations. The great benefit of the next generation mapping approach is the simultaneously mapping and sequencing at a genome wide scale. Due to the low signal to noise ratio, which is based on the large number of unassociated polymorphisms that segregate with the causative mutation in mutagenized populations, further genetic analysis is required additional to the sequence information. Usually, the distribution and origin of polymorphisms detected by re-sequencing against a known genome sequence are used for the identification of the causative mutation (Austin et al. 2011; Blumenstiel et al. 2009; Irvine et al. 2009; Sarin et al. 2008; Schneeberger et al. 2009; Smith et al. 2008; Srivatsan et al. 2008; Zyrin et al. 2010). Latest methods replace the crossing of the mutant with a different accession (e.g. Col-0 x L*er*) by a backcrossing of the mutant with their parental (not mutagenized) line. This is performed to reduce the unlinked polymorphisms, and by using the segregation ratio of unlinked und causative (linked) polymorphisms, the causative mutation can be mapped (Lindner et al. 2012).

1.3 Aim of the thesis

The aim of this thesis was to identify novel components of translation-dependent retrograde signaling pathways. For this purpose, a genetic forward screen was established to identify new mutants that are supposed to participate in further understanding of the regulation and biogenesis of the plant organelles. For the luminescence screen, the *prors1* mutant was used, since due to its defective plastidial and mitochondrial translation machinery it is a good candidate for the research of translational-dependent retrograde signaling pathways. Furthermore, genetic and physiological characterization of found suppressor mutants was performed, including the measurement of chlorophyll fluorescence, the calculation of the starch content and the determination of the expression level of nuclear-encoded photosynthetic genes. The results of these experiments provide new insights into the effects caused by the mutations. Finally, the mutated genes of selected mutants were identified via positional cloning and analysis of next generation sequencing data.

2. Material and methods

2.1 Material

2.1.1 Chemicals and antibodies

Standard chemicals were purchased from Roth (Karlsruhe, Germany), Sigma-Aldrich (Steinheim, Germany), Duchefa (Haarlem, Netherlands), Applichem (Darmstadt, Germany) and Serva (Heidelberg, Germany). Radioactive-labelled dCTP was ordered from Hartmann Analytik (Braunschweig, Germany). Primary antibodies were obtained from Agrisera (Vännäs, Sweden) and the secondary anti-rabbit antibody from Sigma-Aldrich (Steinheim, Germany).

2.1.2 Plant material

All experiments were performed on *Arabidopsis thaliana* plants, ecotype Columbia-0 (Col-0) or Landsberg *erecta* (L*er*). Previous screening of the *Arabidopsis thaliana* GABI-KAT T-DNA insertion collection for plants showing alterations in the effective quantum yield of PSII (Φ_{II}) resulted in the identification of a set of mutants with defects in photosynthesis (Varotto et al. 2000a, 2000b; Rosso et al. 2003). In two of these mutants, the *photosynthesis altered mutant15* (*pam15*) and *pam18*, the same genetic locus was found to be affected. It was identified as the 5`-untranslated region of the nuclear gene *PROLYL-tRNA SYNTHETASE1* (*PRORS1*), the product of which acts in both plastids and mitochondria (Pesaresi et al. 2006). The *prors1-2* (*pam18*) mutant, which showed the more severe phenotype, was used for this work. The mutants found during the screening process (see 2.3.5) were named *rls* (*relaxed LHCB suppression*; Table 1). The wild type accessions Col-0 and L*er* of *Arabidopsis thaliana* were used as control and for crossing. The lines *LHCB3*$_{pro}$*:LUC prors1-2* and *LHCB1.2*$_{pro}$*:LUC prors1-2* were mutagenized for the screening and generation of the so-called parental lines for the *rls* mutants (see 2.2.1).

Table 1: List of mutants identified in the screen, including the respective parental line, i.e. the mutant prior to mutagenesis (see 2.2.1).

name	parental line
rls2(3)	*LHCB3*$_{pro}$*:LUC prors1-2*
rls134	
rls2(1.2)	*LHCB1.2*$_{pro}$*:LUC prors1-2*
rls304	
rls316	
rls336	
rls436	
rls463	
rls478	
rls502	
rls518	
rls608	
rls615	
rls666	
rls681	
rls716	
rls744	

2.1.3 Oligonucleotides

Oligonucleotides were ordered from Metabion (Martinsried, Germany) in standard desalted quality. They were used for positional cloning (Tables 2 - 6), for hybridisation probes (Table 7) and for real-time PCR (Table 8).

Table 2: Genetic markers, location and respective oligonucleotides used for positional cloning of chromosome 1.

name	AGI position (bp)	forward primer sequence (5'-3')	reverse primer sequence (5'-3')
F21M12	3212189-3212389	GGCTTTCTCGAAATCTGTCC	TTACTTTTTGCCTCTTGTCATTG
CIW12	9621357-9621484	AGGTTTTATTGCTTTTCACA	CTTTCAAAAGCACATCACA
CIW1	18363881-18364039	ACATTTTCTCAATCCTTACTC	GAGAGCTTCTTTATTTGTGAT
NGA280	20873698-20873802	GGCTCCATAAAAAGTGCACC	CTGATCTCACGGACAATAGTGC
NGA111	27353212-27353339	TGTTTTTTAGGACAAATGGCG	CTCCAGTTGGAAGCTAAAGGG

Table 3: Genetic markers, location and respective oligonucleotides used for positional cloning of chromosome 2.

name	AGI position (bp)	forward primer sequence (5'-3')	reverse primer sequence (5'-3')
CIW2	1194606-1194710	CCCAAAAGTTAATTATACTGT	CCGGGTTAATAATAAATGT
CIW3	6402846-6403081	GAAACTCAATGAAATCCACTT	TGAACTTGTTGTGAGCTTTGA
CZSOD2	12014513-12016440	GAATCTCAATATGTGTCAAC	GCATTACTCCGGTGTCGTC
NGA168	16291841-16291991	GAGGACATGTATAGGAGCCTCG	TCGTCTACTGCACTGCCG

Table 4: Genetic markers, location and respective oligonucleotides used for positional cloning of chromosome 3.

name	AGI position (bp)	forward primer sequence (5'-3')	reverse primer sequence (5'-3')
NGA162	4608277-4608383	CTCTGTCACTCTTTTCCTCTGG	CATGCAATTTGCATCTGAGG
CIW11	9774308-9774486	CCCCGAGTTGAGGTATT	GAAGAAATTCCTAAAGCATTC
CIW4	18890837-18891025	GTTCATTAAACTTGCGTGTGT	TACGGTCAGATTGAGTGATTC
NGA6	23031050-23031192	ATGGAGAAGCTTACACTGATC	TGGATTTCTTCCTCTCTTCAC

Table 5: Genetic markers, location and respective oligonucleotides used for positional cloning of chromosome 4.

name	AGI position (bp)	forward primer sequence (5'-3')	reverse primer sequence (5'-3')
CIW5	737954-738117	GGTTAAAAATTAGGGTTACGA	AGATTTACGTGGAAGCAAT
CIW6	7892624-7892785	CTCGTAGTGCACTTTCATCA	CACATGGTTAGGGAAACAATA
CIW7	11524350-11524480	AATTTGGAGATTAGCTGGAAT	CCATGTTGATGATAAGCACAA
NGA1107	18096137-18096288	CGACGAATCGACAGAATTAGG	GCGAAAAAACAAAAAAATCCA

Table 6: Genetic markers, location and respective oligonucleotides used for positional cloning of chromosome 5.

name	AGI position (bp)	forward primer sequence (5'-3')	reverse primer sequence (5'-3')
CTR1.2	979764-979922	CCACTTGTTTCTCTCTCTAG	TATCAACAGAAACGCACCGAG
MED24D	1002257-1002562	GGGGGACCTTTTTCTTGATTACC	GCAGAGTCTCACTCTCATCTCC
CIW13	1006717-1006840	CGAACTTGAGACCTCTTGA	GCTTACCTGGAGACAGTCA
MUK11D	1409471-1409873	GGAGAAGGCTTTGTGTCTGTATC	CTTTCTCTTCCACTGAATCTCCTC
NGA158	1698613-1698720	ACCTGAACCATCCTCCGTC	TCATTTTGGCCGACTTAGC
NGA225	1507103-1507222	TCTCCCCACTAGTTTTGTGTCC	GAAATCCAAATCCCAGAGAGG
CIW18	1531045-1531179	AACACAACATGGTTTCAGT	GCCGTTTGTCTCTTCAC
CIW16	1566438-1566576	TGGTTAGATTTGCTGTT	ATTCTGCATTATTAGTTGTC
CIW14	2174597-2174775	CATGATCCATCGTCTTAGT	AATATCGCTTGTTTTTGC
MOJB	2190102-2190275	TGAAAGATTTTAGGAGGACAA	GTAGGAGAAGGGGACAAGTT
EMC	2666002-2666126	AACAGATCGGAAAATCGTCG	AATGACGACGAGACGCTCTT
NGA249	2770216-2770340	GGATCCCTAACTGTAAAATCCC	TACCGTCAATTTCATCGCC
CA72	4254759-4255008	CCCAGTCTAACCACGACCAC	AATCCCAGTAACCAAACACACA
NGA151	4669929-4670078	CAGTCTAAAAGCGAGAGTATGATG	GTTTTGGGAAGTTTTGCTGG
PAT1.2	5957706-5958411	CATGCTTCATCATTGCCC	AGCTGAAGCTCTGCCACC
CIW8	7485585-7485684	TAGTGAAACCTTTCTCAGAT	TTATGTTTTCTTCAATCAGTT
CDPK9	7952512-7952617	TCAATCATTGTCCAAAACTTGG	GAAACTGACTTGGAGAAGGCA
NGA139	8428133-8428314	GGTTTCGTTTCACTATCCAGG	AGAGCTACCAGATCCGATGG
NGA76	10418610-10418840	AGGCATGGGAGACATTTACG	GGAGAAAATGTCACTCTCCACC

PHYC.3	14007897-14008106	AAACTCGAGAGTTTTGTCTAGATC	CTCAGAGAATTCCCAGAAAAATCT
SO191	15004685-15004832	CTCCACCAATCATGCAAATG	TGATGTTGATGGAGATGGTCA
CIW9	17044001-17044166	CAGACGTATCAAATGACAAATG	GACTACTGCTCAAACTATTCGG
M558A.1	23317513-23317972	TTTCTCGGTCTCCGATTAAC	AAAGATAACCAAAGTCAGAGAT
CIW10	24530871-24531007	CCACATTTTCCTTCTTTCATA	CAACATTTAGCAAATCAACTT
ATTED.2	24735924-24736585	CGTAGACAAGGTACTGTCAACC	GATAATCTCGTCTCCAAGTGTCC

Table 7: Oligonucleotides used to generate specific cDNA probes for Northern blot analysis (see 2.2.4).

name of gene	**locus identifier**	**forward primer sequence** (5'-3')	**reverse primer sequence** (5'-3')
LHCB1.2	*AT1G29910*	GACTTTCAGCTGATCCCGAG	CGGTCCCTTACCAGTGACAA
LHCB3	*AT5G54270*	GGAGATGGGCAATGTTGGGA	TAGTTGCGAAAGCCCACGCA
PSAK	*AT1G30380*	ATGGTCTTCCAGCCACCAAA	CGTTCAGGTGCATGAGAATA
PSBO	*AT3G50820*	AGACGGAAGCGTGAAGTTCA	CAATCTGACCGTACCAAACC

Table 8: Oligonucleotides used for real-time PCR experiments (see 2.2.4).

name of gene	**locus identifier**	**forward primer sequence** (5'-3')	**reverse primer sequence** (5'-3')
PRORS1-2	*AT5G52520*	GTATCTAGTAACAGTGTCGT	ATCCACAATGTTACTGTCTC
UBIQUITIN	*AT4G36800*	GGAAAAAGGTCTGACCGACA	CTGTTCACGGAACCCAATTC

2.2 Methods

2.2.1 Plant methods

The starting material for the genetic forward screen, a promoter-luciferase construct (Figure 4), was generated prior to this thesis in Prof. Leister´s lab and transformed into Col-0 *Arabidopsis thaliana* plants as described by Clough and Bent 1998.

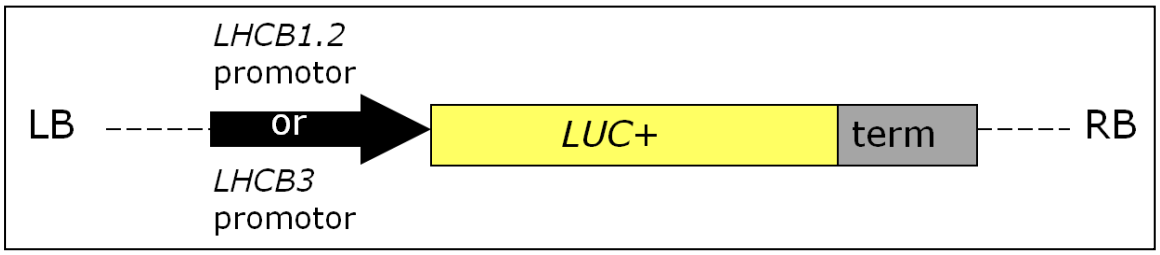

Figure 4: Generation of the promotor-luciferase construct. For this purpose, the *LHCB1.2* or *LHCB3* promotor was cloned in front of the *luciferase* gene and fused to a termination sequence. LB, left border; RB, right border; *LUC*+, luciferase gene; term, Tnos termination sequence; *LHCB1.2* or *LHCB3* promotor, sequence of the promotor of the *LHCB1.2* or *LHCB3* gene, respectively.

These $_{pro}$*:LUC* Col-0 plants were crossed with the *prors1-2* mutant to generate the luciferase-reporter construct in the *prors1-2* mutant genetic background. The plants of the third generation of back-crossing (that are named $_{pro}$*:LUC prors1-2* in this work) were used as the starting plant material.

2.2.1.1 Plant growth and harvesting conditions

Arabidopsis thaliana wild type (ecotypes Col-0 and L*er*) and mutant seeds were sown in Petri dishes on water soaked filter paper and incubated for three days at 4 °C in the dark to break dormancy and to synchronise germination. Plants were grown on soil under greenhouse controlled conditions (70-90 µE m^{-2} s^{-1}, 16 h/8 h light/dark photoperiod) or under controlled environmental chamber (phytotrone) conditions at 22 °C/18 °C with a 16 h/8 h light/dark photoperiod. For *in vitro* growth conditions, after sterilization with 1 ml 70 % (v/v) ethanol for 15 min and three times for 1 min in 1 ml 95 % (v/v) ethanol, the seeds were washed three times with 1 ml ddH_2O. After this treatment, the seedlings were grown on Murashige and Skoog medium (MS medium; Murashige and Skoog, 1962) containing 1 % (w/v) sucrose and 1 % (w/v) agar. All experiments were performed with mutant and wild type plants at the eight leaf rosette stage. Leaf material was collected 8 h after the start of the light period.

2.2.1.2 Ethyl methanesulfonate (EMS) mutagenesis

Seeds (500 mg each) of the lines *LHCB1.2*$_{pro}$*:LUC prors1-2 and LHCB3*$_{pro}$*:LUC prors1-2* were mutagenized by incubation with 35 ml 0.2 % EMS solution (Sigma-Aldrich, Germany) for 15 h. After 10 times washing with water, the seeds were dried. The *LHCB1.2*$_{pro}$*:LUC prors1-2* line was mutagenized a second time, because the germination rate of the mutagenized seeds dropped dramatically after six months.

2.2.1.3 Crossing of *Arabidopsis thaliana*

Anthers in pollen recipient plants were emasculated from closed flowers by dissection. Stigmas in emasculated flowers were then pollinated manually (Weigel et al. 2006).

2.2.1.4 Complementation analysis via crossing of *rls* mutants

The *rls* mutants were grouped into 8 classes (see chapter 3.2.8), dependent on the observed rescue phenotype compared to their respective parental line ($_{pro}$*:LUC prors1-2*) according to the following criteria: (i) the expression level of nuclear-encoded photosynthetic genes, (ii) the maximum quantum yield of PSII (F_v/F_m) and (iii) the growth behavior (leaf size and color at day 21). The mutants from each class were crossed with each other and the F1 and F2 generation was monitored for the phenotype.

2.2.1.5 Chlorophyll fluorescence measurements

The chlorophyll fluorescence measurements were performed with the Dual-PAM 100 (Walz, Germany) as described before (Pesaresi et al. 2006). The fluorescence of dark adapted (15 min) leaves was measured (F_0), before saturation pulses (800 ms) of white light (6000 µmol m^{-2} s^{-1}) were used to determine the maximum fluorescence (F_m) and the ratio $(F_m-F_0)/F_m = F_v/F_m$. After 12 min of illumination with actinic light (80 µmol m^{-2} s^{-1}), which served to drive electron transport between PSII and PSI, the effective quantum yield of PSII (Φ_{II}) and the NPQ (nonphotochemical fluorescence quenching) was measured. Mean values and standard deviations were calculated from at least six plants of each genotype.

2.2.2 Molecular biology methods

2.2.2.1 Nuclear acids extractions

2.2.2.1.1 Genomic DNA extraction

For extraction of genomic DNA from *Arabidopsis thaliana* leaves, 100 mg plant material was homogenized with a plastic pistil in 400 µl extraction buffer containing 200 mM Tris-HCl (pH 7.5), 25 mM NaCl, 25 mM EDTA and 0.5 % (w/v) SDS. Incubation at room temperature for 10 min was followed by centrifugation for 10 min at 10000 g. Subsequently, 300 µl of isopropyl alcohol were added to the supernatant

to precipitate DNA. After 10 min of incubation and 10 min of centrifugation at 10000 g, the pellet was washed with 70 % (v/v) ethanol. Finally, the DNA was resuspended in distilled water.

2.2.2.1.2 Nuclear DNA extraction for next generation sequencing

DNA used for the next generation sequencing approach was extracted according to Carrier et al. 2011: For the nuclei extraction, five to six gram of fresh weight of plant material was grinded in liquid nitrogen to a fine powder and transferred to a 50 ml tube before 45 ml of a sucrose-based extraction buffer (10 % NEB [100 mM Tris (pH 8.0), 1 M KCl, 100 mM EDTA]), 550 mM sucrose, 4 mM spermidine trihydrochloride, 1 mM spermidine tetrahydrochloride, 0.13 % (p/v) carbamic acid, 0.25 % (w/v) PVP40 with 2 % (v/v) β-mercaptoethanol) was added. After incubation on ice for 12 min and mixing regularly, 15 ml of the sample was filtered with a cell strainer (d: 40 µm) into a new 50 ml tube (3 tubes in total) and 1.5 ml of Triton X-100 was added before the next 12 min of incubation on ice. After centrifugation at 600 g for 9 min at 4 °C, the supernatant was discarded and 20 ml of a sucrose-based extraction buffer was used to resuspend the pellet. The obtained 60 ml (3 x 20 ml) were filtered into two new 50 ml tubes using the cell strainer, followed by a centrifugation step at 600 g for 9 min at 4 °C. These last three steps (filtering, centrifugation and resuspension of the pellet) were repeated twice until the pellet was resuspended in 2 ml of sucrose-based extraction buffer and kept at 4 °C over night.

2.2.2.1.3 Nuclear DNA purification

The extracted nuclear DNA was purified according to Carrier et al. 2011: For this purpose, 4 ml of nucleus extraction buffer NEB (100 mM Tris (pH 8.0), 1 M KCl, 100 mM EDTA) was added to the suspension of purified nuclei followed by incubation at 55 °C for 3 h with mixing. Four ml AcK (11.5 % acetic acid, 5 M potassium acetate) was added and mingled for 10 min. After centrifugation at 3000 g for 10 min at 4 °C, the supernatant was transferred into a 50 ml tube, before 15 ml of DNA Binding Buffer DBB (260 mM guanidium chloride in ethanol 96 % (w/v)) and 250 µl of silica matrix (5 g of silicon dioxide (Sigma, S5631), mixed with 50 ml of ultrapure water and adjusted to a pH of 2.0) were added. In the next step, the tube was inverted for 10 min and centrifuged at 1500 g for 2 min at 4 °C. The supernatant was discarded and 5 ml of DNA washing solution (22.5 mM Tris pH 8.0, 160 mM AcK, 1 mM EDTA, 96

% (v/v) ethanol 1.7 : 1) added, incubated for 2 min for resuspending the pellet, followed by centrifugation at 1500 g for 2 min at 4 °C. This step was repeated once. The supernatant was discarded and the tube placed, without its cap, at 37 °C for 10 min, subsequently 600 µl of water were added and incubated at 37 °C for 10 min. The sample was transferred into a 2 ml microtube and centrifuged at 14000 g for 3 min at room temperature. Afterwards, the supernatant was transferred into a new microtube and 60 µl of 3 M NaAc and 1 ml 96 % ethanol (v/v) were added and mixed for 2 min before placing the tube at -20 °C for 5-10 min. Upon centrifugation at 14000 g for 5 min, the DNA was washed with 75 % (v/v) ethanol before the pellet was dissolved in 120 µl ultra-pure water resulting in DNA concentrations of 500 ng to 1 mg. Preparation and performance of the SOLiD^{tm} sequencing of the purified DNAs from the F2 generation of the crosses from *rls2(3)* and *rls478* with L*er* was performed at the sequencing service facility of the University of Düsseldorf.

2.2.2.1.4 RNA extraction

Leaf material of *Arabidopsis thaliana* equivalent to 2.5 ml of a 15 ml tube was grinded in liquid nitrogen with mortar and pestle. Subsequently, 15 ml of trizol reagent was put onto the material and incubated for 5 min at room temperature before centrifugation at 3320 g at 4 °C for 10 min and addition of 3 ml chloroform to the supernatant. After vigorous mixing for 10 sec and incubation for 5 min at room temperature, a centrifugation step at 3320 g at 4 °C for 15 min was performed. To the aqueous phase, ½ of its volume isopropanol and ½ of its volume 0.8 M sodium citrate/1.2 M NaCl was added and mixed gently by inversion. The incubation for 1 h at 4 °C was followed by centrifugation at 3320 g at 4 °C for 40 min. The pellet was washed with 75 % (v/v) ethanol, before resuspending in 100 µl DEPC-water (Roth, Germany). For the extraction of RNA used for microarray and real-time PCR analysis, the RNeasy Kit from QIAgen (Hilden, Germany) or “Maxwell” (Promega, USA), an automated RNA extraction system, was used according to the manufacturer´s instructions.

2.2.2.2 Screening of plants for T-DNA insertion

To screen the plants for the T-DNA insertion in the *PRORS1* gene, the following primers were used: T-DNA PRORSII S: ATATTGACCATCATACTCATTGC and PRORSI screen AS: TCCGGAAAGAGGTCTGTTCC. To analyse the presence of the

wild type allele, PRORSI screen S: CCAAGCATGAGTTTCTCGAG and PRORSI screen AS primers were applied for genotyping. For the performed PCR (polymerase chain reaction), a standard programme was used with an annealing temperature of 55 °C and a duration of 35 cycles (Saiki et al. 1988).

2.2.2.3 Positional cloning (rough mapping)

To generate a mapping population, the *rls2(3)*, *rls2(1.2), rls478* and *rls518* mutants were crossed with L*er* wild type plants. From the F2 generation, only plants were selected which displayed the same phenotype (growth, shape and leave colour) as their parental *rls* mutant, but still possessed the T-DNA insertion in both *PRORS1* alleles. From these plants, leaves of the same size were harvested and pooled before extracting DNA (see chapter 2.2.1.2.). As template for the PCR, DNA from the *rls* mutant (Col-0 genetic background), from L*er,* from the F1 generation (as heterozygous control) and a pool of all plants form the F2 generation were used. Primer pairs used as markers for positional cloning are listed in Tables 2 to 6.

2.2.2.4 Expression analysis via Northern blot and real-time PCR

Northern blotting and hybridisation of probes were performed using standard procedures (Sambrook and Russel 2001). Three to 8 µg of total RNA were denatured for 7 min at 90 °C in loading dye (40 % (w/v) MOPS, 3.1% (v/v) formamide, 20 % (v/v) glycerol, 1.2 M formaldehyde; 0.05 M EDTA) and separated on a denaturing 1.2 % (w/v) agarose gel containing 2 % (v/v) formaldehyde. Afterwards, the RNA was blotted onto a nylon membrane (Roche, Germany) and hybridised for 16 h at 65 °C (hybridisation buffer: 1.8 % (w/v) NaH_2PO_4 x H_2O, 6.6 % (w/v) Na_2HPO_4 x 2 H_2O, 7 % (w/v) SDS, 1 % (w/v) BSA, 1 mM EDTA) with cDNA probes labelled with ^{32}P-dCTP using random hexamer primer and Klenow Fragment (New England Biolabs) reaction. Primer pairs used to generate specific cDNA probes are listed in Table 7. The hybridisation was followed by three times washing for 20 min at 65 °C (washing buffer: 1 % (w/v) SDS, 0.4 % (w/v) 0.5 M EDTA, 8 % (w/v) Na-P [74.4 % (w/v) 0.5 M Na_2HPO_4 x 2 H_2O and 25.6 % (w/v) 0.5 M NaH_2PO_4 x H_2O]). The filters were exposed to a phosphorimager screen and analysed by a Typhoon Variable Mode Imager (GE Healthcare) using ImageQuant 5.2 (GE Healthcare).

For the real-time PCR experiments, cDNA was synthesized from 0.5 µg RNA using the iScript cDNA Synthesis Kit (Bio-Rad, USA) according to the manufacturer's

instructions. For quantification and to determine the quality of the synthesized cDNA, a PCR was performed using primers of the housekeeping gene *UBIQUITIN* (see Table 8). For real-time PCR analysis, 6 µl of 1:20 diluted cDNA and specific primers (see Table 8) were added to iQ™ SYBR® Green Supermix (Bio-Rad, Munich). The thermal cycling started with an initial step at 95 °C for 3 min, followed by 40 cycles of 10 s at 95 °C, 30 s at 55 °C and 10 s at 72 °C, after which a melting curve analysis was carried out. Reactions were performed in triplicate. Real-time PCR was monitored by using the iQ5™ Multi Color Real-Time PCR Detection System (Bio-Rad, Germany). Relative transcript abundances were normalized with respect to the level of the constitutively expressed mRNA of an ubiquitin-protein ligase-like protein (*at4g36800*). The data were analyzed by using LinRegPCR (Ramakers et al. 2003) and according to Pfaffl (2001).

2.2.3 Biochemical methods

2.2.3.1 SDS-PAGE

SDS-PAGE (polyacrylamide gel electrophoresis) was performed according to Laemmli, 1970. Gels were stained with Coomassie Brilliant Blue R250 according to Sambrook, 1989. For the separation of the proteins, a 12 % polyacrylamide SDS gel (for 10 ml: 4 ml 30% acrylamide 37.5:1, 2.5 ml 1.5 M Tris-HCl pH 8.8, 3.5 ml bidest water, 100 µl 10 % APS, 10 µl Temed), with SDS running buffer (25 mM Tris-HCl, 200 mM glycine, 0.1% (w/v) SDS) was used.

2.2.3.2 Preparation of leaf protein extract

Shock frozen (liquid nitrogen) leaves were homogenized in 2 x SDS buffer (62.5 mM Tris-HCl (pH 6.8), 20 % (w/v) glycerine, 4 % (w/v) SDS, 100 mM DTT, 0.05 % (w/v) bromophenol blue). The homogenate was heated at 70 °C for 10 min and centrifuged 10 min at 16100 g at room temperature to remove cellular debris.

2.2.3.3 Immunoblot detection assay

After SDS-PAGE electrophoresis, proteins were transferred onto a PVDF (polyvinylidene fluoride) membrane (Millipore, USA) using a semi-dry blotting apparatus (Biorad, Germany) according to Towbin et al. 1979. The transfer was performed by applying a current corresponding to 0.8 mA * cm^{-2} in transfer buffer (96

mM glycine, 10 mM Tris, 10% (v/v) methanol) for 1 h. After transfer to the membrane, proteins were detected by staining in Ponceau red (3 % (w/v) Ponceau S in 1 % (v/v) acetic acid) for 3-5 min and destained by washing with methanol. Subsequently, the membranes were blocked with TBS buffer (1 M Tris (pH 7.5), 1.5 M NaCl) containing 3 % (w/v) milk powder for 1 h or overnight at 4 °C. After washing for 3 times 10 min with TBS-T (TBS buffer supplemented with 0.1 % (w/v) Tween-20), the membranes were incubated with specific primary and appropriate secondary antibodies as indicated, according to standard protocols (Sambrook et al. 1989). Detection was performed with Pierce ECL Western Blotting Substrate (Thermo Scientific, USA) and Fusion FX7 chemiluminescence and fluorescence imager (Peqlab, Germany).

2.2.3.4 Determination of chlorophyll content

The determination of chlorophyll content was carried out as described by Arnon 1949 and Lichtenthaler 1987. In brief, shock frozen plant material was mixed with 1 ml 80 % aceton (v/v). After incubation for 30 min on ice, the probes were centrifuged at 10000 g for 10 min and the supernatant was transferred to a new microtube. Prior to the measurement at 750 nm, 647 nm and 663 nm, the probes were diluted 1:10 with 80 % aceton (v/v).

2.2.3.5 Luminescence screening and detection assay

For luminescence screening of the plants from the M2 and the M3 generation, one leaf per plant was cut off, brushed with luciferin (Promega, USA) and incubated for 10 min in the dark. For the M2 generation from the first mutagenesis, the leaves were scanned with the Typhoon Variable Mode Imager (GE Healthcare) using ImageQuant 5.2 (GE Healthcare). For the M3 generation of the first and for both generations of the second EMS mutagenesis, the signals were detected by Fusion FX7 chemiluminescence and fluorescence imager (Peqlab, Germany). For quantification of the firefly luciferase, the Luciferase Assay Kit (Promega, USA) was used according to the manufacturer´s instructions.

The firefly luciferase generates light from luciferin in a multistep process. First, D-luciferin is adenylated by MgATP to form luciferyl adenylate and pyrophosphate (1.). After activation by ATP, luciferyl adenylate is oxidized by molecular oxygen to generate a dioxetanone ring. A decarboxylation reaction leads to an excited state of oxyluciferin (2.).

1. luciferin + ATP → luciferyl adenylate + PP_i
2. luciferyl adenylate + O_2 → oxyluciferin + AMP + light

The reaction finally emits light as oxyluciferin returns to the ground state (Shimomura et al. 1977), which can be detected as described.

2.2.3.6 Determination of starch content

A pool of leaves from 10 plants per *rls* mutant (see Table 1) and Col-0 plants as a control were harvested on day 28 after germination at 8 am in darkness and 10 h hours later after 9 hours of light exposure and frozen directly in liquid nitrogen. The determination of starch concentration was carried out with modifications according to Thormälen et al. 2012. For this purpose, 100 mg of pulverized leaf material was extracted three times with 250 µl 80 % ethanol (v/v): upon addition of the first 250 µl of ethanol, the samples were incubated for 30 min at 70 °C. After centrifugation at 10000 g for 5 min, the supernatant was removed and the next extraction volume was added to the pellets for repeating the procedure twice. Subsequently, the pellets were dried for 30 min at 45 °C in a vacuum concentrator (Eppendorf, Germany). To hydrolyze the starch, 400 µl 0.1 M NaOH was added and incubated at 95 °C with 1400 rpm shaking for 1 h. To achieve a neutral pH of 7.0, 75 µl of HCl/Acetat-buffer was mixed with the sample. In the next step, 110 µl aliquots supplemented with 250 µl of the starch degradation mix (AGS-Buffer from Enzytec Starch Kit, Enzytec, Germany) were incubated for 1 h at 55 °C. For the starch measurement, 200 µl glucose determination mix (Solution#1 from Enzytec Starch Kit) was added to 50 µl of this solution and the samples (three technical replicates) were transferred to a 96 well plate, and the stabilized OD_{340} after 10 min (= A_1-value) was determined with the anthos reader HT-3 (Anthos Mikrosysteme Gmbh, Germany). Finally, 10 µl of hexokinase/glucose-9-phosphate dehydrogenase 200 U / 100 U in ammonium sulphate (Solution#2 from Enzytec Starch Kit) was added, and upon stabilization of the OD_{340} (after approximately 1 h), the obtained value was measured once more (A_2- value). For the calculation of the starch concentration, the following equation was used:

$$\Delta A / (\varepsilon * d) * (V_1 / V_2) * (V_3 / V_4) / DW*1000 = \mu mol\ C6/\ g\ DW$$

$\Delta A = (A_2\text{-}A_1)_{sample} – (A_2\text{-}A_1)_{blank}$. ; ε =6,22; d =2,85; DW = dry weight

V_1 (AGS Buffer + neutralized aliquot [µl]) = 360; V_2 (volume for C6-measurement [µl]) = 50

V_3 (pellet volume [µl]) = 475; V_4 (volume for hydrolysis [µl]) = 110

2.2.4 Bioinformatical methods

For evaluation of the real-time PCR, for sequencing and reading frame analyses, as well as for measurement of plant growth and primer design, several software tools were applied that are listed in Table 9.

Table 9: List of references for software tools used in this work.

plant growth:	Visistore: Leister et al. 1999; Plant Physiology Biochem., 37:671-678
primer design:	PerlPrimer v1.1.19: Marshall 2004; Bioinformatics 20:2471-2472.
real-time PCR:	LinReg PCR: Ramakers et al. 2003, Neuroscience Letters 339; 62-66; Pfaffl 2001, Nucleic Acids Res 29: e45
sequencing:	Peak Scanner™ Software Version 1.0 Applied Biosystems 2006; CLC genomics: Workbench (http://www.clcbio.com)
reading frame analysis:	GeneRunner version 3.01 (http://www.generunner.net/)

2.2.4.1 Analysis of next generation sequencing (NGS) data

2.2.4.1.1 Analysis of sequencing data and re-sequencing

The library preparation and the SOLiD™ sequencing (Life Technologies, USA) of the F2 generation from L*er* crosses with *rls2(3)* and *rls478* DNA samples (see 2.2.1.2 and 2.2.1.3) were performed at the sequencing service facility at the Universität Düsseldorf. For the analysis, the files were imported into the CLC Genomics Workbench software (http://www.clcbio.com/products/clc-genomics-workbench/). For both datasets, a quality control of the single reads was performed before the reads were mapped to the reference genome (Tair9 annotation of *Arabidopsis thaliana* ftp://ftp.arabidopsis.org/home/tair/Sequences/whole_chromosomes/).

The following re-sequencing options were chosen to link the reads to the chromosomes: mismatch cost = 2; insertion cost = 3; deletion cost = 3; length fraction = 0.8; similarity fraction = 0.5. As this data was generated by SOLiD™ sequencing, the color-space alignment was used and the color error cost was set to 3. The non-specific matches were ignored and the references not masked. For the SNP calling, the probabilistic variant detection plug-in beta software from CLC bio (Aarhus, Denmark) was used. As input, the read mapping files from the re-sequencing approach were applied, and following parameters were set: minimum coverage = 4; maximal expected variations = 2; variant probability = 90. The non-specific matches were ignored.

2.2.4.1.2 Selection and identification of the rescue locus

The lists of single nucleotide polymorphisms (SNP) for each chromosome were exported to Excel (Microsoft Office 2007), and the SNPs which were derived from the crossing with L*er* were sorted out. For this purpose, the SNP collection of L*er* from Lu et al. 2012 (http://www.personal.psu.edu/hxm16/suppdatafile.zip) was used. In the next step, the SNPs originating from the EMS mutagenesis had to be separated from the SNPs, which were derived from other sources such as sequencing errors. Hence, only SNPs including changes from guanine (G) to adenine (A) or cytosine (C) to thymine (T) remained in the analysis, which constituted more than 98 % of EMS-induced SNPs (Greene et al. 2003). The last filtering step was the selection of SNPs, which possessed coverage of 10 or higher and of which the frequency was above 90. Finally, the localization of the SNPs was determined with regard to their appearance in a locus of interest by the TAIR SeqViewer (http://www.arabidopsis.org/servlets/sv). Of the SNPs identified to be located in an exon, the cause of the nucleotide exchange was analyzed, i.e. an amino acid change or an alteration to a stop codon, with the help of the GeneRunner 3.01 software (http://www.generunner.net/).

3. Results

Previous studies revealed that nuclear-encoded photosynthetic genes are down-regulated in an *Arabidopsis thaliana* knock-down mutant (*prors1-2)* of the *PRORS1* gene, which encodes for the chloroplast-localized prolyl-tRNA synthetase (Pesaresi et al. 2006). Hence, this mutant is a good candidate for use in a genetic forward screen, aiming to identify new mutants suitable for the dissection of translational-dependent retrograde signaling pathways. This project was split into three parts: the first part comprises the identification of *relaxed LHCB suppression* (*rls*) mutants by using a genetic forward luminescence screen. The second part includes the physiological characterization of these *rls* mutants by analysis of the growth phenotype, measurement of chlorophyll fluorescence, determination of chlorophyll *a* and *b* content, calculation of starch (glucose) amount, determination of the expression level of nuclear-encoded photosynthetic genes and the detection of corresponding protein levels. In the third part, the identification and localization of the underlying mutation via positional cloning (rough mapping) and analysis of next generation sequencing data (next generation mapping) from selected *rls* mutants was performed.

3.1. Genetic forward screen to identify *relaxed LHCB suppression* (*rls*) mutants

With the genetic forward screen, new mutants generated by EMS mutagenesis can be identified which have to be characterized later on. In this work, analysis of *LHCB* expression monitored by luciferase and observation of the phenotype of the mutagenized plants were chosen as markers. For this purpose, a promoter-luciferase construct was transferred into a Col-0 *Arabidopsis thaliana* plant ($_{pro}$*:LUC* Col-0). *LHCB1.2* and *LHCB3* were chosen as promotors, which were cloned upstream of the luciferase gene (Figure 4, methods chapter 2.1). These promotors were selected, as the *LHCB1.2* and *LHCB3* transcripts were found to be down-regulated in the *prors1-2* mutant compared to Col-0 (Pesaresi et al. 2006), however the expression remained strong enough to ensure signal detection in the luminescence screen. The $_{pro}$*:LUC* Col-0 plants were crossed with *prors1-2* and the third generation was mutagenized with EMS. The second generation of the mutagenized plants (M2) was screened for a rescue of the phenotype (leaf size and colour) and a rescue of the *LHCB1.2* or

LHCB3 expression using the luciferase marker. A schematical overview of the set-up of the genetic forward screen is depicted in Figure 5.

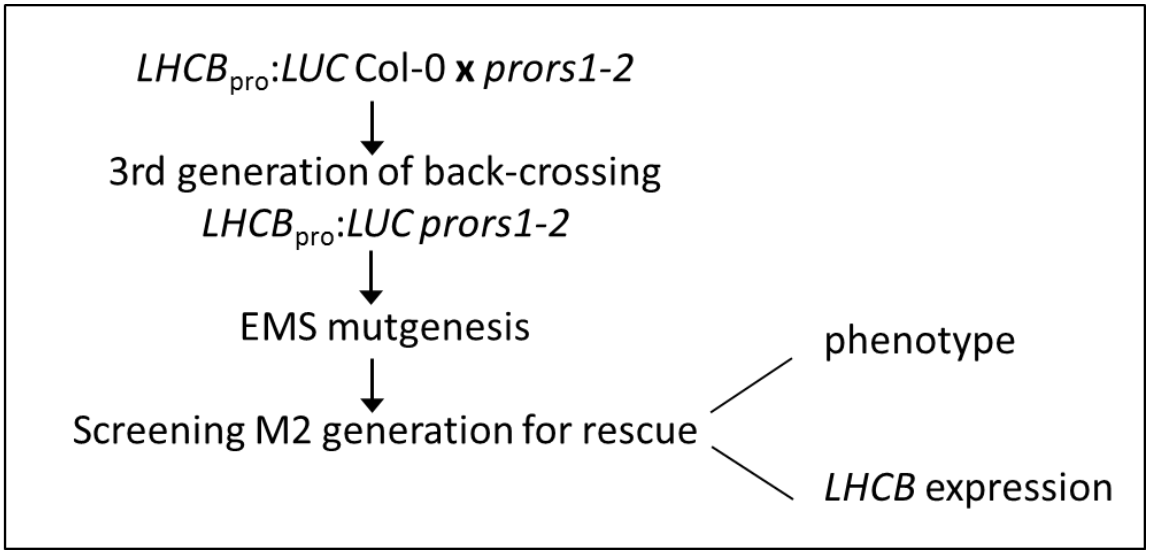

Figure 5: Schematical overview of the genetic forward screen. A promotor-luciferase construct was transferred into a Col-0 plant (*LHCB$_{pro}$:LUC Col-0*) and crossed with the *prors1-2* mutant. The seeds of the third generation of back-crossing with *prors1-2* (*LHCB$_{pro}$:LUC prors1-2*) were mutagenized with EMS. After selfing of the M1 generation, the M2 generation was screened for rescue of the luciferase signal, which was interpreted as a rescue of the *LHCB* expression, or rescue of the phenotype.

3.1.2 Mutants identified by the genetic forward screen

Plants which showed a rescue in the phenotype, i.e. dark green leaves comparable to the wild type and bigger rosette leaves with regard to the parental plants were propagated to the next generation (M3). Additionally, all plants (one rosette leaf from each plant) were screened for detection of the luminescence signal (see chapter 2.2.3.5 in methods; Figure 6). Plants showing a clear luminescence signal in this screen were propagated as well.

At the beginning of this thesis, detection of the luminescence signals could only be performed with the Typhoon Variable Mode Imager (GE Healthcare), which changed with the acquisition of the Fusion FX7 chemiluminescence and fluorescence imager (Peqlab). Both detection methods depicted clear differences in sensitivity and speed (Figure 6), since the sensitivity of the Fusion FX7 was found to be much higher concomitantly with a faster screening process, hence a second screen with the *LHCB1.2$_{pro}$:LUC prors1-2* line was performed.

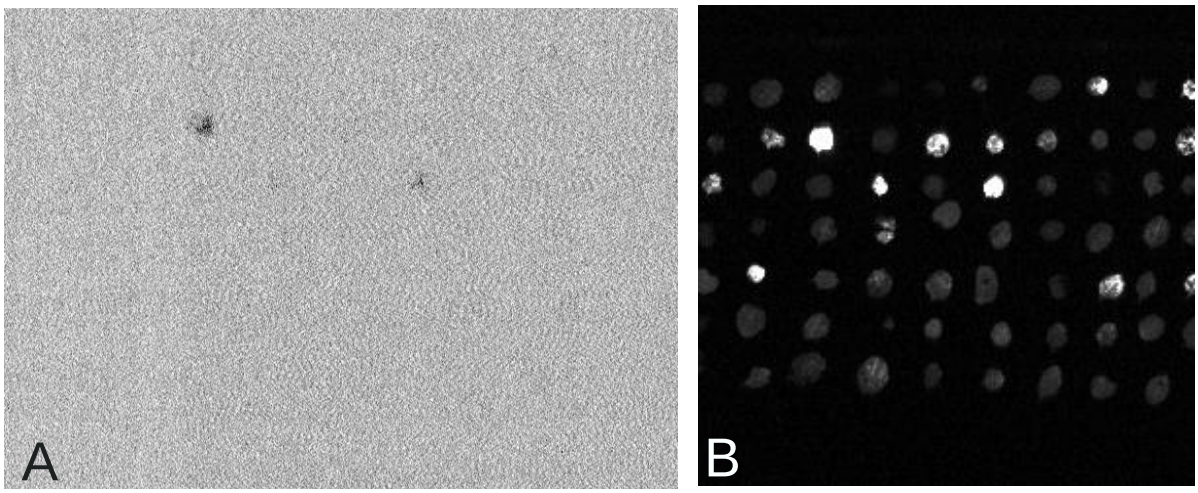

Figure 6: Luminescence screen of the M2 and M3 generation of mutagenized *LHCB*$_{pro}$*:LUC prors1-2* plants. One leaf per plant (25 days after germination) was brushed with luciferin and incubated for 10 min in the dark before detection of the luminescence signals. Identical leaves were used for A and B but different detection methods (scanner) were applied. Scanning of leaves with **A**: Typhoon Variable Mode Imager (GE Healthcare) using ImageQuant 5.2 (GE Healthcare) **B**: Fusion FX7 chemiluminescence and fluorescence imager (Peqlab).

Taken together, 13377 plants were screened, from which 654 were selected in the first round because they either displayed a rescued luciferase signal and/or demonstrated a rescue in the phenotype (Table 10).

Table 10: Numbers of positive tested M2 plants after luminescence screening. The *rls* mutants derived from *LHCB1.2*$_{pro}$*:LUC prors1-2* are divided into the 1st and 2nd mutagenesis due to their different luminescence signal detection method (see text), which explains the higher percentage of positive tested plants from the 2nd mutagenesis.

M2 generation	total	*LHCB1.2* (1st)	*LHCB1.2* (2nd)	*LHCB3*
screened	13377	4636	5621	3120
positive tested	654	144	390	120
positive tested [%]	4.88	3.10	6.93	3.84

In the next step, seeds were harvested from all of these 654 mutants and ~ 10 seeds per mutant from the M3 generation were sown. All plants were screened once more for the luciferase signal and the phenotype was monitored for segregation as well. Additionally, all plants were screened for the presence of the T-DNA insertion and the wild type allele of the *PRORS1* gene via PCR. For a characterization of the photosynthetic performance, the maximum quantum yield of PSII (F_v/F_m) and the

effective quantum yield of PSII (Φ_{II}) were measured for at least 6 plants per mutant. Taken together, 360 *rls* mutants could be confirmed in the M3 generation (Table 11).

Table 11: Numbers of confirmed mutants of the M3 generation in the luminescence screen. The *rls* mutants derived from *LHCB1.2*$_{pro}$*:LUC prors1-2* are divided into the 1st and 2nd mutagenesis due to their different luminescence signal detection in the M2 generation. The analysis of the wild type allele was performed via PCR for all mutants that were confirmed using the luciferase screen.

M3 generation	*LHCB3*	*LHCB1.2* (1st)	*LHCB1.2* (2nd)	total	% of tested lines in M3 generation
Number of confirmed mutants	61	67	232	360	55%
Number of mutants that show no segregation in phenotype and no wild type allele	35	44	197	276	42%
Number of mutants that additionally show no segregation for luciferase signal	5	4	30	39	6%

3.2. Physiological analysis of selected *rls* mutants

The aim of this part of the project was to select the most interesting *rls* mutants for further identification with the mapping approach. With the help of the screening data (luminescence signal and leaf size and color) and the measurement of chlorophyll fluorescence (calculation of PSII parameters), 19 *rls* mutants were selected. Two of them (*rls2(3)* and *rls134*) were descendants of the *LHCB3*$_{pro}$*:LUC prors1-2* mutant, whereas all other chosen *rls* mutants were derived from the *LHCB1.2*$_{pro}$*:LUC prors1-2* mutant. Additional to the luminescence signal (resembling the expression level), the rosette leaf phenotype, PSII parameters, and the chlorophyll *a* and *b* content were determined and the amount of starch (glucose) was calculated. Moreover, the transcript levels of photosynthetic genes and their corresponding protein levels of the selected *rls* mutants were detected.

3.2.1 The *rls* mutants display a broad range of *LHCB* expression levels as revealed by luciferase expression

For quantification of the firefly luciferase expression in leaves, the Luciferase Assay Kit (Promega) was used and established successfully to ensure that the

luminescence signal correctly equates the amount of firefly luciferase protein. The assay was first set-up and monitored by performing a control experiment (Figure 7).

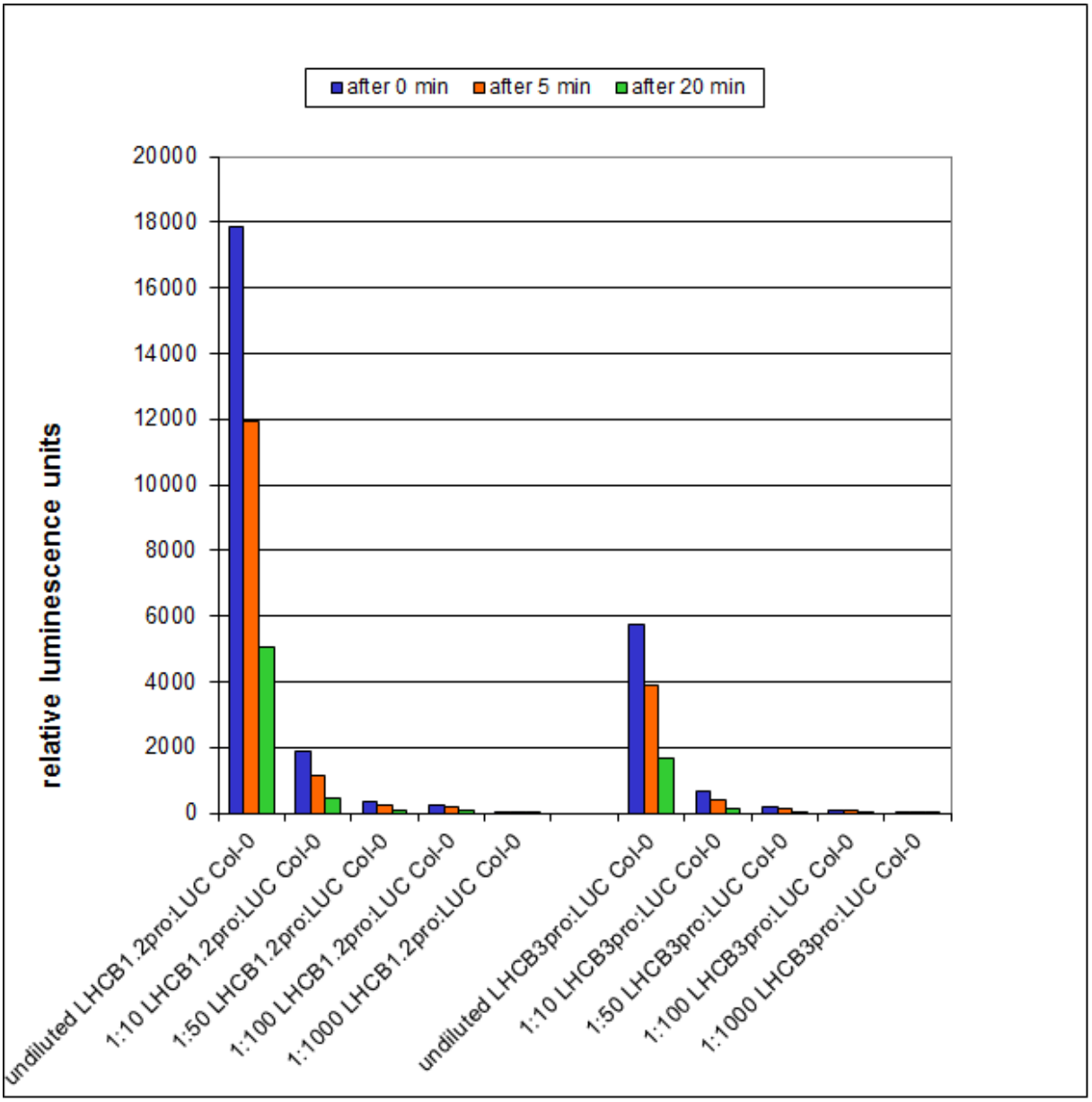

Figure 7: Quantification of the luminescence signal in *LHCB1.2*$_{pro}$*:LUC* Col-0 and *LHCB3*$_{pro}$*:LUC* Col-0 plants. For the quantification of the firefly luciferase in the leaves, a Luciferase Assay Kit (Promega) and the Safire^2 microplate reader (Tecan) were used. A dilution series from the protein extract of leaves from three individual plants was subjected to the analyses and the luminescence reaction was measured at three different time points after the start of the enzymatic assay (blue: after 0 min; orange: after 5 min; green: after 20 min; see methods). Since the mean value was calculated using two technical replicates, no standard deviation is shown.

For this purpose, the firefly luciferase was quantified in a dilution series (20µl undiluted, 1:10, 1:50, 1:100, 1:1000) of leaf protein extract from the two $_{pro}$*:LUC* Col-0 lines (*LHCB1.2*$_{pro}$*:LUC* Col-0, *LHCB3*$_{pro}$*:LUC* Col-0). The luminescence reaction was measured at three different time points after the start of the enzymatic assay, which was achieved by adding luciferin (Figure 7). With this approach, the optimal time point for the measurement was determined, since the enzymatic reaction takes place very fast and is very sensitive to light. The results clearly show that the dilution series of both lines depicted a very good linear correlation. Moreover, it was observed that the *LHCB1.2*$_{pro}$*:LUC* Col-0 line showed a three times higher luminescence value compared to the *LHCB3*$_{pro}$*:LUC* Col-0 line, which fitted to the observed difference in strength of the luminescence signal from the screening process (data not shown).

After the extraction of total protein from a pool of leaves from at least 10 plants for three replicates of each genotype, the signals were detected with the Safire^2 microplate reader (Tecan). The amount of measured luciferase indicated the expression level of the *LHCB* transcripts. This experiment was performed for exact quantification of the luminescence signals, whereas in the luminescence screen the luminescence signals were evaluated optically (Figure 5).

The plants with the promoter-luciferase construct inserted into Col-0 ($_{pro}$*:LUC* Col-0 lines) were used as the positive control (= “wild type”) for this experiment (Table 12). The parental lines of the *rls* mutants, of which the promoter-luciferase construct was in the *prors1-2* background ($_{pro}$*:LUC prors1-2*), showed a very low luciferase signal, which was almost not detectable using the scanner. Most of the *rls* mutants analyzed revealed a rescue of the relative luminescence compared to their parental line ($_{pro}$*:LUC prors1-2*). However, the degree of the rescue varied considerably between the different mutants. While *rls436* and *rls478* depicted luminescence levels almost identical to the parental line *LHCB1.2*$_{pro}$*:LUC prors1-2*, the mutants *rls615* and *rls621* showed the strongest rescue with values in the range of or even above *LHCB1.2*$_{pro}$*:LUC* Col-0 (= “wild type”) level (Table 12, marked in green and red, respectively). This data is in accordance with the luminescence signal strength observed by scanning.

Table 12: Summary of luciferase quantification in the parental lines and *rls* mutants. The firefly luciferase expression was quantified with a Luciferase Assay Kit (Promega) and the Safire^2 microplate reader (Tecan). The normalized relative luminescence units (RLU) as well as the corresponding standard deviations (stdv) are depicted. Lines with similar low levels of luminescence compared to the parental line *LHCB1.2*$_{pro}$*:LUC prors1-2* are highlighted in green, mutants with a high luciferase level comparable to the "wild type" *LHCB1.2*$_{pro}$*:LUC* Col-0 in red.

line	normalized RLU	stdv
LHCB3$_{pro}$*:LUC prors1-2*	39.8	± 4
LHCB3$_{pro}$*:LUC* Col-0	5740.0	± 872
rls2(3)	1268.1	± 42
rls134	705.3	± 21
LHCB1.2$_{pro}$*:LUC prors1-2*	47.2	± 2
LHCB1.2$_{pro}$*:LUC* Col-0	17874.4	± 1275
rls2(1.2)	373.6	± 80
rls304	9988.9	± 1251
rls316	7675.6	± 2074
rls336	8894.5	± 681
rls436	22.7	± 1
rls463	14237.0	± 2333
rls478	63.6	± 22
rls502	1722.8	± 275
rls518	456.1	± 17
rls608	10763.5	± 962
rls615	17250.4	± 5681
rls621	25765.4	± 3055
rls666	8887.6	± 755
rls681	951.9	± 319
rls709	3678.6	± 481
rls716	1918.8	± 199
rls744	2268.7	± 562

3.2.2.1 The *rls* mutants display variable growth phenotypes

For the genetic forward screen, not only the luminescence was used as a marker, but also the growth phenotype and the leaf color of the plants were utilized to identify interesting mutants.

Both parental lines, *LHCB1.2*$_{pro}$*:LUC prors1-2* and *LHCB3*$_{pro}$*:LUC prors1-2*, possessed a very similar phenotype, including a smaller size and a yellowish leaf color. The color of the leaves of the selected mutants varied from yellowish green (like the parental lines) to a darker green (like Col-0) (Figures 8, 9). Moreover, the leaf size of several mutants reached nearly the size of the wild type (e.g. *rls478* and *rls436*), whereas others showed a phenotype comparable to the parental lines *LHCB1.2*$_{pro}$*:LUC prors1-2* or *LHCB3*$_{pro}$*:LUC prors1-2*, including *rls615*, *rls666* or

rls621. Interestingly, these results were in line with the data from the luminescence quantification assay (Table 12), in which the same lines were found to show the best (*rls615* and *rls621*) or the least rescue (*rls478* and *rls436*).

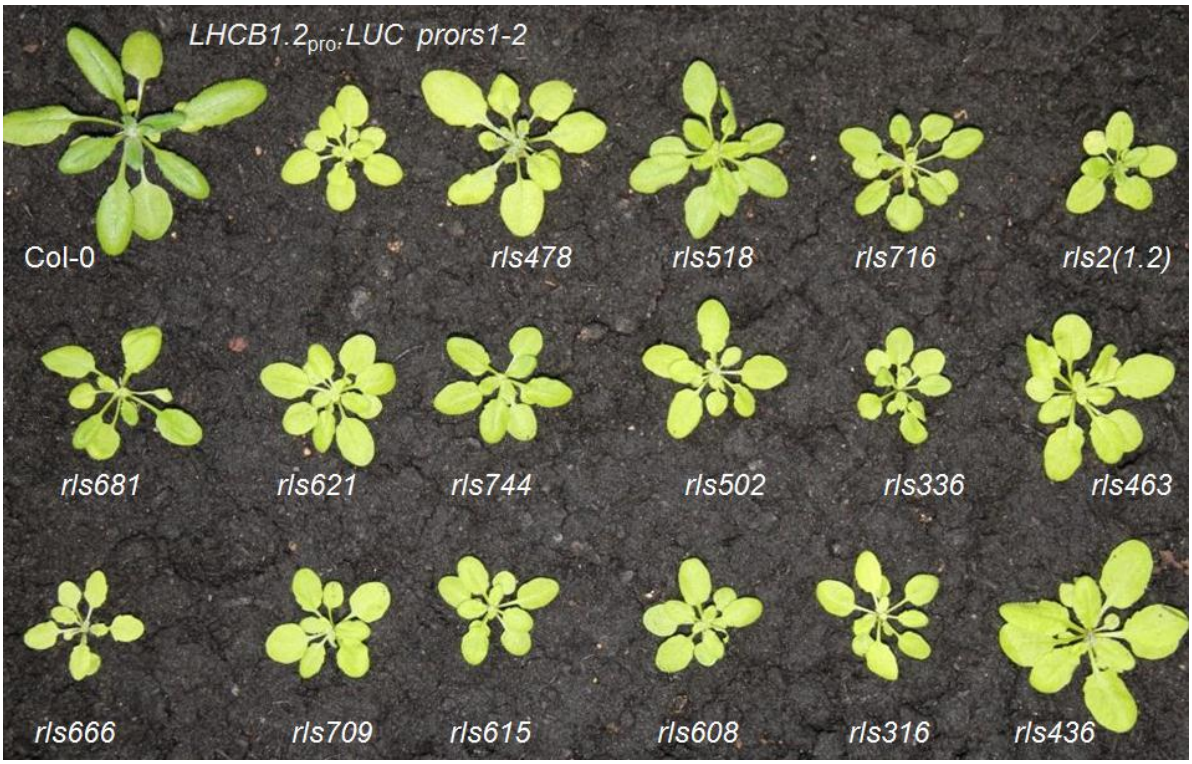

Figure 8: Phenotypic analysis of *rls* mutants containing the *LHCB1.2* promotor-luciferase construct. The picture was taken on day 28 and includes the wild type (Col-0), the parental line (*LHCB1.2*$_{pro}$*:LUC prors1-2* as well as the *rls* mutants.

In contrast to *rls2(3), rls134* showed no rescue compared to the parental line *LHCB3*$_{pro}$*:LUC prors1-2* (Figure 9).

Figure 9: Phenotypic analysis of *rls* mutants containing the *LHCB3* promotor-luciferase construct. The picture was taken on day 28 and shows the wild type (Col-0), the parental line *LHCB3*$_{pro}$*:LUC prors1-2* and the *rls* mutants, which possess the *LHCB3* promotor-luciferase construct.

3.2.2.2 The *rls* mutants exhibit distinct growth performances

After a first phenotypic analysis of the selected *rls* mutants, the plants were next investigated in regard to growth behavior and flowering time. For these developmental studies, the plants were monitored over a period of 50 days. Pictures of six plants per line were taken at five time points beginning with day 10 after germination on a weekly basis. For determination of growth curves, the leaf area was taken as parameter, which was measured and calculated with the software visistore (Leister et al. 1999). The plants were grown in a climate chamber under either long-day conditions with 16 h light and 8 h dark periods or under short-day conditions with 8 h light and 16 h dark periods. For analysis of the flowering time point, the day at which the first flowers emerged and the number of rosette leaves at that time point were noted for the plants growing under long-day conditions. For the plants growing under short-day conditions, no flowers had been observed during the 50 days of monitoring.

Under both long-day and short-day growth conditions, *LHCB3*$_{pro}$*:LUC prors1-2* showed even a worse growth performance than *prors1-2,* which itself possessed a delayed growth compared to wild type (Col-0) plants (Figure 10 A, B). The number of rosette leaves at flowering time (for *prors1-2* three days and for *LHCB3*$_{pro}$*:LUC prors1-2* five days later than Col-0), were for both mutants ~30% reduced compared to the number of Col-0 rosette leaves (Figure 10 C). Interestingly, *rls2(3)* showed a rescue under both growth conditions compared to the parental line *LHCB3*$_{pro}$*:LUC prors1-2* and even to *prors1-2,* confirming the better performance in the former phenotypic analysis. However, *rls2(3)* displayed the same delay in flowering time (5 days) as was observed for *LHCB3*$_{pro}$*:LUC prors1-2*. On the contrary, *rls134* possessed no rescue in growth conditions at all, and was not even germinating under short-day conditions (Figure 10 B).

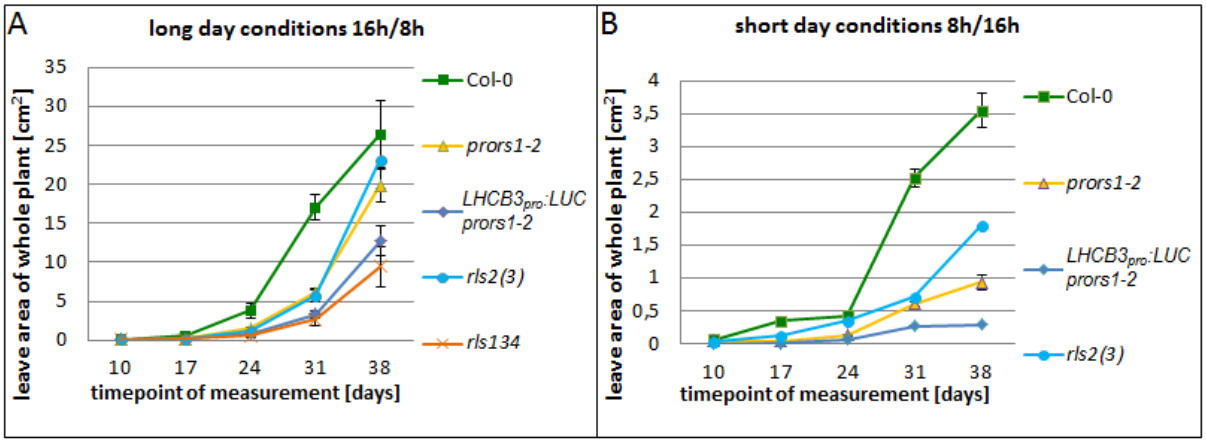

C

name	flowering time at day	number of rosette leaves at flowering time
Col-0	38	19
prors1-2	41	12
LHCB3$_{pro}$:LUC prors1-2	43	11
rls2(3)	43	14
rls134	43	9

Figure 10: Growth curves and flowering time points of Col-0 , *LHCB3$_{pro}$:LUC prors1-2* and its descending *rls* mutants under long-day and short-day conditions. The plants were grown in the climate chamber under 16 h light and 8 h dark (long-day conditions, **A)** or under 8 h light and 16 h dark (short-day conditions, **B**). Pictures of whole plants were taken at 5 time points and the leaf area of at least 5 plants per line was calculated using the software visistore. The mean values per time point and standard deviations are shown, except for the *rls* mutants grown under short-day conditions, because only 2 plants per mutant could be monitored over the whole time period. **C**: The different time points of emerging of flowers and the number of rosette leaves at that time point are depicted of plants grown under long-day conditions.

For mutants deriving from the parental line *LHCB1.2$_{pro}$:LUC prors1-2*, distinct effects in terms of growth and flowering time were observed as well. Due to the larger number of these mutants, they have been divided into several classes. The first group includes the *rls* mutants displaying the “strongest rescue effect” of growth behavior, i.e. the fastest growth (Figure 11). Two of them, *rls436* and *rls478,* showed almost wild type behavior for the growth rate under long-day conditions (Figure 11 A), and also under short-day conditions a rescue compared to their parental line *LHCB1.2$_{pro}$:LUC prors1-2* was observed, although not in the range of wild type growth (Figure 11 B). The flowering time of these mutants was also identical to the wild type, although the number of rosette leaves at that time was clearly reduced.

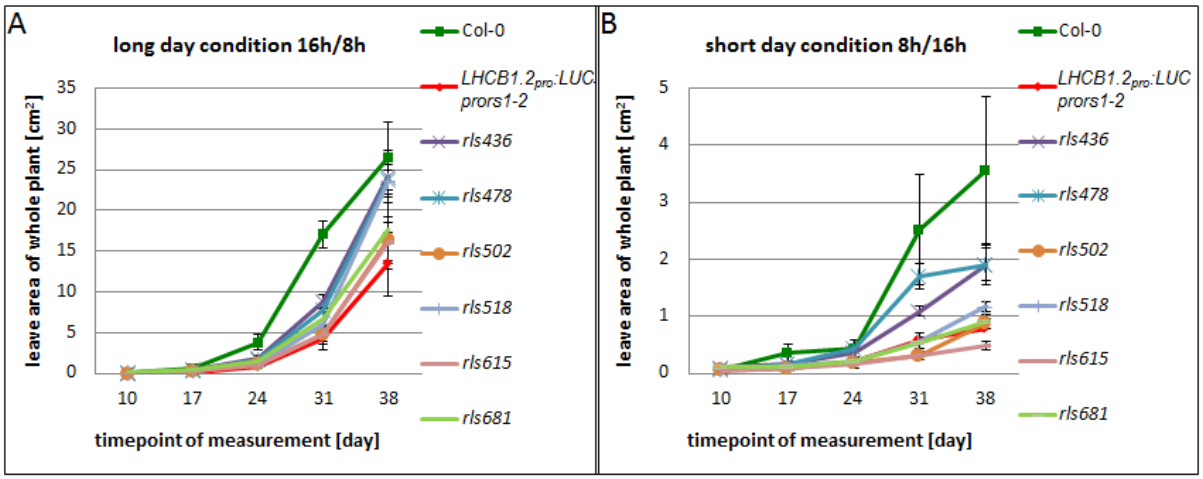

C

name	flowering time at day	number of rosette leaves at flowering time
Col-0	38	19
LHCB1.2pro:LUC prors1-2	41	12
rls436	38	13
rls478	38	13
rls502	43	11
rls518	40	12
rls615	40	11
rls681	40	12

Figure 11: Growth curves and flowering time points of Col-0 and *rls* mutants with a rescue compared to *LHCB1.2*$_{pro}$*:LUC prors1-2* under long-day and short-day conditions. The plants were grown in the climate chamber under 16 h light and 8 h dark (long-day conditions, **A**) and under 8 h light and 16 h dark (short-day conditions, **B**). Pictures of whole plants were taken at 5 time points and using the software visistore, the leaf area of at least 5 plants per mutant was calculated. The mean values per time point and standard deviations are shown. **C**: The different time points of onset of flowering and the number of rosette leaves at that time point are depicted of plants grown under long-day conditions.

The second group of *rls* mutants deriving from the parental line *LHCB1.2*$_{pro}$*:LUC prors1-2* includes the mutants which showed no significant rescue effect regarding growth compared to the parental line (Figure 12 A, B). Additionally, the *rls* mutants from this subgroup featured a clear delay in flowering time, even when analyzed versus the parental line, and also exhibited less rosette leaves at the first flowering time point than *LHCB1.2*$_{pro}$*:LUC prors1-2*. One of the mutants from this group, *rls666,* had the longest delay for onset of flowering of all *rls* mutants monitored (Figure 12 C).

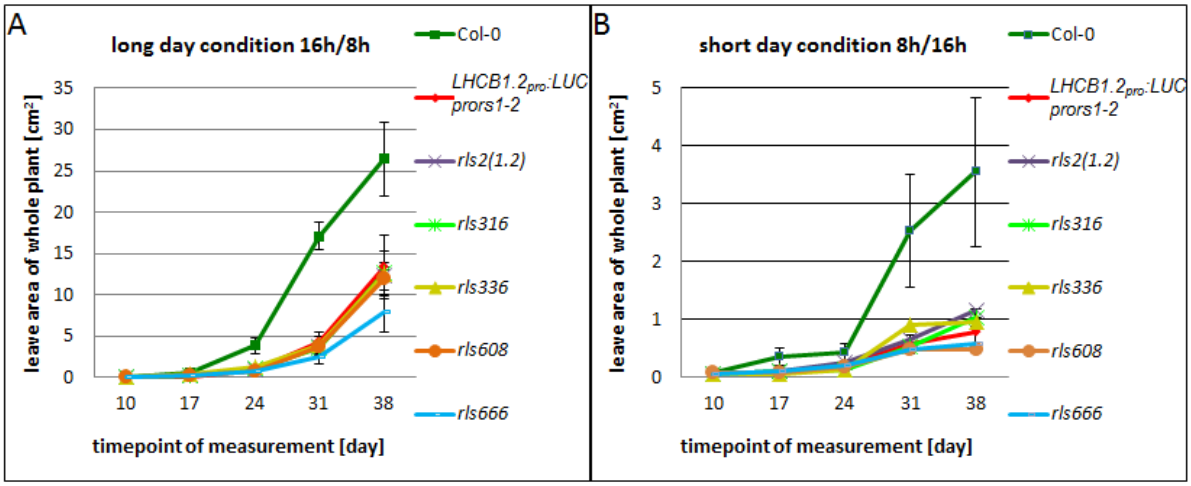

C

name	flowering time at day	number of rosette leaves at flowering time
Col-0	38	19
LHCB1.2$_{pro}$:LUC prors1-2	41	12
rls2-21	41	10
rls316	44	11
rls336	42	10
rls608	42	10
rls666	46	11

Figure 12: Growth curves and flowering time points of Col-0, *LHCB1.2$_{pro}$:LUC prors1-2* and *rls* mutants with no growth rescue under long-day and short-day conditions. The plants were grown in the climate chamber under 16 h light and 8 h dark (long-day conditions, **A**) and under 8 h light and 16 h dark (short-day conditions, **B**). Pictures of whole plants were taken at 5 time points and using the software visistore, the leaf area of at least 5 plants per mutant was calculated. The mean values per time point and standard deviations are shown. **C**: The different time points of onset of flowering and the number of rosette leaves at that time point are depicted of plants grown under long-day conditions.

The third group is composed of the *rls* mutants that showed a similar growth behavior to their parental line *LHCB1.2$_{pro}$:LUC prors1-2* under long-day and a similar or even retarded growth behavior under short-day conditions (Figure 13). Similar to the second group, they exhibited a delay of onset of flowering ranging from 3 to 6 days in comparison to the wild type. However, the number of rosette leaves for these *rls* mutants were found to be in the same range as the leaf number of *LHCB1.2$_{pro}$:LUC prors1-2*.

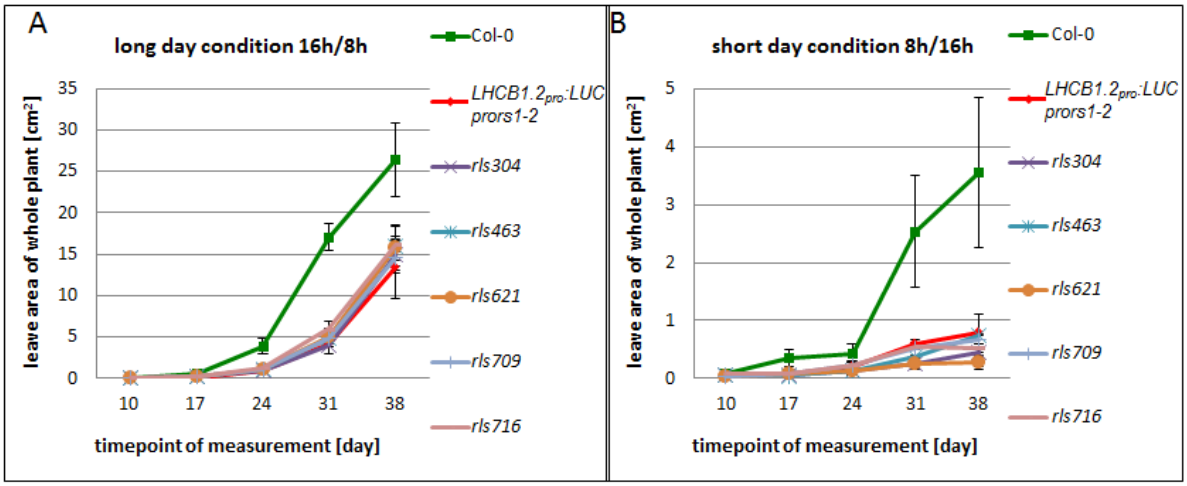

C

name	flowering time at day	number of rosette leaves at flowering time
Col-0	38	19
LHCB1.2$_{pro}$:LUC prors1-2	41	12
Rls304	44	12
rls463	42	11
rls621	44	13
rls709	42	11
rls716	41	12

Figure 13: Growth curves and flowering time points of Col-0 and *rls* mutants with a similar performance as *LHCB1.2$_{pro}$:LUC prors1-2* under long-day and short-day conditions. The plants were grown in the climate chamber under 16 h light and 8 h dark (long-day conditions, **A**) and under 8 h light and 16 h dark (short-day conditions, **B**). Pictures of whole plants were taken at 5 time points and using the software visistore, the leaf area of at least 5 plants per mutant was calculated. The mean values per time point and standard deviations are shown. **C**: The different time points of onset of flowering and the number of rosette leaves at that time point are depicted of plants grown under long-day conditions.

Taken together, three mutants were identified in the growth rate measurements that featured the most obvious rescue effects: *rls2(3)* deriving from *LHCB3$_{pro}$:LUC prors1-2*, and *rls436* and *rls478* with *LHCB3$_{pro}$:LUC prors1-2* as parental line.

3.2.3 Internal transcript level of nuclear-encoded photosynthetic genes in the *rls* mutants

It was described in earlier studies that the mutation of the *PRORS1* gene (*AT5G52520*) results in a down-regulation of nuclear-encoded genes responsible for the light reactions of photosynthesis. The mRNA expression of the *PRORS1* gene, which is a “leaky” mutation, is reduced to 25% in the *prors1-2* mutant compared to Col-0 (Pesaresi et al. 2006). Hence, it has to be investigated that potential rescue effects do not result from a mere up-regulation of *PRORS1* gene expression. For determination of the expression levels of *PRORS1, PSBO, PSAK, LHCB1.2 and LHCB3* transcripts in the *rls* mutants, the RNA was extracted from a pool of at least

10 plants (whole leaves) at the eight rosette leave stage grown under long-day conditions (16 h / 8 h). The expression of the *AT5G52520* transcript in the *rls* mutants and their parental lines (*LHCB3*$_{pro}$*:LUC prors1-2* and *LHCB1.2*$_{pro}$*:LUC prors1-2*) was determined by real-time PCR (Figures 14, 15). For this purpose, the cDNA was synthesized from the isolated RNA using the iScript cDNA Synthesis Kit (Bio-Rad) and the real-time PCR was monitored by using the iQ5™ Multi Color Real-Time PCR Detection System (Bio-Rad) (see methods chapter 2.2.2.4). Reactions were performed in triplicate for each genotype. Relative transcript abundances were normalized with respect to the level of the constitutively expressed mRNA of an ubiquitin-protein ligase-like protein (*AT4G36800*).

For the *LHCB3*$_{pro}$*:LUC prors1-2* originating plants, the *PRORS1* transcript level of *LHCB3*$_{pro}$*:LUC prors1-2* itself and *rls134* was not significantly altered to that of *prors1-2*. However, *rls2(3)* possessed a slight rescue for the *PRORS1* transcript level (Figure 14).

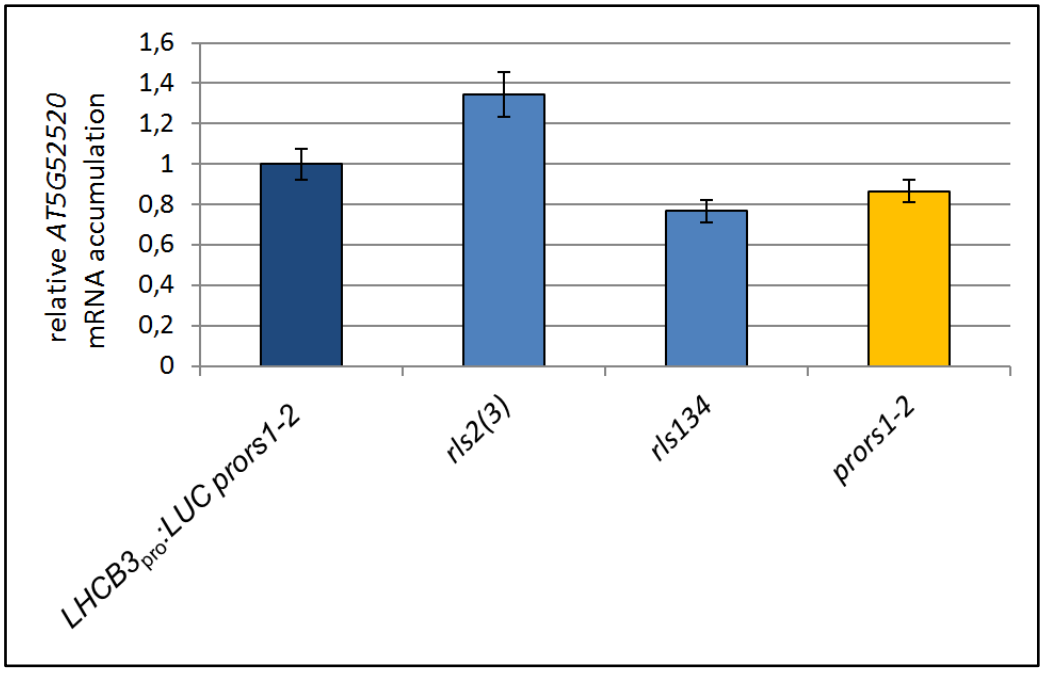

Figure 14: *PRORS1* (*AT5G52520*) mRNA expression level in *LHCB3*$_{pro}$*:LUC prors1-2*, *rls2(3)*, *rls134* and *prors1-2*. The plants were grown under long-day conditions (16 h / 8 h) and harvested at the 8 rosette leave developmental stage for RNA extraction (see methods chapter 2.2.1.4). The cDNA was synthesized from 0.5 µg RNA using the iScript cDNA Synthesis Kit (Bio-Rad) and real-time PCR was performed with the iQ5™ Multi Color Real-Time PCR Detection System (Bio-Rad) (see methods chapter 2.2.2.4). Relative transcript abundances were normalized with respect to the level of the constitutively expressed mRNA of an ubiquitin-protein ligase-like protein (*AT4G36800*).

The *LHCB1.2*$_{pro}$*:LUC prors1-2* originating *rls* mutants featured similar mRNA levels of the *PRORS1* transcript (Figure 15), indicating that the rescue phenotypes observed before are not caused by a difference in the accumulation of *PRORS1* transcript.

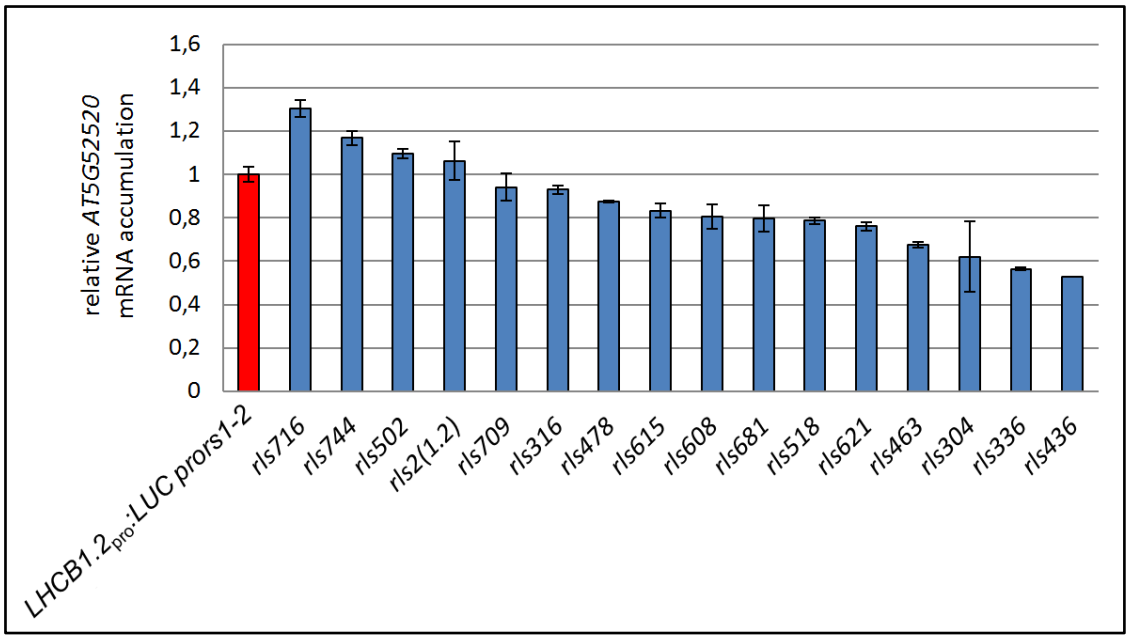

Figure 15: *PRORS1* (*AT5G52520*) expression level of *LHCB1.2*$_{pro}$*:LUC prors1-2* and its descending *rls* mutants. The plants were grown under long-day conditions (16 h / 8 h) and harvested at the 8 rosette leave developmental stage for RNA extraction (see methods chapter 2.2.1.4). The cDNA was synthesized from 0.5 µg RNA using the iScript cDNA Synthesis Kit (Bio-Rad) and real-time PCR was performed with the iQ5™ Multi Color Real-Time PCR Detection System (Bio-Rad) (see methods chapter 2.2.2.4). Relative transcript abundances of *LHCB1.2*$_{pro}$*:LUC prors1-2* (red) and the *rls* mutants (blue) were normalized with respect to the level of the constitutively expressed mRNA of an ubiquitin-protein ligase-like protein (*at4g36800*).

Furthermore, the *PSAK* (*AT1G30380*), *PSBO* (*AT3G50820*), *LHCB1.2* (*AT1G29910*) and *LHCB3* transcript (*AT5G54270*) levels were determined via Northern blot analysis (three biological replicates of each genotype; Figure 16). *LHCB3*$_{pro}$*:LUC prors1-2* showed a reduction of *LHCB3* transcript level compared to Col-0 and *prors1-2,* concomitantly with an increase for the other three transcripts compared to *prors1-2*. Moreover, *rls2(3)* showed an increase of the *LHCB* transcripts in comparison to *LHCB3*$_{pro}$*:LUC prors1-2*, whereas *rls134* featured similar levels of all transcripts. *LHCB1.2*$_{pro}$*:LUC prors1-2* possessed an increased amount of the *PSAK* transcript and slightly reduced *LHCB* transcript levels compared to Col-0. Furthermore, all four transcript amounts were found to be increased in *rls2(1.2),* in contrast to *rls436, rls744, rls502* and *rls336* that exhibited similar levels as compared to *LHCB1.2*$_{pro}$*:LUC prors1-2*. The mutant *rls478* showed a strong rescue of the

LHCB3 transcript, whereas the other three genes were found to be expressed in similar quantities as in *LHCB1.2*$_{pro}$*:LUC prors1-2.*

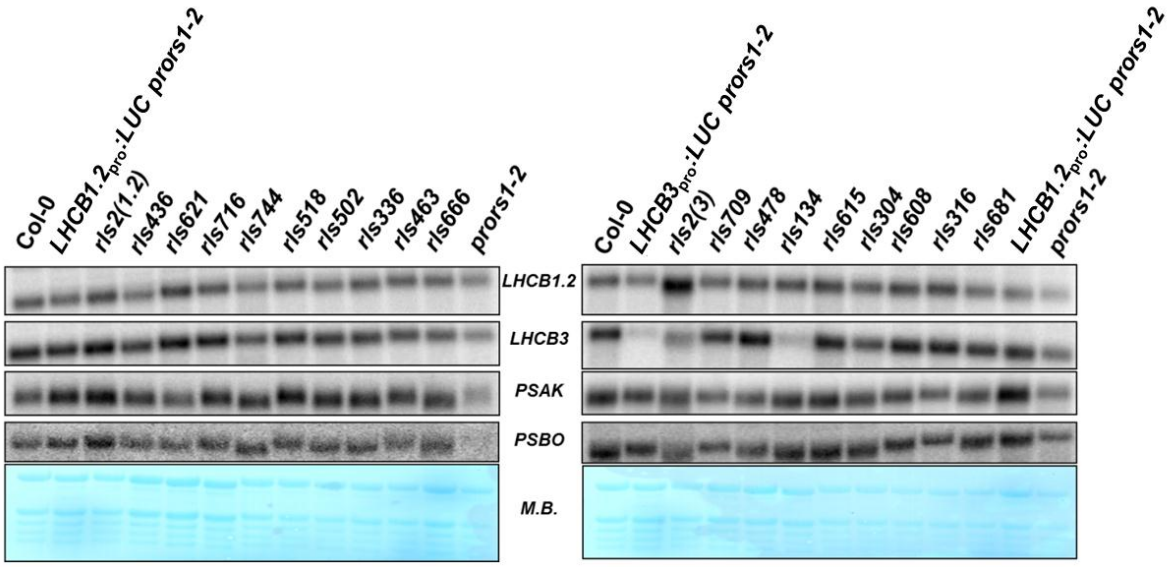

Figure 16: *LHCB1.2*, *LHCB3, PSAK* and *PSBO* transcript levels from Col-0, *prors1-2*, parental lines and *rls* mutants. As a loading control, the methyl blue stained nylon membrane (M.B.) was used. The primers used to generate specific cDNA probes for Northern blot analysis are listed in Table 7.

3.2.4 Detection of nuclear-encoded photosynthetic protein levels

The number of proteins in the chloroplast is estimated to range between 3500 and 4000 (Soll and Schleiff 2004), whereas plastid genomes encode only 75 to 80 proteins (Timmis et al. 2004). Thus, most of the proteins located in the chloroplast are encoded in the nucleus. To verify potential changes in transcript amounts on the protein level, the corresponding protein quantities were determined by an immunoblot detection assay (see methods chapter 2.2.3.3). The plant material used was equal to the one applied for detection of the RNA level, i.e. a pool of at least 10 plants at the 8 rosette leaf stage grown under long-day conditions (16 h / 8 h). The extracted total proteins were separated via polyacrylamide gel electrophoresis (SDS-PAGE), before the immunoblot detection assay was performed.

The protein amounts of PsbO and Lhcb1 were detected for Col-0, *prors1-2*, the parental lines and their descending *rls* mutants (Figure 17). The mutant *rls2(3)* showed a rescue for both proteins compared to its parental line, which did however not reach wild type amounts, while for *rls134* only the PsbO level was increased compared to *LHCB3*$_{pro}$*:LUC prors1-2*. Moreover, *rls666* comprised an even higher

protein amount than Col-0 for both Lhcb1 and PsbO. Almost all *LHCB1.2*$_{pro}$*:LUC prors1-2* descending *rls* mutants showed a higher PsbO protein level than their parental line, except *rls304* and *rls608*. Both *rls436* and *rls478* possessed an increase in Lhcb1 protein as well.

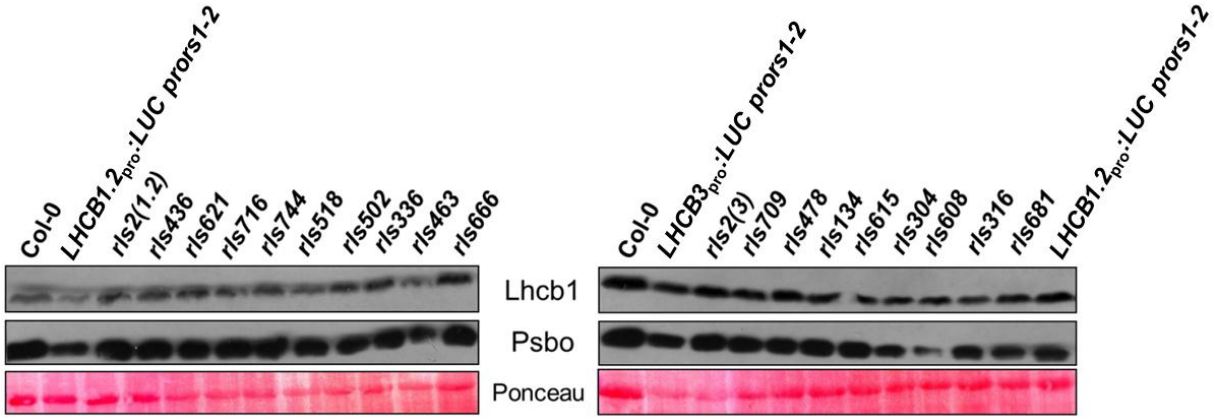

Figure 17: Immunoblot detection assay with LHCB1 and PSBO secondary antibodies. Proteins extracted from equal amounts of plant material from Col-0, the parental lines (*LHCB1.2*$_{pro}$*:LUC prors1-2* and *LHCB3*$_{pro}$*:LUC prors1-2*) and its descending *rls* mutants were separated using SDS-PAGE and were subsequently transferred onto PVDF membrane before incubation with the indicated antibodies. As a loading control, the ponceau red stained PVDF membrane (Ponceau) was used.

3.2.5 A rescue in growth performance does not always correlate with a rescue of PSII parameters

The PSII performance was found to be strongly reduced in *prors1-2* compared to Col-0 (Pesaresi et al. 2006), thus it seems conceivable to observe a potential rescue of the PSII parameters in the *rls* mutants. For this purpose, the measurement of chlorophyll fluorescence of dark adapted (15 min) plants was performed with the Dual-PAM 100 (Walz, Germany). For at least six plants per mutant the fluorescence of the leaves was measured (F_0), before saturation pulses of white light (800ms) were used to determine the maximum fluorescence (F_m) and the ratio $(F_m\text{-}F_0)/F_m$ = F_v/F_m (maximum quantum yield of PSII). After the illumination with actinic light, the effective quantum yield of PSII (Φ_{II}), the nonphotochemical fluorescence quenching (NPQ) and the proportion of closed PSII (1-qP) were detected (see 2.1.4).

The drastically diminished PSII performance of *prors1-2* compared to Col-0 known from previous studies (Pesaresi et al. 2006) was confirmed in the present experiments (Table 14). Interestingly, it has to be noted that *LHCB3*$_{pro}$*:LUC prors1-2*

possessed even a worse PSII performance than *prors1-2,* in contrast to *LHCB1.2*$_{pro}$*:LUC prors1-2*, for which an increased photosynthetic activity compared to *prors1-2* was measured (Tables 14, 15). Regarding the *rls* mutants with *LHCB3*$_{pro}$*:LUC prors1-2* as parental line, values determined for *rls2(3)* for the maximum quantum yield of PSII (F_v/F_m) and the effective quantum yield of PSII (Φ_{II}) reached closest to wild type values, even in comparison to all *rls* mutants analysed, and therefore featured the best rescue of all *rls* mutants (Table 14). Moreover, *rls134* showed a rescue compared to *LHCB3*$_{pro}$*:LUC prors1-2* and *prors1-2* as well, although the effect was not as clear as observed for *rls2(3)*.

Table 14: Chlorophyll fluorescence measurements of dark adapted (15 min) *LHCB3*$_{pro}$*:LUC prors1-2* plants for calculation of PSII parameters. Six plants per mutant were analyzed at day 28 with the Dual-PAM 100 (Walz). The fluorescence was measured (F_0), before saturation pulses of white light were used to determine the maximum fluorescence (F_m) and the ratio (F_m-F_0)/F_m = F_v/F_m (maximum quantum yield of PSII). After illumination with actinic light, the effective quantum yield of PSII (Φ_{II}), the non- photochemical fluorescence quenching (NPQ) and the proportion of closed PSII (1-qP) was detected (see 2.1.4). The mutant showing the strongest rescue (*rls2(3)*) of all *rls* mutants is highlighted in red.

name	F_v/F_m	Φ_{PSII}	NPQ	1-*qP*
Col-0	0.819 ± 0.012	0.703 ± 0.016	0.263 ± 0.051	0.080 ± 0.026
prors1-2	0.501 ± 0.037	0.406 ± 0.054	0.213 ± 0.157	0.203 ± 0.063
LHCB3$_{pro}$*:LUC prors1-2*	0.482 ± 0.015	0.302 ± 0.014	0.418 ± 0.032	0.233 ± 0.020
rls2(3)	0.706 ± 0.020	0.566 ± 0.025	0.226 ± 0.021	0.146 ± 0.016
rls134	0.594 ± 0.043	0.433 ± 0.026	0.284 ± 0.109	0.210 ± 0.006

As mentioned above, *LHCB1.2*$_{pro}$*:LUC prors1-2* possessed a better PSII performance than *LHCB3*$_{pro}$*:LUC prors1-2* and *prors1-2,* hence the range of possible values of the PSII parameters for the *LHCB1.2*$_{pro}$*:LUC prors1-2* originating *rls* mutants was smaller than shown before for the mutants with *LHCB3*$_{pro}$*:LUC prors1-2* as parental line. Interestingly, none of the *LHCB1.2*$_{pro}$*:LUC prors1-2* descending *rls* mutants showed a strong rescue, including *rls436* and *rls478*, which featured a growth behavior similar to the wild type as shown before (Figure 8). Moreover, some mutants (*rls621*, *rls304*, *rls463*, *rls502*) even depicted reduced PSII performance values than observed for *LHCB1.2*$_{pro}$*:LUC prors1-2*. However, *rls2(1.2)*, *rls615* and *rls518* showed the best and slightly enhanced – although not strongly increased compared to *LHCB1.2*$_{pro}$*:LUC prors1-2* – PSII activity.

Table 15: Chlorophyll fluorescence measurements of dark adapted (15 min) *LHCB1.2*$_{pro}$*:LUC prors1-2* descending plants for calculation of PSII parameters. Six plants per mutant were measured at day 28 with the Dual-PAM 100 (Walz). The fluorescence of leaves was measured (F_0), before saturation pulses of white light were used to determine the maximum fluorescence (F_m) and the ratio $(F_m-F_0)/F_m = F_v/F_m$ (maximum quantum yield of PSII). After illumination with actinic light, the effective quantum yield of PSII (Φ_{II}), the non-photochemical fluorescence quenching (NPQ) and the proportion of closed PSII (1-qP) was detected. The *rls* mutants are listed according to the F_v/F_m values descending. The parental line is highlighted in blue and *rls436* and *rls478*, which showed the best growth performance, are highlighted in green.

name	F_v/F_m	Φ_{PSII}	NPQ	1-*qP*
Col-0	0.819 ± 0.012	0.703 ± 0.016	0.263 ± 0.051	0.080 ± 0.026
prors1-2	0.501 ± 0.037	0.406 ± 0.054	0.213 ± 0.157	0.203 ± 0.063
LHCB1.2$_{pro}$*:LUC prors1-2*	0.568 ± 0.065	0.413 ± 0.066	0.224 ± 0.083	0.204 ± 0.005
rls2(1.2)	0.593 ± 0.060	0.417 ± 0.044	0.267 ± 0.084	0.221 ± 0.026
rls615	0.591 ± 0.046	0.450 ± 0.028	0.119 ± 0.090	0.211 ± 0.021
rls518	0.588 ± 0.040	0.408 ± 0.039	0.395 ± 0.104	0.200 ± 0.016
rls436	0.587 ± 0.020	0.451 ± 0.046	0.219 ± 0.127	0.164 ± 0.031
rls336	0.585 ± 0.009	0.409 ± 0.016	0.245 ± 0.045	0.228 ± 0.035
rls666	0.584 ± 0.038	0.413 ± 0.031	0.296 ± 0.059	0.204 ± 0.020
rls478	0.574 ± 0.012	0.433 ± 0.026	0.203 ± 0.063	0.216 ± 0.039
rls709	0.567 ± 0.048	0.408 ± 0.025	0.350 ± 0.097	0.202 ± 0.016
rls716	0.565 ± 0.026	0.419 ± 0.011	0.326 ± 0.105	0.241 ± 0.113
rls744	0.552 ± 0.036	0.378 ± 0.043	0.235 ± 0.060	0.245 ± 0.027
rls666	0.548 ± 0.030	0.368 ± 0.033	0.366 ± 0.127	0.236 ± 0.062
rls621	0.514 ± 0.019	0.371 ± 0.013	0.166 ± 0.024	0.220 ± 0.026
rls304	0.507 ± 0.017	0.362 ± 0.041	0.255 ± 0.033	0.197 ± 0.070
rls463	0.505 ± 0.028	0.341 ± 0.025	0.295 ± 0.090	0.224 ± 0.034
rls502	0.492 ± 0.009	0.355 ± 0.026	0.162 ± 0.040	0.220 ± 0.044
rls316	0.473 ± 0.038	0.363 ± 0.023	0.325 ± 0.059	0.102 ± 0.063
rls608	0.477 ± 0.033	0.333 ± 0.019	0.269 ± 0.159	0.203 ± 0.063

3.2.6 Most of the identified *rls* mutants display a rescue in chlorophyll content

As the phenotypic analysis revealed a yellowish appearance for several *rls* mutants, in the next step the chlorophyll amount was investigated. For the determination of chlorophyll *a* (chl *a*) and chlorophyll *b* (chl *b*) content, pigments were extracted from Col-0, *prors1-2*, *LHCB3*$_{pro}$*:LUC prors1-2*, *LHCB1.2*$_{pro}$*:LUC prors1-2* and *rls* mutant leaves. The extracts of six plants per genotype were photometrically measured at 750 nm, 647 nm and 663 nm (see methods chapter 2.2.3.4). The ratio from chl *a* and chl *b* (= chl (*a*/*b*)) and their sum (= chl (*a*+*b*)) was calculated as well.

Both *rls* mutants originating from *LHCB3*$_{pro}$*:LUC prors1-2* (*rls2(3)* and *rls134*) contained a similar amount of chl *a* and chl *b,* which was found to be ~40% reduced compared to Col-0 (Table 16). The ratio chl (*a*/*b*) was in the range of the wild type, however the sum chl (*a*+*b*) of these *rls* mutants was approximately half of the Col-0 content. Moreover, *rls2(3)* and *rls134* showed a slight rescue of chl *a* and chl *b* content compared to *LHCB3*$_{pro}$*:LUC prors1-2* in terms of chl *a* and chl *b* amount as well as in regard to chl (*a*+*b*). Interestingly, the chl (*a*/*b*) ratio did not differ significantly in any mutant analyzed (compared to Col-0).

Table 16: Determination of chlorophyll *a* (chl *a*) and chlorophyll *b* (chl *b*) content of the *rls* mutants descending from the *LHCB3*$_{pro}$*:LUC prors1-2* line. From 6 plants per genotype, the absorption of chl *a*, chl *b* was measured at 750 nm, 647 nm and 663, and their ratio chl (*a*/*b*) and their sum chl (*a*+*b*) was calculated. The mutant showing the strongest rescue for the maximum quantum yield (F_v/F_m), *rls2(3),* is highlighted in red.

name	chl *a* [µg/mg]	chl *b* [µg/mg]	chl (*a* *b*)	chl (*a*+*b*)
Col-0	0.681 ± 0.05	0.215 ± 0.02	3.1 ± 0.3	0.89 ± 0.07
prors1-2	0.302 ± 0.03	0.106 ± 0.01	2.8 ± 0.3	0.41 ± 0.04
LHCB3$_{pro}$*:LUC prors1-2*	0.341 ± 0.07	0.113 ± 0.05	3.0 ± 0.6	0.45 ± 0.11
rls2(3)	0.368 ± 0.07	0.126 ± 0.03	2.9 ± 0.2	0.50 ± 0.11
rls134	0.355 ± 0.10	0.125 ± 0.04	2.8 ± 0.3	0.48 ± 0.15

For the *LHCB1.2*$_{pro}$*:LUC prors1-2* derived plants, the parental line itself showed an unusual chlorophyll phenotype, as it possessed a lower chl *a* but a higher chl *b* content than *prors1-2,* although the sum chl (*a*+*b*) was almost equal to *prors1-2* (Table 17). The analyzed *rls* mutants depicted distinct chlorophyll features: the majority of them showed an increase in the amounts of both chl *a* and chl *b*, hence suggesting a rescue effect, including *rls478* and *rls436*, for which a rescue of the growth performance – but not of PSII activity – has been detected before. The mutant *rls615* featured the highest chl *a* and chl *b* contents of all tested *rls* mutants, however the ratio chl (*a*/*b*) was – as for nearly all other mutants with increased chlorophyll content – *prors1-2* like. Only for *rls681*, *rls744*, *rls2(2.1)* and, interestingly, for *rls478,* a slight increase in the chl (*a*/*b*) ratio was measured. On the other hand, some mutants including *rls666* and *rls502* possessed an unaltered or even decreased chlorophyll content, especially regarding chl *b*. Finally, for *rls336* and *rls608,* a decrease in the chl (*a*/*b*) ratio was observed.

Despite these distinct patterns in chlorophyll content of the *LHCB1.2*$_{pro}$*:LUC prors1-2* derived *rls* mutants, it has to be noted that *rls615* and *rls518,* which featured a slight rescue for the PSII performance (Table 15), showed also a rescue for the chl (*a*+*b*) content (Table 17). However, to make the situation more complex, *rls2(1.2)* possessed a clearly reduced chl (*a*+*b*) amount compared to the other two mentioned mutants, although their PSII performance was found to be nearly identical (Table 15). Hence, this suggests that the two parameters of PSII activity and chlorophyll content are not as directly related as expected.

Table 17: Determination of chlorophyll *a* (chl *a*) and chlorophyll *b* (chl *b*) content of the *rls* mutants descending from the *LHCB1.2*$_{pro}$*:LUC prors1-2* line. From 6 plants per genotype, chl *a*, chl *b*, their ratio chl (*a*/*b*) and their sum chl (*a*+*b*) was measured at 750 nm, 647 nm and 663 nm, and afterwards the content calculated. The *rls* mutants are listed according to the chl (*a*+*b*) values descending. The parental line is highlighted in blue and *rls436* and *rls478*, which showed the best growth performance, are highlighted in green.

name	chl *a* (µg/mg)	chl *b* (µg/mg)	chl (*a*/*b*)	chl (*a*+*b*)
Col-0	0.681 ± 0.05	0.215 ± 0.02	3.1 ± 0.3	0.89 ± 0.07
prors1-2	0.302 ± 0.03	0.106 ± 0.01	2.8 ± 0.3	0.41 ± 0.04
LHCB1.2$_{pro}$*:LUC prors1-2*	0.286 ± 0.04	0.135 ± 0.02	2.3 ± 0.2	0.42 ± 0.60
rls615	0.518 ± 0.06	0.192 ± 0.01	2.7 ± 0.3	0.71 ± 0.07
rls518	0.456 ± 0.10	0.169 ± 0.03	2.7 ± 0.2	0.62 ± 0.13
rls478	0.434 ± 0.06	0.154 ± 0.01	2.8 ± 0.2	0.59 ± 0.06
rls716	0.424 ± 0.09	0.160 ± 0.04	2.6 ± 0.3	0.58 ± 0.12
rls681	0.430 ± 0.09	0.132 ± 0.03	3.2 ± 0.4	0.56 ± 0.09
rls436	0.410 ± 0.08	0.147 ± 0.02	2.7 ± 0.3	0.55 ± 0.10
rls304	0.400 ± 0.11	0.138 ± 0.03	2.8 ± 0.4	0.54 ± 0.14
rls621	0.387 ± 0.05	0.154 ± 0.03	2.5 ± 0.4	0.54 ± 0.08
rls709	0.386 ± 0.07	0.160 ± 0.03	2.4 ± 0.3	0.54 ± 0.09
rls608	0.392 ± 0.08	0.142 ± 0.03	2.0 ± 0.3	0.53 ± 0.10
rls744	0.402 ± 0.06	0.133 ± 0.03	3.0 ± 0.4	0.53 ± 0.08
rls316	0.376 ± 0.04	0.135 ± 0.02	2.7 ± 0.3	0.51 ± 0.05
rls2(1.2)	0.368 ± 0.07	0.127 ± 0.02	2.8 ± 0.1	0.49 ± 0.09
rls463	0.335 ± 0.07	0.137 ± 0.02	2.4 ± 0.4	0.47 ± 0.08
rls666	0.330 ± 0.07	0.111 ± 0.02	2.9 ± 0.3	0.44 ± 0.09
rls336	0.278 ± 0.02	0.169 ± 0.04	1.6 ± 0.5	0.44 ± 0.05
rls502	0.298 ± 0.04	0.123 ± 0.01	2.4 ± 0.2	0.42 ± 0.06

3.2.7 The starch (glucose) content of *rls* mutants shows a high variation

The glucose produced during photosynthesis is stored mainly as starch ($(C_6H_{10}O_5)_n$); hence starch functions as an energy storage system for the plants and constitutes another – more indirect – parameter for photosynthetic activity and plant viability. For

determination of the starch content of Col-0, the parental lines and the *rls* mutants, the leaves were harvested at two different time points: at 8 am at the end of the dark period as indication of the amount of glucose/starch used during the night as energy source, and at 6 pm (nine hours after light exposure) for determination of the production rate of starch upon photosynthetic activity. From pools of at least 10 plants (whole leaves) per genotype, the starch was extracted and hydrolyzed before three replicates for each genotype were quantified (methods chapter 2.2.3.6). For the quantification, a stabilized OD_{340} after 10 min (= A_1-value) was determined with the anthos reader HT-3 (Anthos Mikrosysteme Gmbh), before an enzyme mix of hexokinase/glucose-9-phosphate dehydrogenase was added. Upon the stabilization of the OD_{340} (after approximately 1 h), the obtained value was measured once more (A_2- value) and the starch calculation was calculated.

The measurement revealed that the relative difference of starch content of the two harvesting time points from *LHCB3*$_{pro}$*:LUC prors1-2* was similar to Col-0, although the overall starch amount was clearly reduced (Figure 18 A). By contrast, *prors1-2* and *LHCB1.2*$_{pro}$*:LUC prors1-2* showed no difference for both harvesting time points, however the general amount was drastically diminished with regard to the starch content of Col-0 as well (Figure 18 B). Additionally, the starch amount of *LHCB3*$_{pro}$*:LUC prors1-2* after the dark period was reduced compared to *prors1-2* and *LHCB1.2*$_{pro}$*:LUC prors1-2*, and the content after 9 h light exposure was higher than the content in *prors1-2* and *LHCB1.2*$_{pro}$*:LUC prors1-2* (Figure 17 A, B). For the *LHCB3*$_{pro}$*:LUC prors1-2* descending plants, *rls2(3)* showed a rescue compared to the parental line for both measurements, whereas *rls134* possessed less starch than *LHCB3*$_{pro}$*:LUC prors1-2* (Figure 18 A), once more corroborating previous results regarding a rescue phenotype of *rls2(3)*. The *rls* mutants derived from *LHCB1.2*$_{pro}$*:LUC prors1-2* were grouped into three subfamilies: the first group includes mutants that feature a similar starch content as Col-0 (*rls304*) or produced more starch than Col-0 during light exposure, when the starch amount at the end of the day was calculated proportionally to the content determined at the beginning of illumination (Figure 18 B; *rls316*, *rls436*, *rls666*, *rls716*). Hence, mutants from this subgroup – interestingly including *rls436* – depict a clear rescue phenotype. The *rls* mutants with a slighter, however still detectable rescue effect, are summarized in the next group (Figure 18 C). Part of this group is *rls478*, for which a strong starch generation during illumination was observed, although the starch content after the

dark period was low. The last subgroup contains *rls* mutants with a lower starch content than the parental line *LHCB1.2*$_{pro}$*:LUC prors1-2*, and thus with no rescue phenotype (Figure 18 D; *rls2(1.2), rls336, rls463, rls608, rls615, rls621, rls744*).

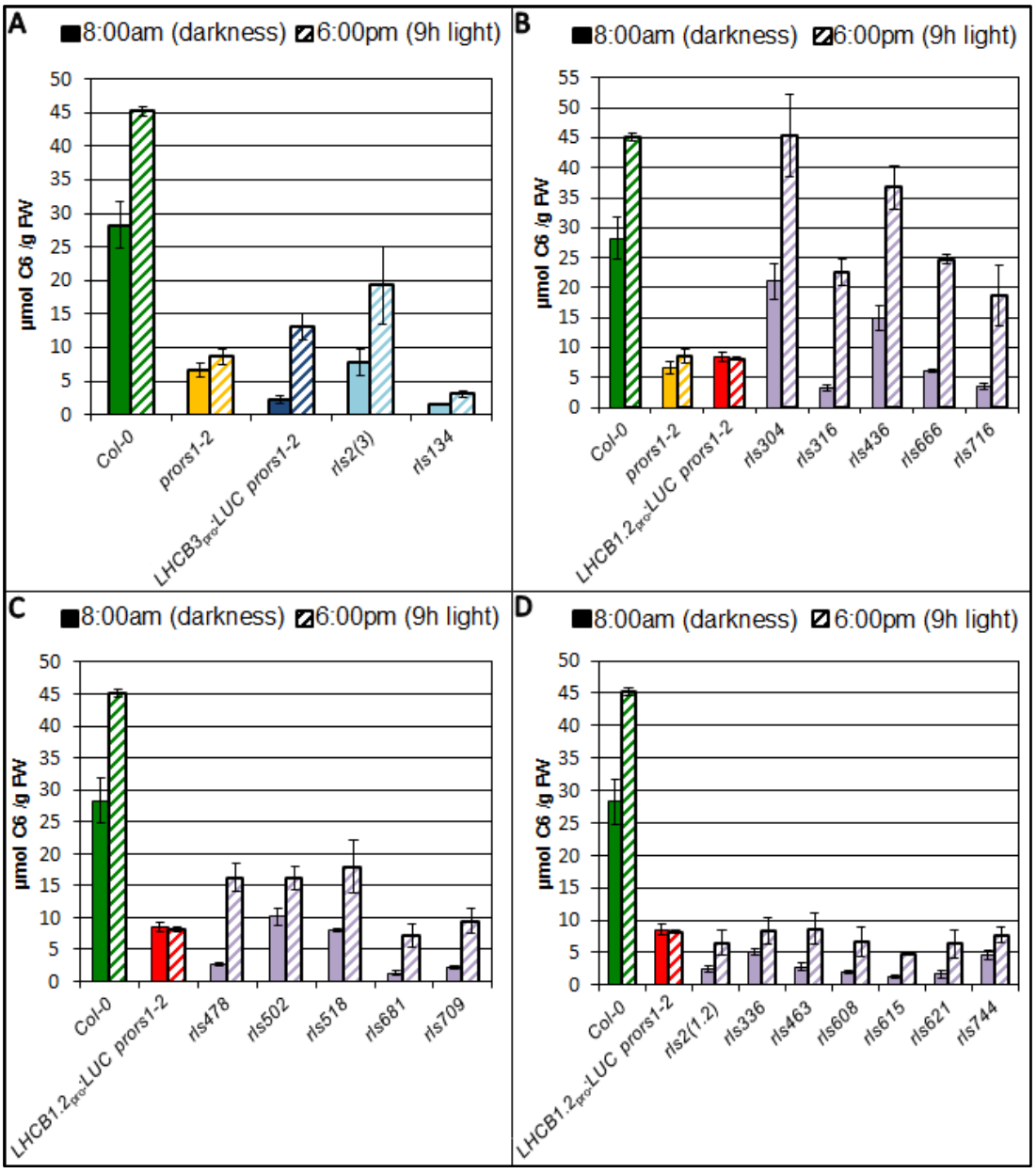

Figure 18: Determination of glucose content at the end of dark period (8 am, solid bars) and after 9 h of light (6 pm, scattered bars). The plants were grown under long-day conditions (16 h light 8 h dark) and harvested at day 28. From a pool of at least 10 plants, three technical replicates were measured (see methods). **A**: Glucose content of Col-0 (green), *prors1-2*(yellow), *rls2(3), rls134* (light blue) and their parental line *LHCB3*$_{pro}$*:LUC prors1-2* (dark blue). **B**: Glucose content of Col-0 (green), *prors1-2* (yellow), *LHCB1.2*$_{pro}$*:LUC prors1-2* (red) and *rls* mutants showing wild type behavior, especially regarding the ratio between the two time points (lilac). **C**: Glucose content of Col-0 (green), *LHCB1.2*$_{pro}$*:LUC prors1-2* (red) and *rls* mutants showing a slight rescue (lilac). **D**: Glucose content of Col-0 (green), *LHCB1.2*$_{pro}$*:LUC prors1-2* (red) and *rls* mutants (lilac) with less starch than their parental line *LHCB1.2*$_{pro}$*:LUC prors1-2*.

Thus, it can be concluded that once more *rls2(3)*, *rls436* and *rls478* are good candidates for containing interesting rescue mutations, however, for *rls304* a strong rescue effect regarding starch synthesis was observed as well.

3.2.8 Crossing of *rls* mutants to analyze complementation

So far, several *rls* mutants proved to be good candidates for possessing mutations causing a rescue effect. To determine if the different *rls* mutants do not comprise the same mutations, which were responsible for their respective rescue phenotypes, the *rls* mutants were crossed with each other. For this approach, the 19 *rls* mutants were grouped into 8 classes (Table 18), and mutants within one class were controlled for complementation via crossing. By sorting the mutants into subgroups, the number of crossings was reduced from 171 to 23. The parameters used for classification included (i) the expression level of nuclear-encoded photosynthetic genes, (ii) the maximum quantum yield of PSII (F_v/F_m) and (iii) the growth behavior (leaf size and color at day 21). For none of the resulting F1 and F2 generations of the crossings, a complementational phenotype was observed, suggesting that none of the mutants contained the same allele for one of the rescue mutations.

Table 18: Grouping of *rls* mutants. The *rls* mutants were grouped into 8 classes, dependent on whether they showed a rescue (+) compared to their parental line ($_{pro}$*:LUC prors1-2*) or not (0). The parameters used for classification were the expression of nuclear-encoded photosynthesis genes, the maximum quantum yield of PSII (F_v/F_m) and the growth performance.

class	1	2	3	4	5	6	7	8
expression of photosynthetic genes (nucleus)	+	+	+	+	0	0	0	0
photosynthesis F_v/F_m	+	+	0	0	+	+	0	0
growth performance	+	0	+	0	+	0	+	0
number of mutants	**1**	**1**	**1**	**4**	**2**	**4**	**1**	**5**
	rls2(3)	*rls615*	*rls478*	*rls316* *rls608* *rls621* *rls716*	*rls436* *rls518*	*rls134* *rls2(1.2)* *rls336* *rls666*	*rls681*	*rls304* *rls463* *rls502* *rls709* *rls744*

3.2.9 Summary of characterization data of *rls* mutants showing different rescue phenotypes

To get an overview of the different rescue phenotypes of the *rls* mutants presented in this chapter compared to their parental lines (*LHCB3*$_{pro}$*:LUC prors1-2* and *LHCB1.2*$_{pro}$*:LUC prors1-2*), the obtained results are summarized in Table 19 and 20. The data used for this evaluation included the growth curves, the maximum quantum yield (F_v/F_m), the sum of chlorophyll *a* and *b* (chl (*a* + *b*)), the starch content and the expression level of the *LHCB*s (Northern blots).

Regarding the *LHCB3*$_{pro}$*:LUC prors1-2* derived lines, the summary clearly demonstrates that *rls2(3)* features a rescue phenotype for all parameters determined, except for the *LHCB* transcript expression level, whereas *rls134* showed a rescue only for the PSII performance (Table 19). This makes *rls2(3)* an ideal candidate for further investigation, especially for the identification of the mutation responsible for this rescue phenotype.

Table 19: Summary of physiological characterization of Col-0, *prors1-2, LHCB3*$_{pro}$*:LUC prors1-2*, *rls2(3)* and *rls134*. The behavior of the *rls* mutants compared to *LHCB3*$_{pro}$*:LUC prors1-2* is depicted: like Col-0 = **++**, rescue effect = **+**, similar to *LHCB3*$_{pro}$*:LUC prors1-2* = **0**. The *rls2(3)* mutant is marked in red.

name	growth	PSII (F_v/F_m)	chlorophyll chl (*a* + *b*)	starch	*LHCB* expression
Col-0	++	++	++	++	++
LHCB3$_{pro}$*:LUC prors1-2*	0	0	0	0	0
rls2(3)	+	+	+	+	+
rls134	0	+	0	0	0
prors1-2	+	0	0	0	0

Two of the *LHCB1.2*$_{pro}$*:LUC prors1-2* originating *rls* mutants (*rls436* and *rls478*) possessed a strong growth rescue leading to a wild type (Col-0) like growth. Moreover, *rls436* and *rls518* showed a rescue phenotype for all parameters tested, except for *LHCB* mRNA expression, in contrast to *rls478* that exhibited a retarded PSII performance. Hence, this makes *rls478* an ideal candidate for the mapping approach to identify the mutation which is responsible for wild type like growth without featuring the same PSII performance. Another mutant showing a strong specific rescue effect was *rls304*, which comprised a wild type like starch content. However, the only other rescue phenotype observed referred to the chlorophyll content, thus this mutant was not chosen for further analysis.

Table 20: Summary of rescue phenotypes for *LHCB1.2*$_{pro}$*:LUC prors1-2* originating *rls* mutants. The behavior of the *rls* mutants compared to *LHCB1.2*$_{pro}$*:LUC prors1-2* is depicted: like Col-0 = **++**, rescue effect = **+**, similar to *LHCB3*$_{pro}$*:LUC prors1-2* = **0**. The strongest effects (like Col-0= ++) are marked in dark green. The two lines with a growth performance comparable to Col-0 are highlighted in light green.

name	growth	PSII (F_v/F_m)	chlorophyll chl (*a* + *b*)	starch	*LHCB* expression
Col-0	++	++	++	++	++
prors1-2	0	0	0	0	0
LHCB1.2$_{pro}$*:LUC prors1-2*	0	0	0	0	0
rls2(1.2)	0	+	0	0	0
rls304	0	0	+	++	0
rls316	0	0	+	+	+
rls336	0	+	0	0	0
rls436	++	+	+	+	0
rls463	0	0	0	0	0
rls478	++	0	+	+	+
rls502	0	0	0	+	0
rls518	+	+	+	+	0
rls608	0	0	+	0	+
rls615	0	+	+	0	+
rls621	0	0	+	0	0
rls666	0	+	0	+	0
rls681	+	0	+	0	0
rls709	0	0	+	0	0
rls716	0	0	+	+	+
rls744	0	0	+	0	0

3.3 Towards the identification of mutations responsible for the rescue phenotypes of *rls2(3)* and *rls478*

Another aim of this thesis was the genetic localization of the mutation which is responsible for the respective *rls* phenotype. For this purpose, the lines *rls2(3)* and *rls478* were chosen, as they showed the best rescue effect for the measured PSII parameter F_v/F_m or featured wild type like growth curves, respectively. To identify the chromosome to which the rescue mutation is linked, rough mapping was carried out. This approach was also conducted for *rls2(1.2)*. Additionally, to precisely localize the mutation, next generation sequencing with subsequent bioinformatic analyses was performed for the mutants *rls2(3)* and *rls478*.

3.3.1 Rough mapping of *rls2(3)*, *rls2(1.2)* and *rls478*

To link the suppression mutation to one specific chromosome, a positional cloning approach was realized for the *rls2(3)*, *rls2(1.2)* and *rls478* mutants. For this purpose, the respective *rls* mutants were crossed with the L*er* accession. In the resulting F2 generation, plants were selected, which displayed the same phenotype (growth, leave shape and color) as their *rls* mutant parent. These plants were additionally analyzed with regard to the *prors1-2* T-DNA insertion via PCR, to ensure that only plants containing both mutations were selected for mapping. Leaves with the same size from at least 80 plants from this subset were pooled and DNA was extracted.

Positional cloning takes advantage of the natural polymorphisms between the various *Arabidopsis thaliana* accessions. The L*er* accession was chosen for crossing with the *rls* mutants, because crossing of Col-0 (in this case the background of the *rls* mutants) and L*er* is most commonly used for mapping approaches, and therefore a variety of markers are already known for this constellation (Chang et al. 1988; Konieczny and Ausubel 1993; Hardtke et al. 1996; Pingli Lu et al. 2012). For this study, only simple sequence length polymorphism (SSLP) markers (downloaded from The Arabidopsis Information Research (Tair) homepage: http://www.arabidopsis.org/servlets/Search?action=new_search&type=marker) were applied: the nucleotide repeats possess a different length in the respective *Arabidopsis thaliana* accessions; hence they can be easily detected and distinguished by PCR (Lukowitz et al. 2000). As homozygous controls, both parental lines used to generate the mapping populations, i.e. the *rls* mutant and the L*er* wild type*,* were used. The F1 generation was utilized as the heterozygous control, which therefore displayed two signals, one resembling the Col-0 accession (the *rls* mutant) and one the L*er* accession. The F2 generation should generally be heterozygous as well, with the exception of the region where the mutation is located: this is supposed to be homozygous for the mutation, because no recombination is thought to occur in this region (Figure 3). Most of the PCRs and the agarose gel electrophoreses were performed under my supervision by Bachelor students Max Fürst (*rls2(3)*) Peter Hagl (*rls2(1.2)*) and Jasmin Waldow (*rls478*).

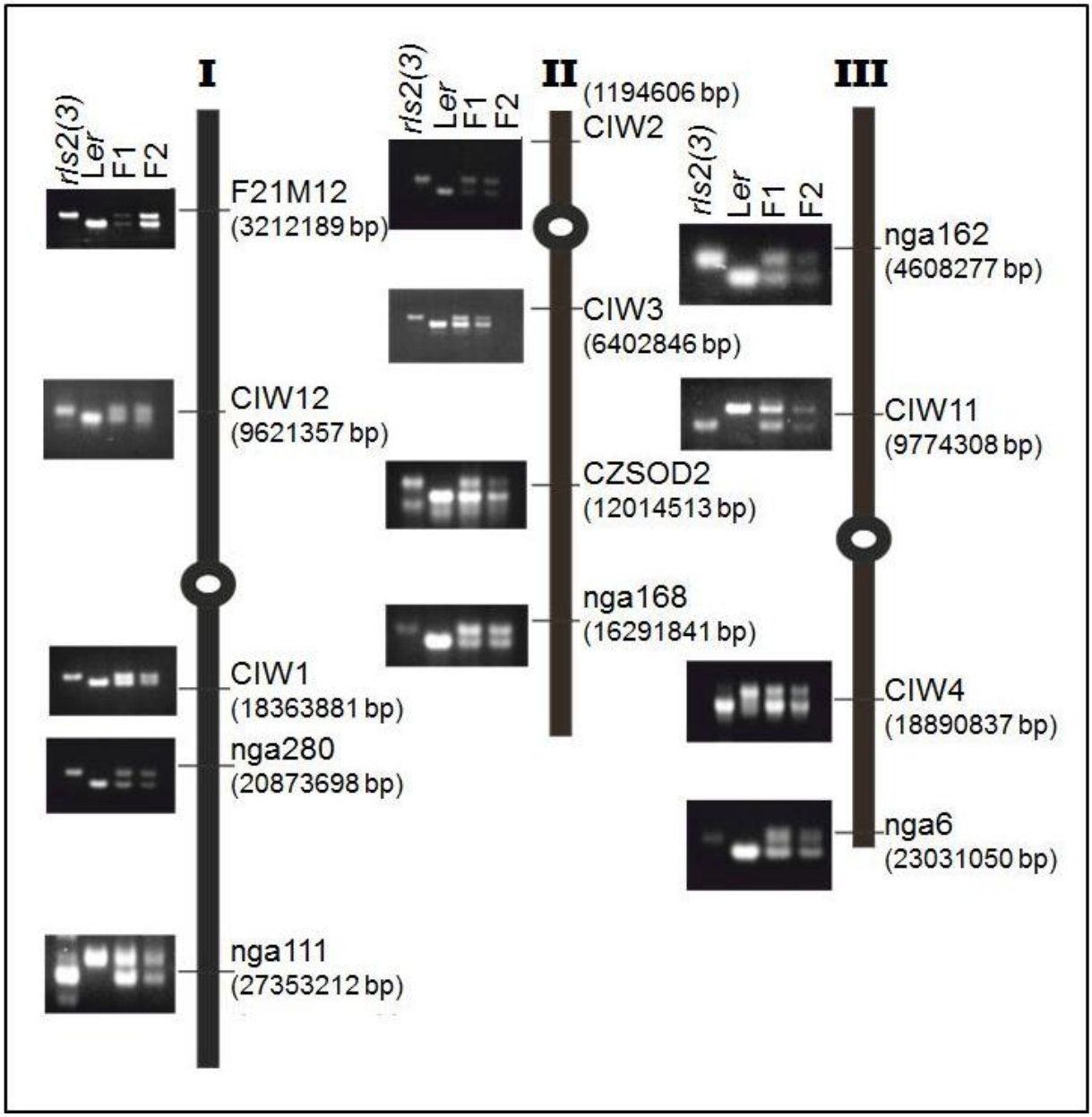

Figure 19: Positional cloning (rough mapping) to identify the rescue mutation of *rls2(3)* using SSLP markers for chromosomes I, II and III. For each chromosome **I**, **II** and **III**, the separated PCR-products are depicted on the left side, whereas the right side includes the markers and their respective position. For the positional cloning (see methods 2.2.2.3), isolated DNA from leaves of L*er* and *rls2(3)* (as homozygous control), of the F1 generation (as the heterozygous control) as well as of the pool of the F2 generation was used for the analyses of the SSLP markers via PCR.

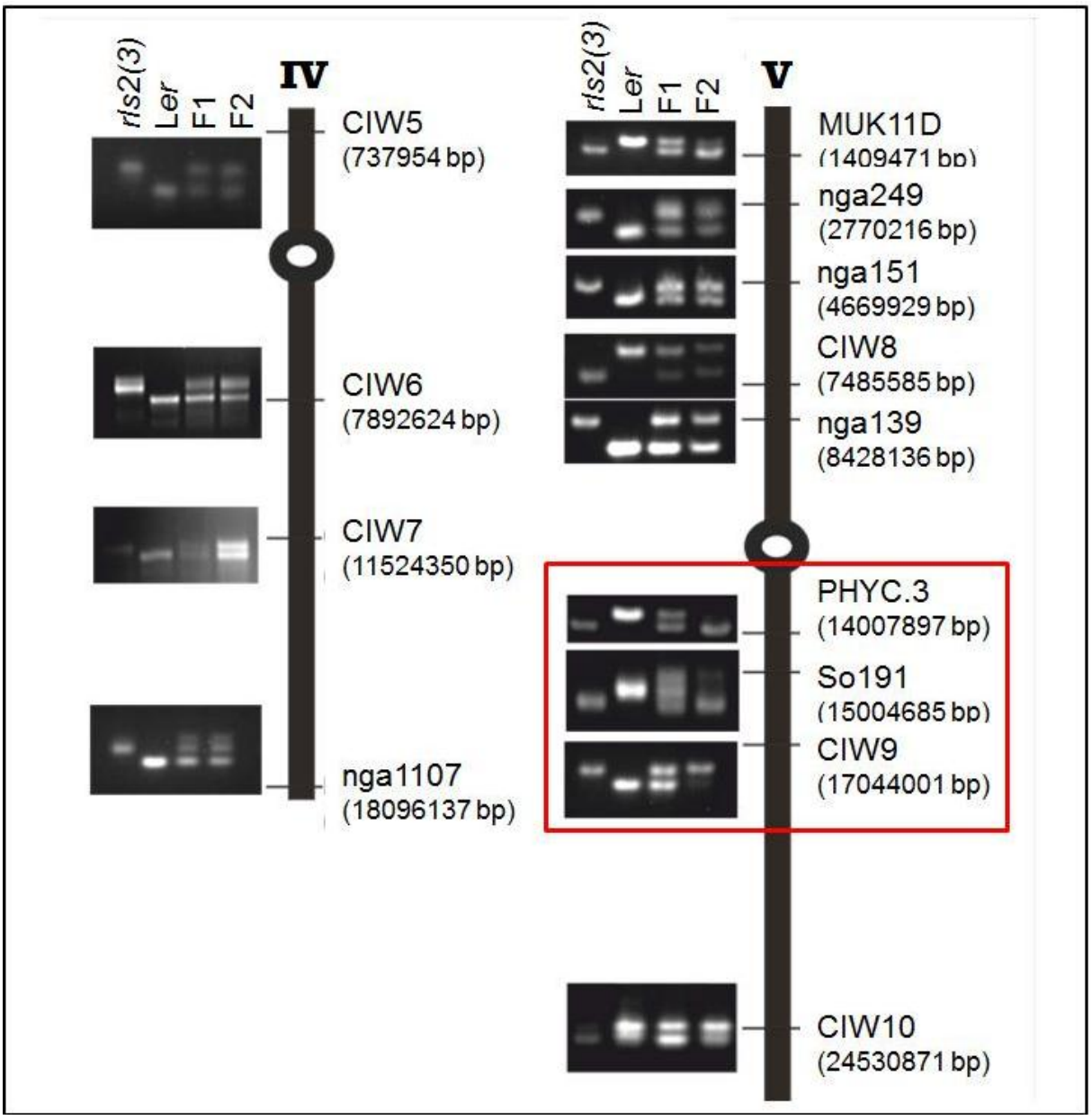

Figure 20: Positional cloning (rough mapping) to identify the rescue mutation of *rls2(3)* using SSLP markers for chromosomes IV and V. For each chromosome **IV** and **V**, the separated PCR-products are depicted on the left side, whereas the right side includes the markers and their respective position. For the positional cloning, isolated DNA from leaves of L*er* and *rls2(3)* (as homozygous control), of the F1 generation upon crossing of both (as the heterozygous control) as well as of the pool of the F2 generation was used for the analyses of the SSLP markers via PCR. The region identified as location of the mutation is marked by a red box.

For the *rls2(3)* mutant, the rough mapping approach revealed that the mutation is located on chromosome **V**, as applying the markers PHYC.3 (position: 14007897bp) and CIW9 (170044001bp) depicted a homozygous signal (Figure 20). Moreover, the marker So191 (15004685bp) that is located in between these markers showed the homozygous pattern as well. These data allowed linking the mutation to a 3 mb

(megabase) region near the centromere at the lower arm of chromosome **V**. To confirm this and to narrow down the region at chromosome **V**, more markers were used for this chromosome than for the others (Figures 19, 20).

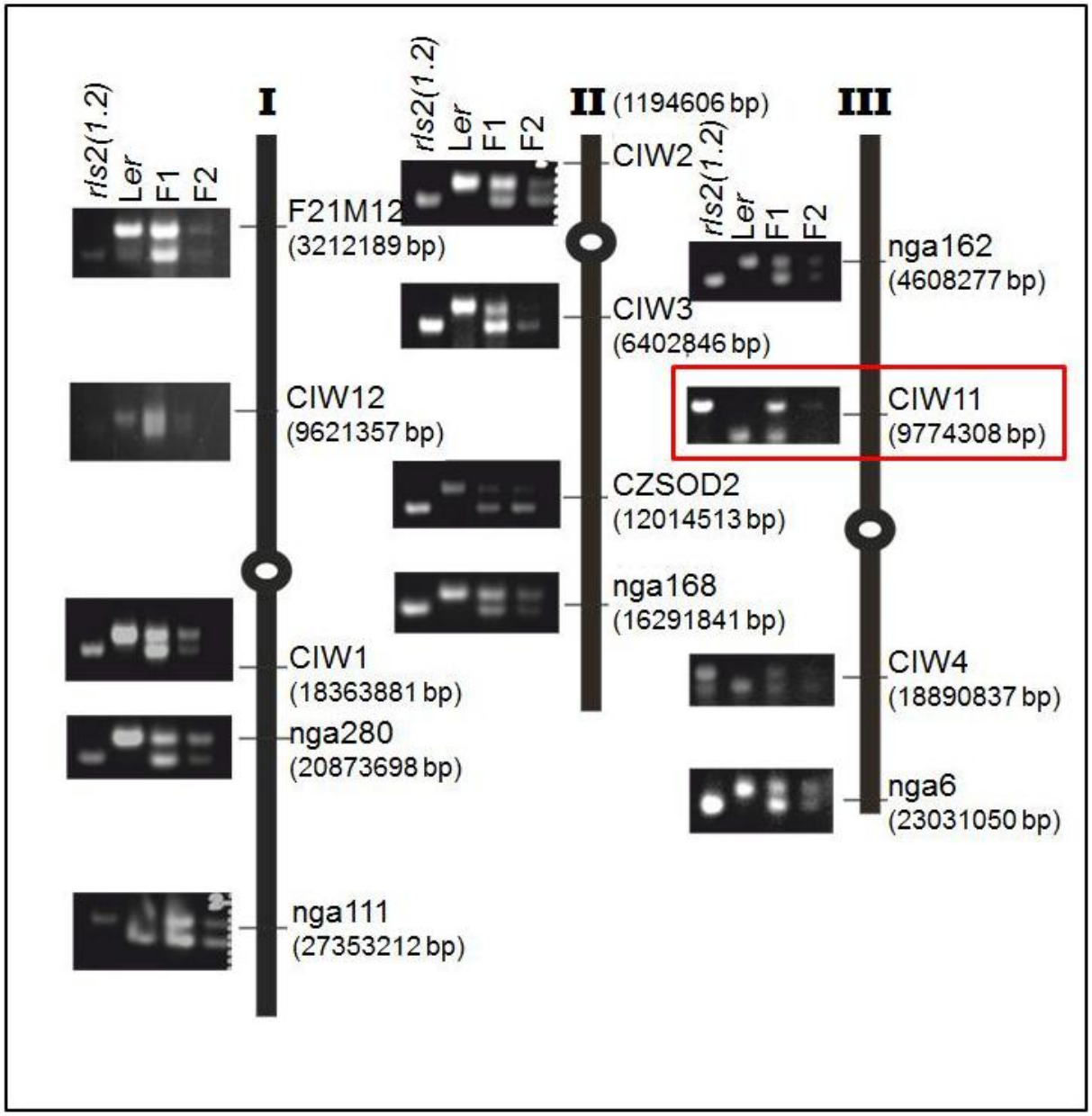

Figure 21: Positional cloning (rough mapping) to identify the rescue mutation of *rls2(1.2)* using SSLP markers for chromosomes I, II and III. For each chromosome **I**, **II** and **III**, the separated PCR-products are depicted on the left side, whereas the right side includes the markers and their respective position. For the positional cloning, isolated DNA from leaves of L*er* and *rls2(1.2)* (as homozygous control), of the F1 generation upon crossing of both (as heterozygous control) as well as of the pool of the F2 generation was used for the analyses of the SSLP markers via PCR. The region identified as potential location of the mutation is marked by a red box.

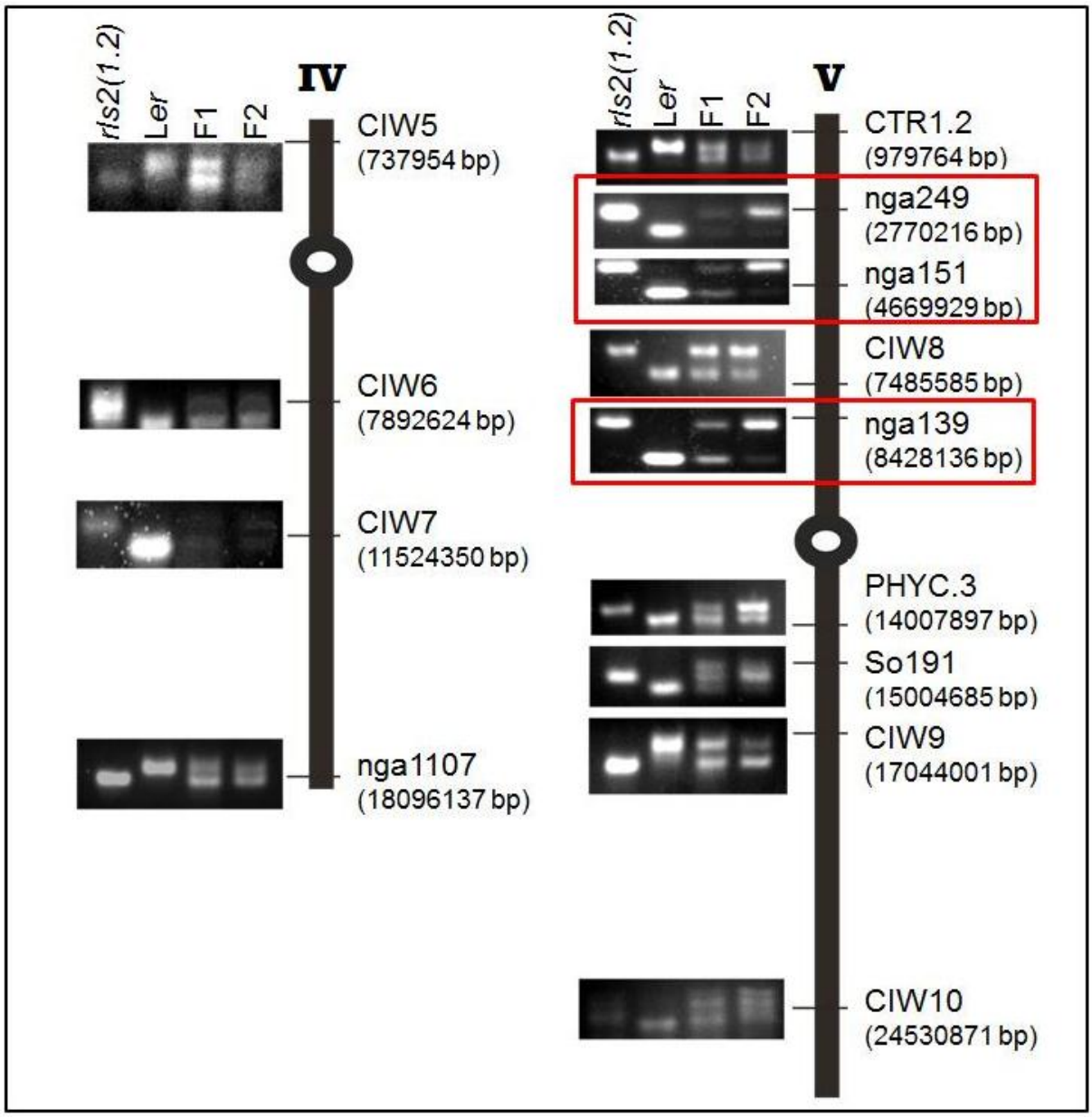

Figure 22: Positional cloning (rough mapping) to identify the rescue mutation of *rls2(1.2)* using SSLP markers for chromosomes IV and V. For each chromosome **IV** and **V**, the separated PCR-products are depicted on the left side, whereas the right side includes the markers and their respective position. For the positional cloning, isolated DNA from leaves of L*er* and *rls2(1.2)* (as homozygous control), of the F1 generation upon crossing of both (as heterozygous control) as well as of the pool of the F2 generation was used for the analyses of the SSLP markers via PCR. The region identified as potential location of the mutation is marked by a red box.

For the *rls2(1.2)* mutant, chromosome **I**, **II** and **IV** could be excluded as mutation sites (Figures 21, 22). On chromosome **III** however, the marker CIW11 (9774308bp) showed a homozygous signal when using DNA from the F2 generation as template, but as the signal was very weak, it was not possible to draw an unambiguous conclusion (Figure 21). On chromosome **V**, the region around the marker So191

(15004685bp), where the mutation was mapped for *rls2(3),* could be excluded, whereas the markers nga249 (2770216bp), nga151 (4669929bp) and nga139 (8428136bp) located at the upper arm of chromosome **V** showed a weak homozygous signal (Figure 22). Although the data indicate that the mutation is most likely located on this region on chromosome **V**, more regions have to be considered and analyzed in more detail to clearly identify the rescue mutation of *rls2(1.2)*.

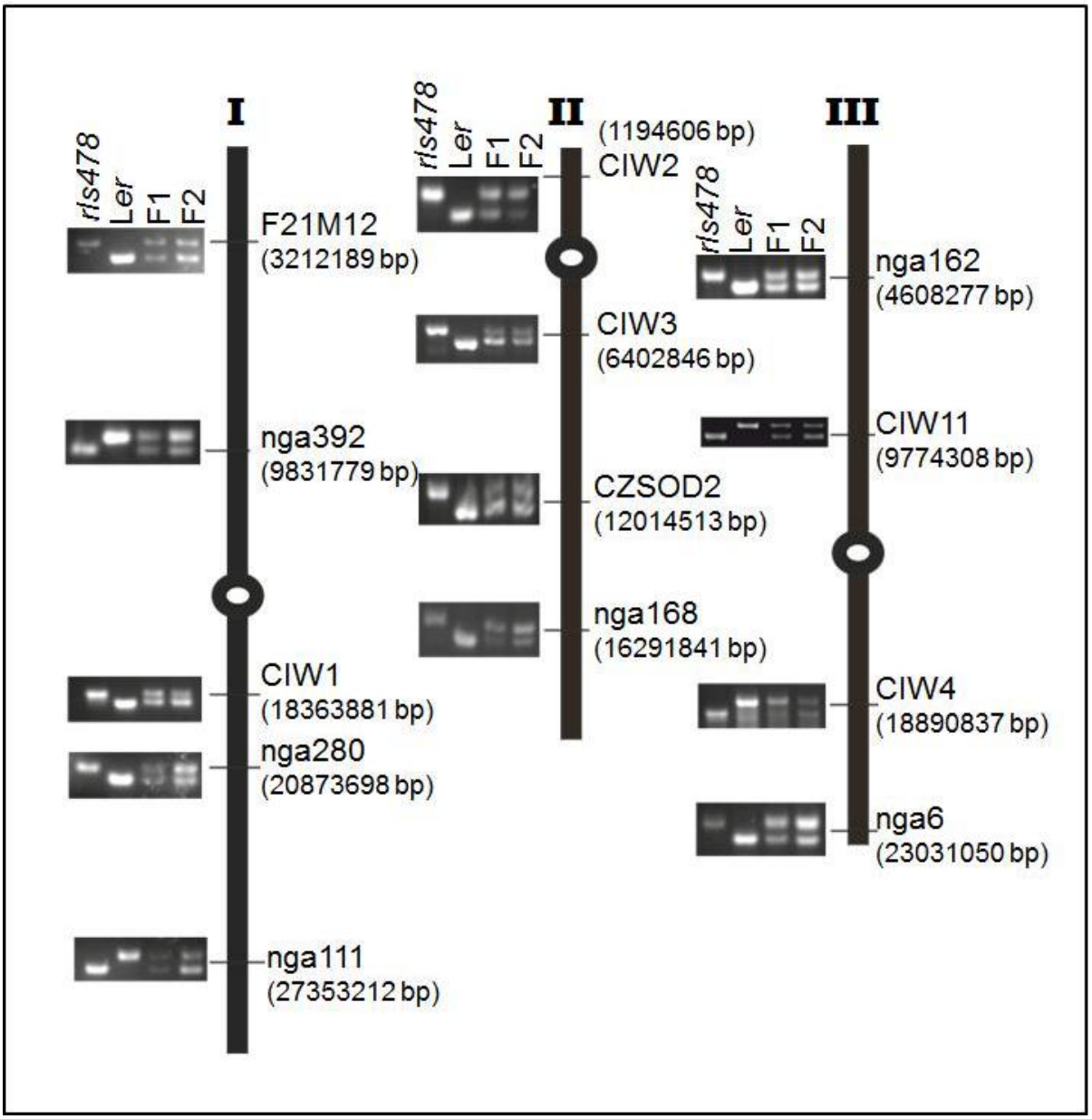

Figure 23: Positional cloning (rough mapping) to identify the rescue mutation of *rls478* using SSLP markers for chromosomes I, II and III. For each chromosome **I**, **II** and **III**, the separated PCR-products are depicted on the left side, whereas the right side includes the markers and their respective position. Isolated DNA from leaves of L*er* and *rls478* (as homozygous control), of the F1 generation upon crossing of both (as heterozygous control) as well as of the pool of the F2 generation was used for the analyses of the SSLP markers via PCR.

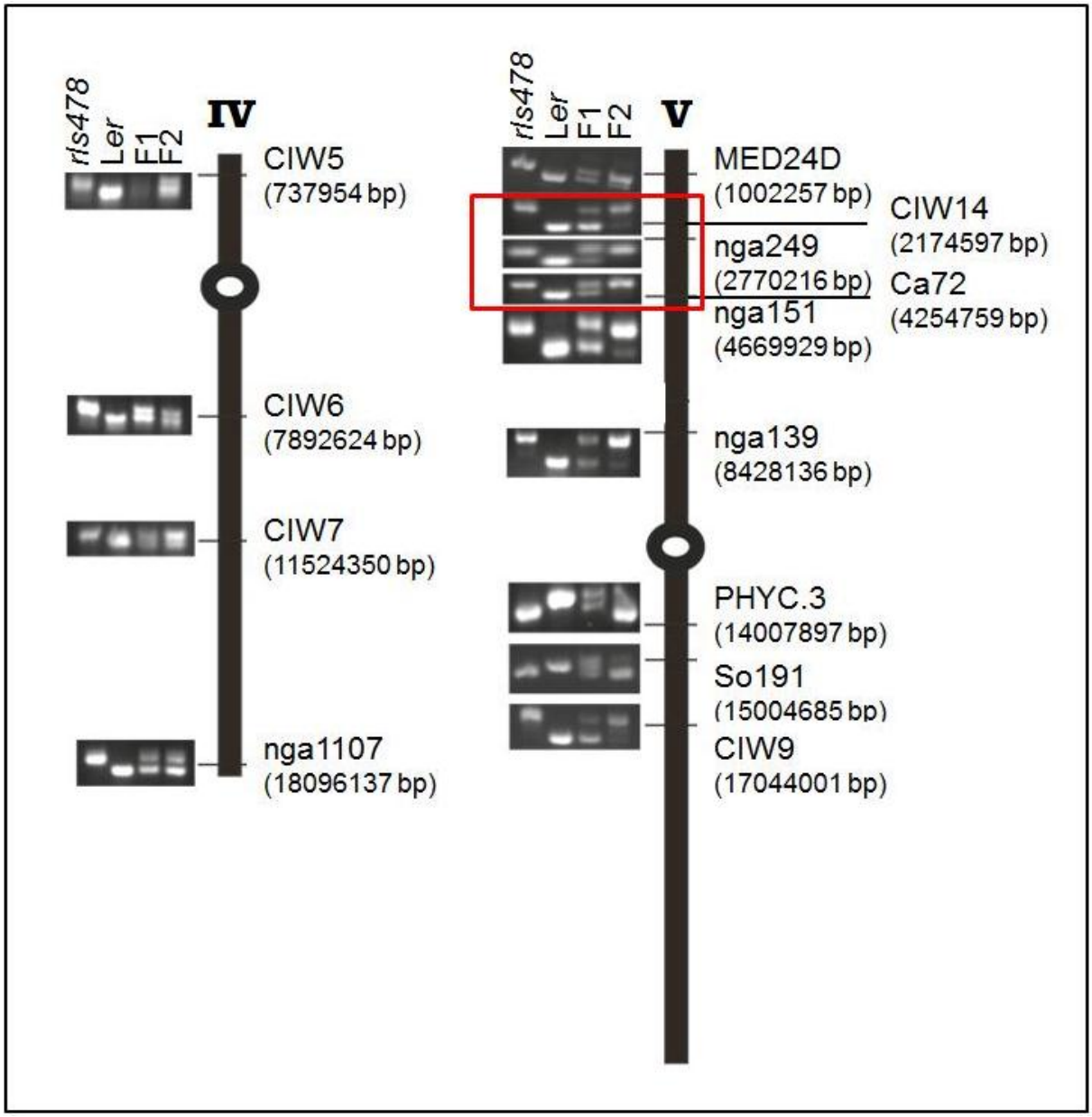

Figure 24: Positional cloning (rough mapping) to identify the rescue mutation of *rls478* using SSLP markers for chromosomes IV and V. For each chromosome **IV** and **V**, the separated PCR-products are depicted on the left side, whereas the right side includes the markers and their respective position. For the positional cloning, isolated DNA from leaves of L*er* and *rls478* (as homozygous control), of the F1 generation upon crossing of both (as the heterozygous control) as well as of the pool of the F2 generation was used for the analyses of the SSLP markers via PCR. The region identified as location of the mutation is marked by a red box.

When investigating the mapping population of *rls478,* chromosomes **I**, **II**, **III** and **IV** could be excluded, as all tested markers from these chromosomes clearly showed heterozygous signals (Figures 23, 24). Moreover, the rescue mutation for the *rls478* mutant was found to be linked to a 2 mb large region at the upper arm of

chromosome **V**, located between the markers nga249 (2770216bp) and Ca72 (4254759bp) (Figure 24). CIW14 (2174597bp), a marker close to nga249 at the telomeric site, showed a tendency towards homozygocity as well, whereas the adjacent marker MED24D (1002257bp) gave a clear heterozygous signal. A similar situation was observed for the centromeric site. Generally, all markers from the lower arm of chromosome **V** gave relatively weak signals, however they appeared rather heterozygous than homozygous. For the only marker available for the telomeric region of the lower arm from chromosome **V** CIW10 (24530871bp), no signal was detected with the rough mapping approach.

Summing up, it can be concluded that the mutated loci of *rls2(3)*, *rls2(1.2)* and *rls478* responsible for the rescue were successfully localized to certain chromosomal regions via positional cloning. However, for *rls2(1.2)*, further markers have to be used in the future to unambiguously clarify the localization. Interestingly, all mutations were found to be most probably linked to chromosome **V**, although to different regions.

3.3.2 Using next generation sequencing to fine map *rls2(3)* and *rls478*

In this thesis, the next generation sequencing technology was used to perform the fine mapping, as this allows conducting the mapping with the information obtained from the SNPs detected in the respective sequence; hence the sequence information is already in hand. The mutants *rls2(3)* and *rls478* were chosen for fine mapping because (i) they could be clearly linked to one specific region at chromosome **V** via rough mapping, which simplifies the fine mapping approach, and (ii) both mutants showed a very interesting rescue, *rls2(3)* in regard to the PSII parameters (F_v/F_m) and *rls478* concerning the growth behavior (like Col-0). Another benefit of analyzing these two *rls* mutants was that they originate from the two different $_{pro}$*:LUC prors1-2* lines: *rls2(3)* from *LHCB3*$_{pro}$*:LUC prors1-2* and *rls478* from *LHCB1.2*$_{pro}$*:LUC prors1-2*. Thus, it was expected that the promoter-luciferase constructs could be mapped with this approach as well, which was so far impossible by positional cloning or genome walking

3.3.2.1 SOLiD™ sequencing of *rls2(3)* and *rls478*

Genomic DNA isolated of both F2 generations from the mapping population of *rls2(3)* and *rls478* was sent for SOLiD™ sequencing to the sequencing service facility at the

Universität Düsseldorf (see methods chapter 2.2.4.1). For *rls2(3),* more than 88 million single reads and for *rls478,* more than 114 million single reads resulted from the sequencing run (Table 21).

Table 21: The output of the SOLiD™ sequencing (Life Technologies) for *rls2(3)* and *rls478*. The read number was in range (100000000 reads ± 25 %).

mutant	number of reads	number of mapped reads	mean depth	genome coverage
rls2(3)	88297875	37873634	22	97%
rls478	114042728	57427747	33	97%

All bioinformatical analyses of the sequencing data was performed with the CLC Genomics Workbench software (www.CLCbio.com). In the following course of this, the reads were mapped to the *Arabidopsis thaliana* genome, which was downloaded from the Tair homepage (ftp://ftp.arabidopsis.org/home/tair/Sequences/whole_chromosomes/). The low number of mapped reads resulted from the heterozygous DNA from the F2 generation used for the experiment. Approximately half of the reads were mapped to the Col-0 genome (Tair9), and the other reads were found to be mapped to the L*er* genome (data not shown). However, the sequencing depth and genome coverage was still high enough to perform fine mapping (Table 21).

3.3.2.2 Detection and filtering of SNPs for *rls2(3)* and *rls478* mutants

The determination of SNPs (named also SNP calling) was performed with the probabilistic variant plug in from the CLC genomics workbench (see methods chapter 2.2.4.1.1). The number of SNPs per chromosome was found to correlate with the respective size (length in bp), except for chromosome **V** (Tables 22, 23): the amount of SNPs of the *rls2(3)* data detected for chromosome **V** was reduced to the number of SNPs for chromosome **IV**, although chromosome **IV** is 30% smaller (shorter) than chromosome **V**. For the *rls478* dataset, the number of SNPs determined for chromosome **V**, was merely ~ 10% of the expected number for this chromosome, deduced from the data of the other four chromosomes.

Table 22: SNP calling for the *rls2(3)* mutant. The analysis was performed with the CLC genomics workbench (CLC bio). The number of the SNPs correlated to the chromosome size (length), except for chromosome **V**. The ratio between SNPs, which were derived from the crossing of the wild type accessions Col-0 with L*er* and EMS induced SNPs is for all chromosomes ~ 6:4.

chromosome	number of SNPs	number of L*er*-SNPs	number of EMS-induced SNPs
I	89147	54242 (61%)	34905 (39%)
II	24855	15441 (62%)	9414 (38%)
III	59579	36357 (61%)	23222 (39%)
IV	61458	35794 (58%)	25664 (42%)
V	60100	36986 (61%)	23114 (39%)

The low number of SNPs at chromosome **V** might be due to a very low recombination rate during meiosis for this chromosome. The sequence data showed that chromosome **V** was almost homozygous for the *rls478* mutant, and for *rls2(3)* there was a clear tendency to the Col-0 sequence for chromosome **V**. A reason for this could be that both mutation sites, the T-DNA insertion in the *PRORS1* gene and the rescue mutation, are located on chromosome **V** and were found to be linked; hence the selection of the mapping population was excluding plants with recombination events at chromosome **V**, because they were selected to contain both mutations (see methods chapter 2.2.4.1.2).

Table 23: SNP calling for the *rls478* mutant. The analysis was carried out with the CLC genomics workbench (CLC bio). The number of the SNPs correlated to the chromosome size (length), except for chromosome **V**. Chromosome **V** was found to be ~ 90 % identical to the Col-0 sequence, which explains the low SNP number and the turned around ratio (3:7) between SNPs, which were derived from the crossing of the wild type accessions Col-0 with L*er* and EMS induced SNPs.

chromosome	number of SNPs	number of L*er*-SNPs	number of EMS-induced SNPs
I	83180	52278 (63 %)	30902 (37 %)
II	43887	29233 (67 %)	14654 (33 %)
III	53664	34219 (64 %)	19445 (36 %)
IV	52265	31840 (61 %)	20425 (39 %)
V	8051	2520 (31 %)	5531 (69 %)

To distinguish between the SNPs derived from the crossing of the *rls* mutants with L*er* and the EMS-induced SNPs, the SNP collection for L*er* from Lu et al. 2012 (http://www.personal.psu.edu/hxm16/suppdatafile.zip) was used. The ratio between the L*er* SNPs and EMS-induced SNPs was for all chromosomes approximately 6:4,

except for chromosome **V** of *rls478* (see Tables 22, 23). Because of a sequence identity of ~ 90% of the sequence of chromosome **V** from the *rls478* mapping population and the Col-0 sequence, the ratio of the SNPs was in this case found to be 3:7.

3.3.2.3 Identification of EMS-induced SNPs possibly responsible for the *rls* phenotypes of mutants *rls2(3)* and *rls478*

In order to reduce the number of SNPs, which could be responsible for the *rls* phenotype, more filtering steps were performed. To separate the EMS-induced SNPs from other SNPs, *e.g.* sequencing errors, only SNPs including changes from guanine (G) to adenine (A) or cytosine (C) to thymine (T) remained in the analysis, which are known to constitute more than 99 % of EMS-induced SNPs (Green et al. 2003). In the last filtering step, only SNPs were selected with a coverage of > 10 and a frequency of > 90%, meaning that the SNP is covered by 10 sequencing reads or more and 9 out of 10 nucleotide transitions are identical.

Table 24: Description and localization of EMS-induced SNPs as possible candidates for the *rls* phenotype of *rls478.* Depicted are the candidates, which showed a coverage of > 10 (the SNP is covered from 10 sequencing reads or more), a frequency of 100 % of the mutated allele, and whether the SNP is located in a coding region leading to an amino acid change. The nucleotide change was either from cytosine (C) to thymine (T) or guanine (G) to adenine (A). The most likely candidate for causing the *rls478* phenotype is highlighted in red.

chromosome	reference position (bp)	nucleotide change	amino acid change	locus
1	6790420	C/T	Ala/Val	*AT1G19640*
3	15142935	G/A	Ala/Thr	*AT3G43148*
4	12087278	C/T	Ser/Leu	*AT4G23060*
4	12087281	C/T	Ala/Val	*AT4G23060*
4	17276567	G/A	Ala/Thr	*AT4G36630*
4	9227408	G/A	Asp/Asn	*AT4G16330*
4	2715173	C/T	His/Tyr	*AT4G05310*
5	**2906927**	**C/T**	**Glu/stop**	***AT5G09360***
5	**14327194**	**G/A**	**Gln/Gln**	***AT5G36320***

After these filtering steps, 115 candidate SNPs (chromosome **I** = 30; **II** = 5; **III** = 8; **IV** = 46; **V** = 26) remained for *rls478*. Regarding the localization of the SNPs, first it was determined whether they were located to a gene. Second, if localization to a gene was observed, it was analyzed whether they located to an exon or an intron.

The SNPs which were located in an exon were subsequently analyzed if they were responsible for an amino acid change. The resulting candidate SNPs, potentially including the one responsible for the *rls* phenotype of *rls478,* are listed in Table 24. All of them were found to be located in an exon and led to an amino acid change.

Out of these candidates, the SNP at position 2906927 was the only SNP located in the region of chromosome **V**, which was previously identified with the rough mapping approach (Figure 24). This mutation is located in the 5th of 6 exons of gene *AT5G09360* and results in a stop codon instead of a glutamic acid. *AT5G09360* encodes for the *LACCASE14* (*LAC14*) gene, which belongs to the laccase gene family (Cai et al. 2006; Turlapati et al. 2011). Hence, this mutation is the best candidate to be responsible for the *rls* phenotype of *rls478*.

For *rls2(3),* 126 candidate SNPs (chromosome **I** = 26; **II** = 19; **III** = 12; **IV** = 39; **V** = 30) remained after the filtering steps mentioned above. In Table 25, all candidates are listed which were located in an exon and led to a codon change.

Table 25: EMS induced SNPs and their localization as possible candidates for the rls phenotype of *rls2(3).* Depicted are the candidates which showed a coverage higher than 10 (the SNP is covered from 10 sequencing reads or more), a frequency of 90 % of the mutated allele, and where the SNP is located in a coding region leading to an amino acid change. The nucleotide change occurred either from cytosine (C) to thymine (T) or guanine (G) to adenine (A). The most likely candidate for causing the *rls2(3)* phenotype is highlighted in red.

chromosome	reference position (bp)	nucleotide change	amino acid change	locus
4	17361415	G/A	Gly/Arg	*AT4G36860*
4	9227408	G/A	Asp/Asn	*AT4G16330*
4	12087281	C/T	Ser/Leu	*AT4G23060*
4	12087278	C/T	Ala/Val	*AT4G23060*
4	8980228	C/T	Arg/Cys	*AT4G15780*
5	**2906927**	**C/T**	**Glu/Glu**	***AT5G09360***
5	1097774	C/T	Thr/Ile	*AT5G04050*
5	4896800	G/A	Val/Ile	*AT5G15110*
5	**14327194**	**G/A**	**Gln/stop**	***AT5G36320***

Only one of these SNPs was found to be located in the region on chromosome **V,** which was determined by rough mapping (Figure 20). This candidate SNP at position 14327194 leads to a stop codon instead of a glutamine and is located in the exon of the *AT5G36320* gene. *AT5G36320* encodes for an ECA1 gametogenesis-related family protein with an unknown function. These mapping results make the mutation in

the *AT5G36320* gene the most likely candidate to be responsible for the *rls* phenotype of *rls2(3)*. However, this mapping data has to be confirmed via complementation experiments in the future.

4. Discussion

During evolution, the conversion from endosymbiont to the organelle was accompanied by a massive genomic transfer from the organelles to the nucleus. Therefore, signaling pathways evolved to mediate the communication between the cell compartments (Kleine et al. 2009). Today, most of the organelle-located proteins are encoded in the nucleus (Abdallah et al. 2000); hence the signaling pathways from the organelles to the nucleus (retrograde signaling), which deliver information about the developmental stage of the organelles or environmental influences are crucial for plants to react accordingly (Pogson et al. 2008). The *prors1-2* mutant is a very good candidate for research of the translation-dependent retrograde signaling pathways, due to its reduced organelle translation in both chloroplasts and mitochondria (Pesaresi et al. 2006) without the need of applying herbicides such as lincomycin or norflurazon.

From a genetic screen of mutagenized *prors1-2* mutants performed in this study, 19 *rls* (*relaxed LHCB suppression*) mutants were selected for further physiological characterization. The two mutants showing the most interesting phenotypes (*rls2(3)* and *rls478*) were mapped to localize the respective suppression mutation, which play most likely a role in the translation-dependent signaling process. The mutant *rls2(3)* possessed the best PSII performance of all 654 measured mutants, which is almost equal to wild type (Col-0) level. However, this mutant could not convert the energy generated by photosynthesis into growth, as its growth performance remained retarded compared to Col-0 (Figure 9), especially under short-day conditions (Figure 10 B). The very strong rescue effect in PSII activity for *rls2(3)* with regard to its parental line *LHCB3*$_{pro}$*:LUC prors1-2* might be due to the strong rescue of the *LHCB1.2* transcript and presumably other transcripts compared to *LHCB3*$_{pro}$*:LUC prors1-2* (Figure 16). However, as the other tested transcripts showed no (*PSAK and PSBO*) or just a slight (*LHCB3*) rescue in expression (Figure 16), the assumption can be drawn that this is not the only reason for the increase in PSII performance of ~40% (Table 26).

The mutants *rls478* and *rls436* both feature wild type like growth rates including the same time point of flowering, therefore they possess the best growth rescue of the 19 selected *rls* mutants compared to their parental line (*LHCB1.2*$_{pro}$*:LUC prors1-2*) (Figure 11). Interestingly, in regard to the PSII performance, both mutants show no

rescue compared to *LHCB1.2*$_{pro}$*:LUC prors1-2*, especially *rls478,* which has an even worse performance than *rls436* (Table 15). Nevertheless, these mutants feature differences in the starch content: whereas the amount of starch determined for *rls436* is almost at the wild type level, the starch content of *rls478* is much lower than the wild type (Figure 17 B and C). The strongly reduced amount of starch measured at the end of the dark period for *rls478* leads to the hypothesis that all the energy produced by the mutant is used directly for plant growth, therefore the mutant is not capable of storing the energy in form of starch during the day as other mutants like *rls436*. Due to these data, *rls2(3)* (descending from *LHCB3*$_{pro}$*:LUC prors1-2*) and *rls478* (descending from *LHCB1.2*$_{pro}$*:LUC prors1-2*) were chosen as candidates for the identification of their suppression mutation.

Table 26: Summary of physiological rescue phenotypes of *rls2(3), rls478* and *rls436* compared to their parental lines. The behavior of the *rls* mutants compared to their parental mutants *LHCB3*$_{pro}$*:LUC prors1-2* and *LHCB1.2*$_{pro}$*:LUC prors1-2* is depicted: like Col-0 = **++**, rescue effect = **+**, similar to *LHCB3*$_{pro}$*:LUC prors1-2*; *LHCB1.2*$_{pro}$*:LUC prors1-2* = **0**.

name	**growth**	**PSII**	**starch**	***LHCB* expression**
LHCB3$_{pro}$*:LUC prors1-2*	0	0	0	0
rls2(3)	+	+	+	+
LHCB1.2$_{pro}$*:LUC prors1-2*	0	0	0	0
rls436	++	+	+	0
rls478	++	0	+	+

4.1 Are *LACCASE14* and *AT5G36320* possible candidates for suppression mutations?

4.2.1 *LACCASE14 (LAC14)*, the best candidate for the suppression mutation of *rls478*

The fine mapping of the mutation causing the observed rescue effects in *rls478* revealed a nucleotide exchange from C to A at position 2906927 bp on chromosome **V,** causing an amino acid change from glutamic acid to a stop codon in the 5th exon of the *LAC14* gene (*AT5G09360*). This position was additionally located with the rough mapping approach (Figure 24; region from 2174597 bp to 4254759 bp) for *rls478.*

LACCASES are multi-copper containing glycoprotein oxidases, for which the physiological and biochemical role in higher plants is mostly unknown. Copper is a crucial trace element required in redox-mediated physiological processes, and its levels were found to affect plant growth and development (Burkhead et al. 2009). Moreover, copper is known to function as a cofactor for several plant enzymes, including plastocyanin, cytochrome *c* oxidases and ethylene receptors (Burkhead et al. 2009). It was additionally proposed that LACCASES play a role in lignification (LaFayette 1999; Ranocha et al. 2002; Cesarino et al. 2012) or in functioning as redox mediators in maize (Galuszka et al. 2005). However, although 17 members of the *LACCASE* gene family were detected in *Arabidopsis thaliana* (McCaig et al. 2005), only for one of these the physiological function is known: *TRANSPARENT TESTA 10* (*LAC15/TT10*) is involved in mediating flavonoid polymerization, leading to seed coat colour/maturation, although without any clear determination of substrates and products (Pourcel et al. 2005). For two others LACCASES, *LAC4* and *LAC17*, there is evidence that they contribute to constitutive lignification in *Arabidopsis thaliana* stems (Berthet et al. 2011).

The *LAC14* gene is one of two *Arabidopsis thaliana LACCASE* genes that lack the cis copper response elements in the promotor region, which leads to the assumption that *LAC14* is not directly regulated by copper levels (Turlurpati et al. 2011). Furthermore, LAC14 belongs to the subgroup of LACCASES with a low redox potential. *LAC14* was found to be mainly expressed in reproductive organs, although it was detected in low levels in all tissues. *LAC14* possesses the longest N-terminal signal peptide (length 33 residues; average 25) of all 17 family members and contains 9 predicted glycosylation sites. The *in silico* expression pattern of *LAC14* revealed an up-regulation in roots and shoots after cold stress (4 °C) and an up-regulation merely in roots after osmotic stress (mannitol) and salt stress (Turlurpati et al. 2011). Moreover, upon drought (16 day old seedling 15 min dry airstream) and oxidative (10 µM methyl viologen) stress conditions, *LAC14* was found to be down-regulated in the shoots. Generally, *LAC14* - together with *LAC16* - seems to be regulated in an early response pathway to stress conditions (Turlurpati et al. 2011).

From the mapping results and from previous studies of *LAC14,* it is reasonable that the mutation in *LAC14* is responsible for the suppression of the *prors1-2* mutation leading to the phenotype of *rls478*. To confirm this assumption in future experiments, it is required to complement the *LAC14* gene in *rls478* with the wild type gene.

4.2.2 The *AT5G36320* gene as a candidate for the suppression mutation of *rls2(3)*

For determination of the mutation causing the phenotype of the second candidate chosen for the mapping approach, the only SNP remaining after filtering (see 3.3.2.3) is located in the *AT5G36320* gene. The respective mutation leads to a stop codon and is located in the region of chromosome **V** at position 14327194 bp (Figure 20), which was also mapped by rough mapping. The gene *AT5G36320* is 356 bp long, consists of merely one exon and codes for a ECA1 gametogenesis related family protein, similar to all neighboring genes from *AT5G36310* to *AT5G36550*. However, no data regarding the exact physiological function is available for *AT5G36320* to date. From the mapping data, this gene includes most likely the causative mutation of the *rls2(3)* phenotype, although it has to be noted that the mutation is located in a highly repetitive region of the chromosome (in close proximity to the centromere), and it can therefore not be excluded that it represents a mapping artifact.

4.2 Is there a link between the *prors1-2* mutation and the potential suppression mutations caused by a reduced recombination frequency of chromosome **V**?

The evolutionary importance of meiosis for allelic shuffling, which is caused by crossing-over events and gene conversion is undisputed. For *Arabidopsis thaliana,* less than 10 crossing-over events per meiosis are estimated (Salome et al. 2012; Lu et al. 2012; Giraut et al. 2011; Toyota et al. 2011), however relatively little is known about gene conversion rates (Innan et al. 2002; Yang et al. 2012). Generally, the frequency of crossing-over (= recombination) between two locations depends on their distance. By observing the recombination frequency (with the help of markers), the distance (linkage disequilibrium) between two locations can be calculated (Sturtevant 1913; Haldane 1956). Gene conversions are ignored for mapping approaches and treated as genotyping errors (Yang et al. 2012). The linkage disequilibrium in *Arabidopsis thaliana* decays within 50 kb (Nordborg et al. 2000).

The recombination frequency of chromosome **V** for both mapping populations of *rls2(3)* and *rls478* was much lower than expected, leading to strongly reduced numbers of SNPs. A reason for this could be the distorted segregation ratios, which

differ considerably from the Mendelian expectation for three of the five chromosomes in *Arabidopsis thaliana*. Chromosomes **II** and **V** are Col-0 dominant, whereas Chromosome **IV** is L*er* dominant (Salome et al. 2012; Giraut et al. 2011; Yang et al. 2012). The underlying reason for this is still unclear. The data of this project suggest that there is only evidence for chromosome **V** to be Col-0 dominant, (Tables 22, 23), due to the reduced number of SNPs for this chromosome. The most likely reason for the observed Col-0 dominant segregation for chromosome **V** is a linkage between the *prors1-2* mutation and the suppression mutations. The gene *prors1-2* is located at the lower arm of chromosome **V** at position 21311063 bp (Figure 25).

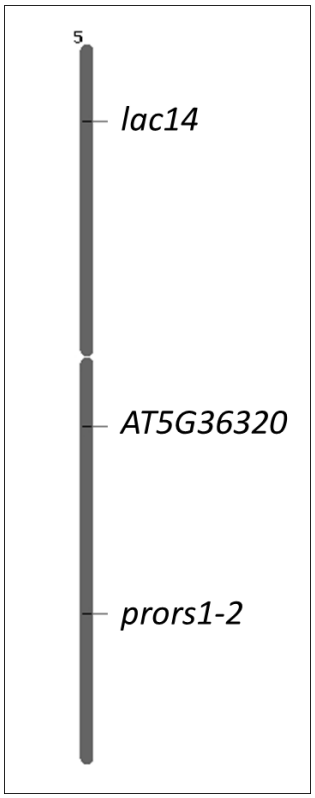

Figure 25: Locations of mutations on chromosome V. The exact positions true to scale for *lac14* (2906426 bp), *AT5G36320* (14326901 bp) and *prors1-2* (21311063 bp) are shown.

Crucial for determination of mapping mutations is the selection of the mapping population from which pool the DNA will be sequenced. For this study, the selection was based on the visual phenotype of the suppression mutants *rls2(3)* and *rls478* and the presence of the *prors1-2* allele, analyzed via PCR. All plants which fulfill these requirements were selected to represent the mapping population. If the two respective mutations are linked, which seems possible as they are both located on chromosome **V**, then only plants are selected which include both mutations; hence

plants with no or strongly reduced recombination events between the two mutation sites are selected for the mapping population. This would lead to the drastically reduced number of SNPs on chromosome **V**.

4.3 Outlook on SNP Ratio Mapping (SRM)

Former mapping approaches rely on the recovering of homozygotes or backcrossing, which leads to difficulties if lethal or poorly transmitted mutations are mapped (Austin et al. 2011; Blumenstiel et al.2009; Irvine et al. 2009; Sarin et al. 2008; Schneeberger et al. 2009; Smith et al. 2008; Srivatsan et al 2008; Zyrin et al. 2010). Second-site modifiers in a complex genetic/transgenic background, as in this project, are problematic as well. In the SNP ratio mapping approach (SRM), the mutant is backcrossed to the non-mutagenized parent, leading to a segregation ratio of unlinked SNP, created by EMS mutagenesis, of 1:3 in a pool of the whole mapping population (Lindner et al. 2012). By selecting only mutant individuals in the F1 of the second backcrossing, the causative (linked) SNP is enriched and segregates in a ratio of 1:1. A calculated 50-fold sequence coverage should be sufficient to distinguish between a 1:3 and 1:1 ratio. The peak of the causative SNP (peak size ~0.5) should have a “round form”, as the peak size of the neighbouring SNPs is between 0.5 and 0.25. By statistical testing of the neighbouring SNPs (possessing an expected recombination rate) from SNPs segregating 1:1, the causative SNP can be distinguished from other SNPs segregating 1:1, as they are located in regions displaying unusual segregation ratios, including the highly repetitive centromeric regions (Lindner et al. 2012). With SRM, the mapping of the suppression mutation in a complex genetic background is easier and faster than by other NGM methods, as the EMS mutagenized SNPs do not have to be filtered from the SNPs that derive from crossing of different accessions. However, problems might occur if the mutation of interest is in a region with unusual segregation ratios, *e.g.* in proximity to the centromere and telomere. To solve this problem, an improved maximum likelihood algorithm (iML) can be applied, by which a high genotyping accuracy can be achieved for organisms without a fully sequenced reference genome. Additionally, incorrect SNP calls, resulting from repetitive genomic regions, can be efficiently prevented (Dou et al. 2012). In the future, the mapping of mutations will be much faster and more efficiently with the help of next generation sequencing technologies.

Reference list

Abdallah F, Salamini F, Leister D (2000). A prediction of the size and evolutionary origin of the proteome of chloroplasts of Arabidopsis. *Trends Plant. Sci*. 5:141-2.

Andriankaja M, Dhondt S, De Bodt S, Vanhaeren H, Coppens F, De Milde L, Mühlenbock P, Skirycz A, Gonzalez N, Beemster GT, Inzé D (2012). Exit from proliferation during leaf development in *Arabidopsis thaliana*: a not-so-gradual process. *Dev. Cell.* 22:64-78.

Apel K, Hirt H (2004). Reactive oxygen species: metabolism, oxidative stress, and signal transduction. *Annu. Rev. Plant. Biol.* 55:373-99.

Arnon DI (1949). Copper enzyme in isolated chloroplast polyphenoloxidase in *Beta vulgaris*. *Plant. Physiol.* 24:1-15.

Austin RS, Vidaurre D, Stamatiou G, Breit R, Provart NJ, Bonetta D, Zhang J, Fung P, Gong Y, Wang PW, McCourt P, Guttman DS (2011). Next-generation mapping of Arabidopsis genes. *Plant. J.* 67:715-25.

Bell CJ, Ecker JR (1994). Assignment of 30 microsatellite loci to the linkage map of *Arabidopsis. Genomics* 19:137–44.

Berthet S, Demont-Caulet N, Pollet B, Bidzinski P, Cézard L, Le Bris P, Borrega N, Hervé J, Blondet E, Balzergue S, Lapierre C, Jouanin L (2011). Disruption of LACCASE4 and 17 results in tissue-specific alterations to lignification of Arabidopsis thaliana stems. *Plant Cell.* 23:1124-37.

Blumenstiel JP, Noll AC, Griffiths JA, Perera AG, Walton KN, Gilliland WD, Hawley RS, Staehling-Hampton K (2009). Identification of EMS-induced mutations in Drosophila melanogaster by whole-genome sequencing*. Genetics.* 182:25-32.

Bradbeer JW, Atkinson YE, Börner T, Hagemann R (1979). Cytoplasmic synthesis of plastid polypeptides may be controlled by plastid-synthesized RNA. *Nature* 279:816–7.

Burch-Smith TM, Brunkard JO, Choi YG, Zambryski PC (2011). Organelle-nucleus cross-talk regulates plant intercellular communication via plasmodesmata. *Proc. Natl. Acad. Sci. U. S. A*. 108:1451–60.

Cai X, Davis EJ, Ballif J, Liang M, Bushman E, Haroldsen V, Torabinejad J, Wu Y (2006). Mutant identification and characterization of the laccase gene family in *Arabidopsis*. *J. Exp. Bot.* 57:2563-9.

Carrier G, Santoni S, Rodier-Goud M, Canaguier A, Kochko Ad, Dubreuil-Tranchant C, This P, Boursiquot JM, Le Cunff L (2011). An efficient and rapid protocol for plant nuclear DNA preparation suitable for next generation sequencing methods. *Am. J. Bot.* 98:13-5.

Cesarino I, Araújo P, Sampaio Mayer JL, Paes Leme AF, Mazzafera P (2012). Enzymatic activity and proteomic profile of class III peroxidases during sugarcane stem development. *Plant. Physiol. Biochem.* 55:66-76.

Chan KX, Crisp PA, Estavillo GM, Pogson BJ (2010). Chloroplast-to-nucleus communication: current knowledge, experimental strategies and relationship to drought stress signaling. *Plant. Signal. Behav*. 5:1575-82.

Chang C, Bowman JL, DeJohn AW, Lander ES, Meyerowitz EM (1988). Restriction fragment length polymorphism linkage map for Arabidopsis thaliana. *Proc. Natl. Acad. Sc.i U. S. A.* 85:6856-60.

Clough SJ, Bent AF (1998). Floral dip: a simplified method for Agrobacterium-mediated transformation of *Arabidopsis thaliana*. *Plant. J.* 16:735-43.

Dyall SD, Brown MT, Johnson PJ (2004). Ancient invasions: From endosymbionts to organelles. *Science* 304:253-7.

Dou J, Zhao X, Fu X, Jiao W, Wang N, Zhang L, Hu X, Wang S, Bao Z (2012). Reference-free SNP calling: improved accuracy by preventing incorrect calls from repetitive genomic regions. *Biol. Direct.* 8:7-17.

Elstner (1991). Mechanism of oxygen activation in different compartments of plant cells. In E.J. Pell and K.L. Steffen (eds) Active Oxygen/Oxidative Stress and Plant Metabolism, American Society of Plant Physiologists, Rockville, pp. 13-25

Enami K, Ozawa T, Motohashi N, Nakamura M, Tanaka K, Hanaoka M (2011). Plastid-to-nucleus retrograde signals are essential for the expression of nuclear starch biosynthesis genes during amyloplast differentiation in tobacco BY-2 cultured cells. *Plant. Physiol.* 157:518–30.

Estavillo GM, Crisp PA, Pornsiriwong W, Wirtz M, Collinge D, Carrie C, Giraud E, Whelan J, David P, Javot H, Brearley C, Hell R, Marin E, Pogson BJ (2011). Evidence for a SAL1-PAP chloroplast retrograde pathway that functions in drought and high light signaling in *Arabidopsis*. *Plant Cell* 23:3992–4012.

Fernández AP, Strand Å (2008). Retrograde signaling and plant stress: plastid signals initiate cellular stress responses. *Curr..Opin. Plant. Biol.* 11:509–13.

Galuszka P, Frébortová J, Luhová L, Bilyeu KD, English JT, Frébort I (2005). Tissue localization of cytokinin dehydrogenase in maize: possible involvement of quinone species generated from plant phenolics by other enzymatic systems in the catalytic reaction. *Plant. Cell. Physiol*. 46:716-28.

Gálvez-Valdivieso G, Mullineaux PM (2010). The role of reactive oxygen species in signaling from chloroplast to the nucleus. *Physiol. Plant*. 138:430–9.

Giraut L, Falque M, Drouaud J, Pereira L, Martin OC, Mézard C (2011). Genome-wide crossover distribution in Arabidopsis thaliana meiosis reveals sex-specific patterns along chromosomes. *PLoS. Genet.* 7:e1002354.

Greene EA, Codomo CA, Taylor NE, Henikoff JG, Till BJ, Reynolds SH, Enns LC, Burtner C, Johnson JE, Odden AR, Comai L, Henikoff S (2003). Spectrum of chemically induced mutations from a large-scale reverse-genetic screen in *Arabidopsis*. *Genetics.* 164:731-40.

Haldane JB (1956). The estimation and significance of the logarithm of a ratio of frequencies. *Ann. Hum. Genet.* 20:309-11.

Hardtke CS, Berleth T (1996). Genetic and contig map of a 2200-kb region encompassing 5.5 cM on chromosome 1 of *Arabidopsis thaliana*. *Genome*. 39:1086-92.

Innan H (2002). A method for estimating the mutation, gene conversion and recombination parameters in small multigene families. *Genetics*. 161:865-72.

Irvine DV, Goto DB, Vaughn MW, Nakaseko Y, McCombie WR, Yanagida M, Martienssen R (2009). Mapping epigenetic mutations in fission yeast using whole-genome next-generation sequencing. *Genome Res.* 19:1077-83.

Jung HS, Chory J (2010). Signaling between chloroplasts and the nucleus: can a systems biology approach bring clarity to a complex and highly regulated pathway? *Plant Physiol*. 152:453-9.

Kakizaki T, Matsumura H, Nakayama K, Che FS, Terauchi R, Inaba T (2009). Coordination of plastid protein import and nuclear gene expression by plastid-to-nucleus retrograde signaling. *Plant. Physiol.* 151:1339-53.

Kleine T, Voigt C, Leister D (2009). Plastid signaling to the nucleus: messengers still lost in the mists? *Trends. Genet.* 25:185-92.

Kobayashi Y, Kanesaki Y, Tanaka A, Kuroiwa H, Kuroiwa T, Tanaka K (2009). Tetrapyrrole signal as a cell-cycle coordinator from organelle to nuclear DNA replication in plant cells. *Proc. Natl. Acad. Sci. U. S. A.* 106:803–7.

Konieczny A, Ausubel F (1993). A procedure for mapping *Arabidopsis* mutations using co-dominant ecotypespecific PCR-based markers. *Plant. J.* 4:403–10.

Koussevitzky S, Nott A, Mockler TC, Hong F, Sachetto-Martins G, Surpin M, Lim J, Mittler R, Chory J (2007). Signals from chloroplasts converge to regulate nuclear gene expression. *Science.* 316:715-9.

Laemmli UK (1970). Cleavage of Structural Proteins During Assembly of Head of Bacteriophage-T4. *Nature.* 227:680-6

LaFayette PR, Eriksson KE, Dean JF (1999). Characterization and heterologous expression of laccase cDNAs from xylem tissues of yellow-poplar (*Liriodendron tulipifera*). *Plant. Mol. Biol.* 40:23-35.

Larkin RM, Alonso JM, Ecker JR, Chory J (2003). GUN4, a regulator of chlorophyll synthesis and intracellular signaling. *Science*. 299:902-6.

Lee KP, Kim C, Landgraf F, Apel K (2007). EXECUTER1- and EXECUTER2-dependent transfer of stress-related signals from the plastid to the nucleus of *Arabidopsis thaliana*. *Proc. Natl. Acad. Sci. U. S. A.* 104:10270–5.

Leister, D (2005). Genomics-based dissection of the cross-talk of chloroplasts with the nucleus and mitochondria in Arabidopsis. *Gene* 354:110–6.

Leister D, Varotto C, Pesaresi P, Niwergall A, Salamini F (1999). Large-scale evaluation of plant growth in *Arabidopsis thaliana* by non-invasive image analysis. *Plant Phys. and Biochem.* 37:671-8.

Lichtenthaler HK (1987). Chlorophylls and carotenoids: Pigments of photosynthetic biomembranes. *Methods Enzymol.* 148:350-82.

Lindner H, Raissig MT, Sailer C, Shimosato-Asano H, Bruggmann R, Grossniklaus U (2012). SNP-Ratio Mapping (SRM): identifying lethal alleles and mutations in complex genetic backgrounds by next-generation sequencing. *Genetics*.191:1381-6.

Lu P, Han X, Qi J, Yang J, Wijeratne AJ, Li T, Ma H (2012). Analysis of Arabidopsis genome-wide variations before and after meiosis and meiotic recombination by resequencing Landsberg erecta and all four products of a single meiosis. *Genome Res.* 22:508-18.

Lukowitz W, Gillmor CS, Scheible WR (2000). Positional cloning in Arabidopsis. Why it feels good to have a genome initiative working for you. *Plant. Physiol.* 123:795-805.

Marshall OJ (2004). PerlPrimer: cross-platform, graphical primer design for standard, bisulphite and real-time PCR. *Bioinformatics*. 20:2471-2.

McCaig BC, Meagher RB, Dean JF (2005). Gene structure and molecular analysis of the laccase-like multicopper oxidase (LMCO) gene family in *Arabidopsis thaliana*. *Planta*. 221:619-36.

Meskauskiene R, Nater M, Goslings D, Kessler F, op den Camp R, Apel K (2001). FLU: A negative regulator of chlorophyll biosynthesis in *Arabidopsis thaliana*. *Proc. Natl. Acad. Sci. U. S. A*. 98:12826–31.

Mochizuki N, Brusslan JA, Larkin R, Nagatani A, Chory J (2001). Arabidopsis genomes uncoupled 5 (GUN5) mutant reveals the involvement of Mg-chelatase H subunit in plastid-to-nucleus signal transduction, *Proc. Natl. Acad. Sci. U. S. A.* 98:2053–8.

Mullineaux P, Karpinski S (2002). Signal transduction in response to excess light: getting out of the chloroplast. *Curr. Opin. Plant.* Biol. 5:43-8.

Nordborg M (2000). Linkage disequilibrium, gene trees and selfing: an ancestral recombination graph with partial self-fertilization. *Genetics*. 154:923-9.

Nordborg M, Hu TT, Ishino Y, Jhaveri J, Toomajian C, Zheng H, Bakker E, Calabrese P, Gladstone J, Goyal R, Jakobsson M, Kim S, Morozov Y, Padhukasahasram B, Plagnol V, Rosenberg NA, Shah C, Wall JD, Wang J, Zhao K, Kalbfleisch T, Schulz V, Kreitman M, Bergelson J (2005). The pattern of polymorphism in *Arabidopsis thaliana*. *PLoS. Biol.* 3:e196.

Nott A, Jung HS, Koussevitzky S, Chory J (2006). Plastid-to-nucleus retrograde signaling. *Annu. Rev. Plant. Biol.* 57:739–59.

Oelmüller R, Mohr H (1986). Photooxidative destruction of chloroplasts and its consequences for expression of nuclear genes. *Planta.* 167:106–13.

Page DR, Grossniklaus U (2002). The art and design of genetic screens: *Arabidopsis thaliana. Nat. Rev. Genet.* 3:124-36.

Pesaresi P, Masiero S, Eubel H, Braun HP, Bhushan S, Glaser E, Salamini F, Leister D (2006). Nuclear photosynthetic gene expression is synergistically modulated by rates of protein synthesis in chloroplasts and mitochondria. *Plant Cell.* 18:970-91.

Pesaresi P, Schneider A, Kleine T, Leister D (2007). Interorganellar communication. *Curr. Opin. Plant. Biol*. 10:600-6.

Pfaffl MW (2001). A new mathematical model for relative quantification in real-time RT-PCR. *Nucleic. Acids. Res.* 29:e45.

Pfannschmidt T (2010). Plastidial retrograde signaling-a true "plastid factor" or just metabolite signatures? *Trends. Plant. Sci.* 15:427-35.

Pogson BJ, Woo NS, Forster B, Small ID (2008). Plastid signaling to the nucleus and beyond, *Trends. Plant. Sci.* 13:602–9.

Pontier D, Albrieux C, Joyard J, Lagrange T, Block MA (2007). Knock-out of the magnesium protoporphyrin IX methyltransferase gene in Arabidopsis. Effects on chloroplast development and on chloroplast-to-nucleus signaling. *J. Biol. Chem*. 282:2297–304.

Pourcel L, Routaboul JM, Kerhoas L, Caboche M, Lepiniec L, Debeaujon I (2005). TRANSPARENT TESTA10 encodes a laccase-like enzyme involved in oxidative polymerization of flavonoids in Arabidopsis seed coat. *Plant Cell.* 17:2966-80.

Ramakers C, Ruijter JM, Deprez RH, Moorman AF (2003). Assumption-free analysis of quantitative real-time polymerase chain reaction (PCR) data. *Neurosci. Lett.* 339:62-6.

Ranocha P, Chabannes M, Chamayou S, Danoun S, Jauneau A, Boudet AM, Goffner D (2002). Laccase down-regulation causes alterations in phenolic metabolism and cell wall structure in poplar. *Plant. Physiol*. 129:145-55.

Saiki RK, Gelfand DH, Stoffel S, Scharf SJ, Higuchi R, Horn GT, Mullis KB, Erlich HA (1988). Primer-directed enzymatic amplification of DNA with a thermostable DNA polymerase. *Science.* 239:487-91.

Salomé PA, Bomblies K, Fitz J, Laitinen RA, Warthmann N, Yant L, Weigel D (2012). The recombination landscape in *Arabidopsis thaliana* F2 populations. *Heredity (Edinb)*. 108:447-55.

Salomé PA, Oliva M, Weigel D, Krämer U (2013). Circadian clock adjustment to plant iron status depends on chloroplast and phytochrome function. *EMBO. J.* 32:511-23.

Sambrook J, Russel DW (2001). Molecular cloning: a laboratory manual 3rd edition; *Cold Spring Harbour Laboratory Press*, New York.

Sambrook J, Fritsch EF, Maniatis T (1989). Molecular Cloning - A Laboratory Manual. *Cold Spring Harbour Laboratory Press*, New York.

Sarin S, Prabhu S, O'Meara MM, Pe'er I, Hobert O (2008). Caenorhabditis elegans mutant allele identification by whole-genome sequencing. *Nat. Methods*. 5:865-7.

Schneeberger K, Ossowski S, Lanz C, Juul T, Petersen AH, Nielsen KL, Jørgensen JE, Weigel D, Andersen SU (2009). SHOREmap: simultaneous mapping and mutation identification by deep sequencing. *Nat. Methods.* 6:550-1.

Shimomura O, Goto T, Johnson FH (1977). Source of oxygen in the CO_2 produced in the bioluminescent oxidation of firefly luciferin. *Proc Natl Acad Sci U. S. A*. 74:2799-802.

Skovsen E, Snyder JW, Lambert JD, Ogilby PR (2005). Lifetime and diffusion of singlet oxygen in a cell. *J Phys. Chem. B.* 109:8570-3.

Smith DR, Quinlan AR, Peckham HE, Makowsky K, Tao W, Woolf B, Shen L, Donahue WF, Tusneem N, Stromberg MP, Stewart DA, Zhang L, Ranade SS, Warner JB, Lee CC, Coleman BE, Zhang Z, McLaughlin SF, Malek JA, Sorenson JM, Blanchard AP, Chapman J, Hillman D, Chen F, Rokhsar DS, McKernan KJ, Jeffries TW, Marth GT, Richardson PM (2008). Rapid whole-genome mutational profiling using next-generation sequencing technologies. *Genome Res*. 18:1638–42.

Soll J, Schleiff E (2004). Protein import into chloroplasts. *Nat. Rev. Mol. Cell Biol*. 5:198–208.

Srivatsan A, Han Y, Peng J, Tehranchi AK, Gibbs R, Wang JD, Chen R (2008). High-precision, whole-genome sequencing of laboratory strains facilitates genetic studies. *PLoS. Genet.* 4:e1000139.

Strand Å, Asami T, Alonso J, Ecker JR, Chory J (2003). Chloroplast to nucleus communication triggered by accumulation of Mg-protoporphyrinIX. *Nature.* 421:79–83.

Sturtevant AH (1913). The linear arrangement of six sex-linked factors in *Drosophila*, as shown by their mode of association. *Journal of Experimental Zoology*, 14:43-59.

Sullivan JA, Gray JC (1999). Plastid translation is required for the expression of nuclear photosynthesis genes in the dark and in roots of the pea lip1 mutant. *Plant Cell* 11:901–10.

Sun X, Feng P, Xu X, Guo H, Ma J, Chi W, Lin R, Lu C, Zhang L (2011). A chloroplast envelope-bound PHD transcription factor mediates chloroplast signals to the nucleus. *Nat. Commun.* 2:477.

Susek RE, Ausubel FM, Chory J (1993). Signal transduction mutants of Arabidopsis uncouple nuclear CAB and RBCS gene expression from chloroplast development. *Cell* 74:787–99.

Terry MJ, Smith AG (2013). A model for tetrapyrrole synthesis as the primary mechanism for plastid-to-nucleus signaling during chloroplast biogenesis. *Front. Plant. Sci.* 4:14.

Thormählen I, Ruber J, von Roepenack-Lahaye E, Ehrlich SM, Massot V, Hümmer C, Tezycka J, Issakidis-Bourguet E, Geigenberger P (2013). Inactivation of thioredoxin f1 leads to decreased light activation of ADP-glucose pyrophosphorylase and altered diurnal starch turnover in leaves of Arabidopsis plants. *Plant Cell Environ.* 36:16-29.

Timmis JN, Ayliffe MA, Huang CY, Martin W (2004). Endosymbiotic gene transfer: organelle genomes forge eukaryotic chromosomes. *Nat. Rev. Genet.* 5:123–35.

Towbin H, Staehelin T, Gordon J (1979). Electrophoretic transfer of proteins from polyacrylamide gels to nitrocellulose sheets: procedure and some applications. *Proc. Natl. Acad. Sci. U. S. A.* 76: 4350-4.

Toyota M, Matsuda K, Kakutani T, Terao Morita M, Tasaka M (2011). Developmental changes in crossover frequency in *Arabidopsis*. *Plant. J.* 65:589-99.

Turlapati PV, Kim KW, Davin LB, Lewis NG (2011). The laccase multigene family in *Arabidopsis thaliana*: towards addressing the mystery of their gene function(s). *Planta.* 233:439-70.

Varotto C, Pesaresi P, Meurer J, Oelmüller R, Steiner-Lange S, Salamini F, Leister D (2000). Disruption of the *Arabidopsis* photosystem I gene psaE1 affects photosynthesis and impairs growth. *Plant. J.* 22:115-24.

Weigel D, Glazebrook J (2006). Setting up *Arabidopsis* crosses. *Cold Spring Harbour Laboratory Press*, New York.

Woodson JD, Chory J (2008). Coordination of gene expression between organellar and nuclear genomes. *Nat. Rev. Genet.* 9:383-95.

Woodson JD, Pérez-Ruiz JM, Chory J (2011). Heme synthesis by plastid ferrochelatase I regulates nuclear gene expression in plants. *Curr. Biol.* 21:897–903.

Xiao Y, Savchenko T, Baidoo EE, Chehab WE, Hayden DM, Tolstikov V, Corwin JA, Kliebenstein DJ, Keasling JD, Dehesh K (2012). Retrograde signaling by the plastidial metabolite MEcPP regulates expression of nuclear stress-response genes. *Cell.* 149:1525-35.

Yang S, Yuan Y, Wang L, Li J, Wang W, Liu H, Chen JQ, Hurst LD, Tian D (2012). Great majority of recombination events in *Arabidopsis* are gene conversion events. *Proc. Natl. Acad. Sci. U S A*. 109:20992-7.

Zhang ZW, Yuan S, Feng H, Xu F, Cheng J, Zhang DW, Hong H, Lin HH (2011). Transient accumulation of Mg-protoporphyrinIX regulates expression of PhANGs: new evidence for the signaling role of tetrapyrroles inmature *Arabidopsis* plants. *J. Plant. Physiol.* 168:714–21.

Zuryn S, Le Gras S, Jamet K, Jarriault S (2010). A strategy for direct mapping and identification of mutations by whole-genome sequencing. *Genetics,* 186:427–30.

Acknowledgements

Ich möchte mich bei Prof. Dr. Dario Leister für die Möglichkeit bedanken, dass ich meine Doktorarbeit in einem sehr interessanten internationalen Umfeld erarbeiten konnte, sowie für die wissenschaftlichen Möglichkeiten die mir geboten wurden.

Des Weiteren bedanken möchte ich mich bei meiner Betreuerin Dr. Tatjana Kleine für ihr großes Vertrauen in meine Fähigkeiten im Labor sowie in meinen Umgang mit den zu betreuenden Studenten.

Ein großer Dank gilt Elli, die mir im Labor nicht nur mit Rat und sehr viel Tat zur Seite stand, sondern mit der ich auch viele interessante Gespräche über jedwede Sportart führen konnte, was mir sehr viel Spaß bereitet hat.

Bedanken möchte ich mich auch bei meinen Kollegen für die tolle gemeinsame Zeit, besonders bei meinen Bürokollegen Ari, Jafar und Steffi, sowie Wenteng der mir ein guter Freund und „Spielkontrahent“ geworden ist.

Den fleißigen Bachelorstudenten Max, Pit, Maya und Jasmin gilt ebenso mein Dank.

Ohne meine Familie wäre das alles nicht möglich gewesen und ich bin überglücklich über ihre immerwährende Unterstützung in allen Lebenslagen. Dafür und, dass sie diese Zeit mit mir erlebten, bin ich sehr dankbar.

Ohne den wichtigsten Menschen in meinem Leben wäre vieles nicht möglich gewesen, von dieser Arbeit ganz zu schweigen. Du zeigst mir jeden Tag, auf was es im Leben ankommt. Du bist meine Kraftquelle. Ich danke dir von ganzem Herzen das du der wesentliche Teil meines/unseres Lebens bist. Vielen Dank für alles!

Declaration / Eidesstattliche Erklärung

Ich versichere hiermit an Eides statt, dass die vorliegende Dissertation von mir selbständig und ohne unerlaubte Hilfe angefertigt wurde.

München, den 18.7.2013 Lukas Mittermayr

Erklärung

Hiermit erkläre ich,

dass die Dissertation nicht ganz oder in wesentlichen Teilen einer anderen Prüfungskommission vorgelegt worden ist.

dass ich mich anderweitig einer Doktorprüfung ohne Erfolg **nicht** unterzogen habe

München, den 18.7.2013 Lukas Mittermayr